Alma Mater Studiorum · Università di Bologna

Scuola di Scienze
Corso di Laurea Magistrale in Fisica

TWO-DIMENSIONAL RELAXATION-DIFFUSION ANALYSIS TO STUDY WATER COMPARTMENTALIZATION IN CELLS BY A SINGLE-SIDED NMR DEVICE

Relatore:
Prof.ssa Paola Fantazzini

Presentata da:
Filippo Pedrazzini

Correlatore:
Dott. Leonardo Brizi

Sessione III
Anno Accademico 2014/2015

Alla mia famiglia.

Abstract

In questo lavoro di tesi è presentato un metodo per lo studio della compartimentalizzazione dell'acqua in cellule biologiche, mediante lo studio dell'autodiffusione delle molecole d'acqua tramite uno strumento NMR single-sided. Come sistema modello è stato assunto un campione di cellule di lievito, *Saccharomyces cerevisiae*.
Le misure sono state eseguite nel laboratorio NMR all'interno del Dipartimento di Fisica e Astronomia di Bologna.
Inizialmente sono stati misurati i coefficienti di autodiffusione di tre campioni in condizione di non confinamento, soltrol 130, soltrol 170 e acqua, ottenendo risultati consistenti con i dati in letteratura. Si è passati quindi all'analisi di un campione di lievito allo stato solido, ottimizzando le procedure per l'ottenimento di mappe di correlazione 2-dimensionali, aventi come assi il coefficiente di autodiffusione D e il tempo di rilassamento trasversale T_2. In questo sistema l'acqua è confinata e l'autodiffusione è ristretta dalle pareti cellulari, si parla quindi di coefficiente di autodiffusione apparente. Le mappe hanno portato all'individuazione di due famiglie di nuclei ^{1}H, aventi un coefficiente di autodiffusione apparente che cala all'aumentare del tempo di diffusione, fino a raggiungere un valore asintotico.
Il campione è stato poi analizzato in diluizione in acqua distillata ($1 : 1.5$ (w/w)) confermando la separazione del segnale in due distinte famiglie.
L'utilizzo di un composto chelato, il CuEDTA, al posto di acqua distillata, ha permesso di affermare che la famiglia con il coefficiente di autodiffusione apparente maggiore corrisponde all'acqua esterna alle cellule. L'analisi e il fit dei dati ottenuti sulle due famiglie al variare del tempo lasciato alle molecole d'acqua per la diffusione hanno portato alla stima di due compartimenti. Con l'assunzione dell'ipotesi di forma sferica si è ottenuta una stima del raggio dei due compartimenti: $r = 2.3 \pm 0.2\mu$m per l'acqua extracellulare, $r = 0.9 \pm 0.1\mu$m per quella intracellulare, che è probabilmente acqua scambiata tra gli organelli e il citoplasma. L'incertezza associata a tali stime tiene conto soltanto dell'errore nel calcolo dei parametri liberi del fit dei dati, è pertanto una sottostima, dovuta alle approssimazioni connesse all'utilizzo di equazioni valide per un sistema poroso costituito da pori sferici connessi non permeabili. Gli ordini di grandezza dei raggi calcolati sono invece consistenti con quelli osservabili dalle immagini ottenute con il microscopio ottico.

Contents

Introduction

The Nuclear Magnetic Resonance (NMR) studies on diffusion phenomenon, particularly of the molecular self-diffusion play an important role in scientific research. An interesting field of application of this phenomenon is the study of the porous media, from which MRPM (*Magnetic Resonance for fluids in Porous Media*) branch has been developed [1]. By the NMR analysis of a fluid diffusing in a porous medium, it's possible to study the properties of the porous structure such as the porosity, the pore size distribution, the connectivity, the permeability [2]. The nuclear spin relaxation and diffusion of the fluids molecules allow the study by NMR of important properties of the systems investigated. The diffusion phenomenon is related to the Brownian motion, for which the fluids molecules travel tracing paths called *random walks*; if the random walk is not limited by any obstacle, the diffusion is free and it is associated to the bulk diffusion coefficient D_0, depending on the fluid nature. In the case of molecules confined, the diffusion is limited, and this condition is called *restricted diffusion*. The consequence of this confinement condition is the reduction of D_0 into the *apparent diffusion coefficient* $D_{app}(t)$ [3]. The attenuation of D_{app} respect to D_0 shows a time dependence related to the molecules interactions with the confinement structure, probing its geometry.
Porous media could be modelled as packages of solid particles with interstitial space occupied by fluids; in this condition fluid molecules have a space available for displacement reduced, since the solid wall can't be penetrated [4]. In biological tissues, cell membranes exhibit finite permeability to water transport, thus limiting the diffusion displacement through the membranes [1].
There are two aspects of the selfdiffusion reduction dependence on time.
For short diffusion times, for which the diffusion distance $\sqrt{D_0 t}$ is much less than pore size, the reducing of the diffusion coefficient is proportional to the Surface-to-Volume ratio of the pores [2][5][6]. At long times, diffusing molecules probe the connectivity of the pore space and the restricted diffusion is defined by tortuosity: this feature leads to many properties of confined fluids, as permeability or electrical conduction [7][8].
The study of self-diffusion coefficient attenuation has led to an improvement of diagnostic imaging techniques obtaining high-contrast images weighted by the different restricted selfdiffusion coefficients in several biological tissues. For example, the computing of Surface-to-Volume ratio has a substantial role in the detection of ischemia cell sizes changes [9].
In this work of thesis, the $D_{app}(t)$ of internal-external water in biological cells (*Saccharomyces cerevisiae*) is investigated in order to study water compartmentalization.
The measurements were performed at the NMR laboratory of the Department of Physics

and Astronomy of the University of Bologna using the Profile NMR MOUSE (*MObile Universal Surface Explorer*). It consists in a small single-sided NMR sensor weighting of the order of 1 kg which generates a polarizing magnetic field up to 0.5 T [10]. The pulse sequences performed to measure the signal attenuation due to diffusion don't use pulsed gradients; they exploit the intrinsic gradient perpendicular to the magnet surface. Hence, the main object of this work is the feasibility study of the use of this portable and cheap instrument in a branch where usually in-situ mangets are used. The main pulse sequence performed consists in a Stimulated Spin Echo for data encoding, followed by a CPMG for data decoding. The data elaboration is realized through two-dimensional correlation maps having self-diffusion coefficient D and ^{1}H transverse relaxation time T_2 as axis.

The first part of this thesis, *Material and methods*, consists of four chapters containing:

- a theoretical description of diffusion and self-diffusion in bulk and restricted conditions, focusing on diffusion in porous media and the measurement of this phenomenon by NMR;

- a presentation of the NMR-MOUSE and of the NMR pulse sequences performed in data acquisition;

- the description of 1D and 2D Laplace inversion which constitute the mathematical basis of the software used in the data elaboration.;

- the description of the materials and samples used in the study of both bulk and restricted self-diffusion.

The second part, *Results*, consists of four chapters containing:

- the preliminary tests performed in order to test the procedures adopted to measure the molecular self-diffusion coefficients on bulk liquids, by exploiting the intrinsic magnetic field gradient of the NMR MOUSE;

- the optimization of the procedure for the study of compartmentalization by measurements of restricted diffusion on solid yeast sample;

- the measurements of T_2 on yeast sample in different distilled water dilutions, followed by restricted diffusion measurements on 1 : 1.5 (w/w) diluted yeast both in not-doped and CuEDTA-doped water;

- a discussion about the restricted diffusion behaviour in the three samples studied and the results obtained by their analysis, which interpretation leads to the conclusion that two compartments, intra-cellular and extra-cellular water, can be distinguished in the yeast samples and their sizes estimated.

Part I

Material and methods

Chapter 1

Diffusion

Molecules inside a liquid are exposed to *Brownian motion*: a phenomenon consisting in a random motion of thermic origins. The motion of each molecule is independent of others, however, collisions between molecules originate mutual moves of random nature, without a favourite direction. Hence, the diffusion phenomenon has origin. The paths traced by molecules travelling in a liquid are called *random walks*. Although diffusion is the results of random processes, it's governed by a mechanism whose features are dependent on probe nature and temperature.

1.1 Diffusion and self-diffusion

It's possible to analize fluid diffusion in terms of the concentration, the number of particles per unit volume [3]. This process is described by Fick's first law of diffusion, which bounds the flux of a particle $\mathbf{J}$ as the number of particles crossing the unit area for unit of time at the point $\mathbf{r}$ at time t as:

$$\mathbf{J}(\mathbf{r}, t) = -D\nabla c(\mathbf{r}, t) \tag{1.1}$$

The minus sign indicates that (in isotropic media) the direction of flow is from larger to smaller concentration. The D factor stands for the *diffusion coefficient*. Due to the conservation of mass, the continuity theorem applies, and thus,

$$\frac{\partial c(\mathbf{r}, t)}{\partial t} = -\nabla \cdot \mathbf{J}(\mathbf{r}, t) \tag{1.2}$$

The equation above states that $\frac{\partial c(\mathbf{r},t)}{\partial t}$ is the difference between the influx and efflux from the point located at $\mathbf{r}$. Combining eqs. (1.1) and (1.2), Fick's second law of diffusion can be derived:

$$\frac{\partial c(\mathbf{r}, t)}{\partial t} = D\nabla^2 c(\mathbf{r}, t) \tag{1.3}$$

In this mathematical description, we have assumed that the diffusion process is isotropic and can therefore be described by the diffusion coefficient D (i.e., a scalar). In the anisotropic media, the diffusion coefficient depends on the direction. It is a symmetric tensor (3×3 matrix). Fick's first law changes to:

$$\mathbf{J}(\mathbf{r}, t) = -\mathbf{D}\nabla c(\mathbf{r}, t) \tag{1.4}$$

which is an abbreviated version of:

$$\begin{vmatrix} J(x,t) \\ J(y,t) \\ J(z,t) \end{vmatrix} = - \begin{vmatrix} D_{xx} & D_{xy} & D_{xz} \\ D_{yx} & D_{yy} & D_{yz} \\ D_{zx} & D_{zy} & D_{zz} \end{vmatrix} \begin{vmatrix} \frac{\partial c(x,t)}{\partial t} \\ \frac{\partial c(y,t)}{\partial t} \\ \frac{\partial c(z,t)}{\partial t} \end{vmatrix} \tag{1.5}$$

It may be expressed as follows:

$$\frac{\partial c(\mathbf{r}, t)}{\partial t} = \nabla \cdot \mathbf{D}\nabla c(\mathbf{r}, t) \tag{1.6}$$

In the case of self-diffusion, there's not net concentration gradient. For this reason, the discussion about this phenomenon should be done in terms of the total probability $P(\mathbf{r}_1, t)$ of finding a particle at position $\mathbf{r}_1$ at time t. This is given by:

$$P(\mathbf{r}_1, t) = \int \rho(\mathbf{r}_0) P(\mathbf{r}_0, \mathbf{r}_1, t) d\mathbf{r}_0 \tag{1.7}$$

where $\rho(\mathbf{r}_0)$ is the particle density in $\mathbf{r}_0$, and thus, $\rho(\mathbf{r}_0)P(\mathbf{r}_0\mathbf{r}_1, t)$ is the probability of starting from $\mathbf{r}_0$ and moving to $\mathbf{r}_1$ in time t. The integration over $\mathbf{r}_0$ accounts for all possible starting positions. Similar to concentration, $P(\mathbf{r}_1, t)$ describes the probability of finding a particle in a certain position at a certain time. In the free diffusion case $\rho(\mathbf{r}_0) = 1$. It's reasonable to assume that $P(\mathbf{r}_0, \mathbf{r}_1, t)$ obeys the diffusion equation. For this reason $P(\mathbf{r}_0, \mathbf{r}_1, t)$ is called *diffusion propagator function*. We can rewrite Fick's laws in terms of $P(\mathbf{r}_0, \mathbf{r}_1, t)$ with the initial condition,

$$P(\mathbf{r}_0, \mathbf{r}_1, t) = \delta(\mathbf{r}_0 - \mathbf{r}_1) \tag{1.8}$$

(where δ is the Dirac delta function). Substituting $c(r, t)$ with $P(\mathbf{r}_0, \mathbf{r}_1, t)$ in Eq. (1.1), $\mathbf{J}$ becomes the conditional probability flux:

$$\mathbf{J} = -D\nabla P \tag{1.9}$$

For the continuity theorem, we have $\frac{\partial P(\mathbf{r}_0, \mathbf{r}_1, t)}{\partial t} = -\nabla \mathbf{J}$ from which Fokker-Planck equation is obtained. It's equivalent to the Frick's second law

$$\frac{\partial P(\mathbf{r}_0, \mathbf{r}_1, t)}{\partial t} = D\nabla^2 P(\mathbf{r}_0, \mathbf{r}_1, t) \tag{1.10}$$

Equation (1.10) can be written in terms of $P(\mathbf{R}, t)$, where $\mathbf{R} = \mathbf{r}_1 - \mathbf{r}_0$ is the displacement vector. For the case of three-dimensional free diffusion of a homogeneous and isotropic medium, with boundary condition $\lim_{r\to\infty} P = 0$, we obtain:

$$P(\mathbf{r}_0, \mathbf{r}_1, t) = (4\pi D t)^{-\frac{3}{2}} e^{-\frac{(\mathbf{r}_1 - \mathbf{r}_0)^2}{4Dt}} \tag{1.11}$$

Due to the Markovian nature of Brownian motion, P depends only on the net displacement $(\mathbf{r}_1 - \mathbf{r}_0)$ after a time t and not on $\mathbf{r}_0$. The mean squared path is given by

$$\left\langle (\mathbf{r}_1 - \mathbf{r}_0)^2 \right\rangle = \int_{-\infty}^{\infty} (\mathbf{r}_1 - \mathbf{r}_0)^2 \rho(\mathbf{r}_0) P(\mathbf{r}_0, \mathbf{r}_1, t) d\mathbf{r}_0 d\mathbf{r}_1 \tag{1.12}$$

We can rewrite Eq. 1.11 in Cartesian coordinates ($\mathbf{r} = x\mathbf{i} + y\mathbf{j} + z\mathbf{k}$)

$$P(\mathbf{r}_0, \mathbf{r}_1, t) = (4\pi Dt)^{-\frac{3}{2}} e^{-\frac{(x_1 - x_0)^2}{4Dt}} e^{-\frac{(y_1 - y_0)^2}{4Dt}} e^{-\frac{(z_1 - z_0)^2}{4Dt}} \tag{1.13}$$

This is the first step toward obtaining the mean-squared displacement in the case of free diffusion. The second consists in considering $\rho(\mathbf{r}_0) = 1$. Finally, using the standard integral [11] we obtain

$$\int_{-\infty}^{\infty} x^2 e^{-\mu x^2 + 2\nu x} dx = \frac{1}{2\mu} \sqrt{\frac{\pi}{\mu}} \left(1 + \frac{2\nu^2}{\mu} \right) e^{\frac{\nu^2}{\mu}} \qquad [|arg\nu| < \pi, Re \quad \mu > 0] \tag{1.14}$$

with $\mathbf{x} = \mathbf{x}_1 - \mathbf{x}_0$, $\mathbf{y} = \mathbf{y}_1 - \mathbf{y}_0$, $\mathbf{z} = \mathbf{z}_1 - \mathbf{z}_0$, $\mu = (4Dt)^{-1}$ and $\nu = 0$. The result of this process is the Einstein relation (also known as Einstein-Smoluchowski relation) which states that mean-squared displacement varies linearly with time

$$\left\langle (\mathbf{r}_1 - \mathbf{r}_0)^2 \right\rangle = nDt \tag{1.15}$$

where $n = 2, 4, 6$ for one, two, or three dimensions, respectively.

1.1.1 Restricted diffusion

The diffusion of a particle in a fluid depends on diffusing medium features. The diffusion process could be influenced by the presence of obstacles. In fact, generally, diffusion could be:

- *isotropic*: when the diffusive medium has no favoured diffusion direction;
- *anisotropic*: in presence of barriers or obstacles with a certain structural organization, the diffusion of particles changes according to spatial directions.

The case of free diffusion, described in the previous paragraph, refers to medium without any foreign body that could interfere with the random walk. Instead, if these bodies (barriers or obstacles) are present in the fluid, they limit the diffusion of particles, so a regime of *restricted diffusion* emerges. The consequence of the presence of obstacles is a sensible reduction of the so-called bulk diffusion coefficient (which we have described in the case of a bulk fluid); it becomes *apparent diffusion coefficient* $D_{app}(t)$.
The problem can be modelled by the following approach [3]. Let us consider two situations in which a particle has the same diffusion coefficient. In one case the particle is diffusing freely in the (isotropic and homogeneous) fluid, in the other it's confined (so there's no

way out) in a sphere with its radius R.
Let us define the adimensional variable ξ from Eq 1.12:

$$\xi = \frac{D\Delta}{R^2} \tag{1.16}$$

where Δ is the time left to diffuse. Contrary to the bulk diffusion coefficient, the apparent diffusion coefficient has a dependence on time.

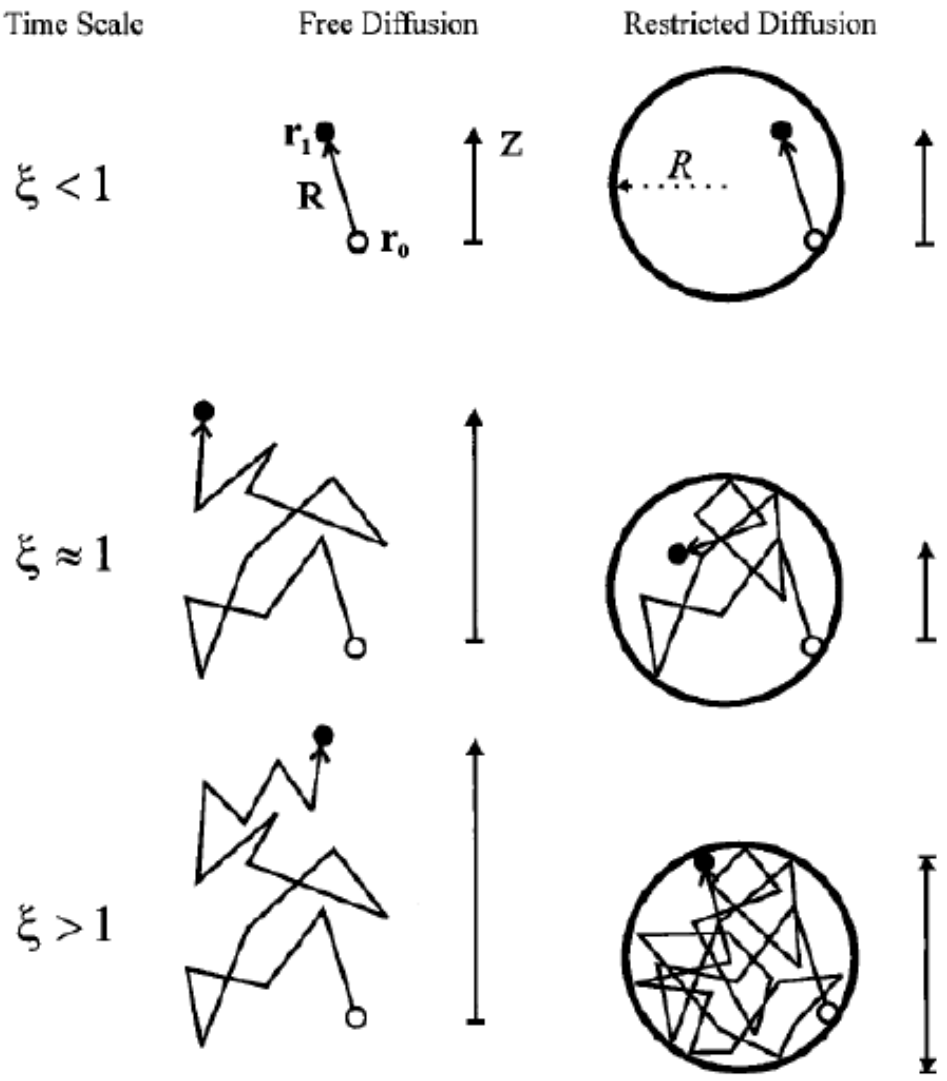

Figure 1.1: A scheme representing the particle paths in free diffusion (middle column) and in restricted diffusion (right column) for time scales increasing from the top to the bottom [3].

For really shorts Δ, the diffusing particle doesn't move enough to be influenced by the confinement (i.e $\xi << 1$); hence, the measured coefficient is equivalent to the bulk one. Increasing Δ (i.e. $\xi \approx 1$), there is a percentage of particles which are influenced by the presence of barriers; hence the mean squared displacement doesn't vary linearly with time anymore and the measured coefficient has a dependence on Δ.

For very long Δ (i.e. $\xi > 1$) the particles displacements are limited by the barriers, consequently, the measured coefficient reaches a minimum and it became independent on time again.
Therefore, for very short measurement times, the NMR signal attenuation is sensible to the "true" diffusion coefficient, while for long times it's sensible to the confinement shape and geometry.

1.2 Diffusion in porous media

As stated in the above subsection, it's possible to study the effects of restriction on diffusion, by measuring the apparent diffusion coefficient as a function of time. This kind of research is important to establish the features of solid porous media [12] as sedimentary rocks, and can be applied also to biological media, as cells.
Let us consider the case of biological cells.
In a confined geometry, the mean squared displacement is bounded at long time by the size of the confining cell L_S [13] (Fig 1.2).

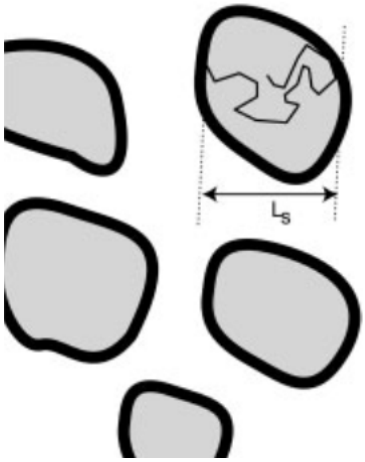

Figure 1.2: Isolated cell containing mobile molecules whose mean squared displacement in the long time limit becomes in the order of the cell size squared L_S^2 up to a numerical constant depending on the geometry [13].

1.2.1 Short-time limit

At short times, as stated in subsection (1.1.1), only a percentage of spins interact with the pore walls, implying a reduction of the diffusion coefficient. In these cases, $D_{app}(t)$ has information of surface-to-volume ratio S/V. The average of the molecules far away from the pore walls (so they behave like in bulk fluids) and the ones that have interact with the wall results in the mean square displacement [13]. Initially we consider the motion in

direction x. In Section 1.1 we have defined the propagator P as a Gaussian distribution for the free diffusion case. In presence of restriction, it results a non-Gaussian distribution (Fig 1.3):

$$P(x_0, x_1, t) = \begin{cases} (4\pi D_0 t)^{-1/2} e^{-\frac{(x_1-x_0)^2}{4D_0 t}}, & -\infty \leqslant x \leqslant \infty, \text{ bulk diffusion} \\ (4\pi D_0 t)^{-1/2} (e^{-\frac{(x_1-x_0)^2}{4D_0 t}} + e^{-\frac{(x_1+x_0)^2}{4D_0 t}}), & 0 \leqslant x \leqslant \infty, \text{ reflecting wall} \\ (4\pi D_0 t)^{-1/2} (e^{-\frac{(x_1-x_0)^2}{4D_0 t}} - e^{-\frac{(x_1+x_0)^2}{4D_0 t}}), & 0 \leqslant x \leqslant \infty, \text{ absorbing wall} \end{cases} \tag{1.17}$$

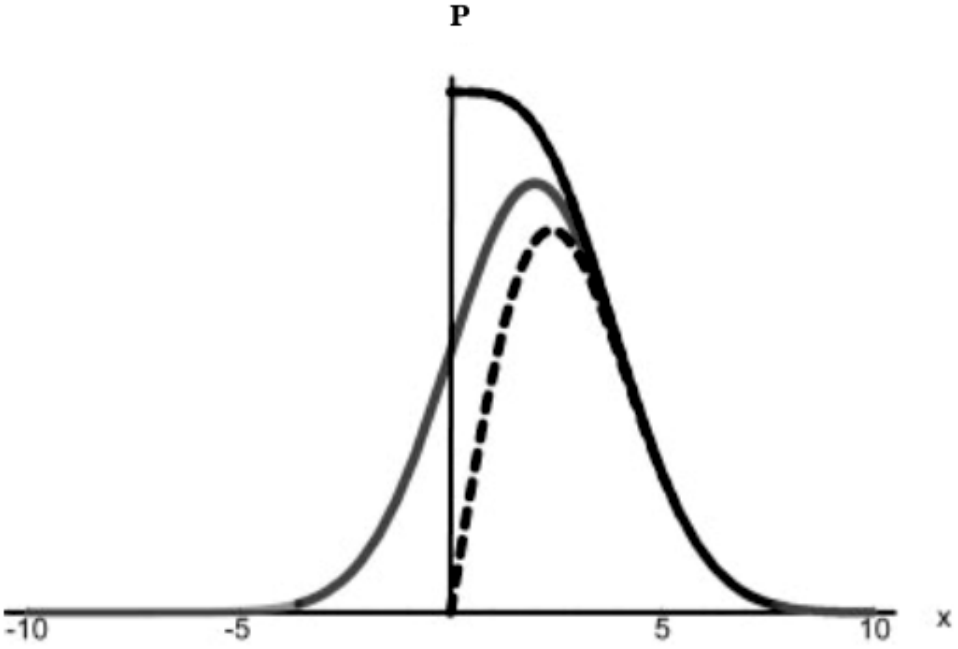

Figure 1.3: The probability density $P(x_0 = 2, x_1, t)$ for a particle in different conditions: reflecting wall condition (top curve) unrestricted condition (middle curve) and absorbing wall condition (bottom curve) [13].

The mean-square displacement for a single wall is given by

$$\left\langle (x_1 - x_0)^2 \right\rangle = \int_0^\infty \int_0^\infty dx_1 dx_0 (x_1 - x_0)^2 M(x_0, 0) P(x_0, x_1, t) \tag{1.18}$$

where $M(x_0, 0) = \frac{1}{L_S}$ is the initial density of walkers. Let us narrow the integration range to $0 \leq x \leq L_S$ In the limit $L_S \ggg L_D = \sqrt{2D_0 t}$ (where L_D stands for the diffusion length), we obtain:

$$D_{app}(t) = \frac{\left\langle (x_1 - x_0)^2 \right\rangle}{2t} = \begin{cases} D_0, & \text{unbounded} \\ D_0 \left[1 - \frac{4\sqrt{D_0 t}}{3\sqrt{\pi} L_S} \right], & \text{bounded} \end{cases} \tag{1.19}$$

Because of the early time, the wall looks flat, so the mean square displacements along y and z directions are unaffected by the confinement:

$$\left\langle (y(t) - y(0))^2 \right\rangle = \left\langle (z(t) - z(0))^2 \right\rangle \equiv 2D_0 t \tag{1.20}$$

Hence we have:

$$\begin{aligned} D(t) &= \frac{1}{6t}\left[\left\langle (x(t)-x(0))^2\right\rangle + \left\langle (y(t)-y(0))^2\right\rangle + \left\langle (z(t)-z(0))^2\right\rangle\right] \\ &= D_0\left(1-\frac{4}{9\sqrt{\pi}}\frac{S}{V}\sqrt{D_0 t}\right) + O(D_0 t) \end{aligned} \tag{1.21}$$

1.2.2 Long time limit

At long times, diffusing molecules probe the connectivity of the pore space, they will loose memory of their initial positions [13]. So, Eq. 1.15 is given by the volume integral over initial and final positions:

$$\frac{\int \left(\mathbf{r'}-\mathbf{r}\right)^2 d^3r d^3r'}{V^2} \propto L_S^2 \tag{1.22}$$

Where V is the pore volume and L_S is the pore size.
Thus:

$$D_{app}(t) \propto \frac{L_S^2}{6t} \underset{t\longrightarrow\infty}{\longrightarrow} 0 \tag{1.23}$$

In well connected porous medium, $D_{app}(t)$ approaches to a nonzero finite value, called *effective diffusion coefficient*:

$$\lim_{t\longrightarrow\infty} D_{app}(t) = D_{eff} \tag{1.24}$$

This reduction is due to a geometrical factor, known as the tortuosity α

$$\lim_{t\longrightarrow\infty} \frac{D_{app}(t)}{D_0} = \frac{D_{eff}}{D_0} = \frac{1}{\alpha} \tag{1.25}$$

This dimensionless factor is critical in various transport processes in porous media; it's related to the porosity of the medium ϕ through a geometrical factor F

$$\alpha = F\phi \tag{1.26}$$

Consequently:

$$D_{eff} = \frac{D_0}{F\phi} \tag{1.27}$$

For reflecting spheres, the diffusion coefficient approaches its final asymptote [14] as:

$$\frac{D_{app}(t)}{D_0} = \frac{1}{\alpha} + \frac{\beta}{D_0 t} - \frac{\gamma}{(D_0 t)^{3/2}} \tag{1.28}$$

For a general porous medium, β and γ are coefficients depending on the details of the pore geometry.

1.2.3 Padé approximant

In NMR experiments involving diffusion in porous media (i.e. Latour et al. [12]), a Padé approximant between the two limites descripted above is used:

$$\frac{D_{app}(t)}{D_0} = 1 - \left(1 - \frac{1}{\alpha}\right) \frac{\left(\frac{4}{9\sqrt{\pi}}\right)\left(\frac{S}{V}\right)\sqrt{D_0 t} + \left(1 - \frac{1}{\alpha}\right)\left(\frac{D_0 t}{D_0 \theta}\right)}{\left(1 - \frac{1}{\alpha}\right)\left(\frac{4}{9\sqrt{\pi}}\right)\left(\frac{S}{V}\right)\sqrt{D_0 t} + \left(1 - \frac{1}{\alpha}\right)\left(\frac{D_0 t}{D_0 \theta}\right)} \tag{1.29}$$

where θ is a fitting parameter which represents the typical time that the molecules need to diffuse a macroscopic distance l to reach the tortuosity limit [13].

$$\theta = \frac{l^2}{D_0} \tag{1.30}$$

This approximation let us to study the evolution of $D_{app}(t)$ taking into account the two limits described (Fig 1.4).

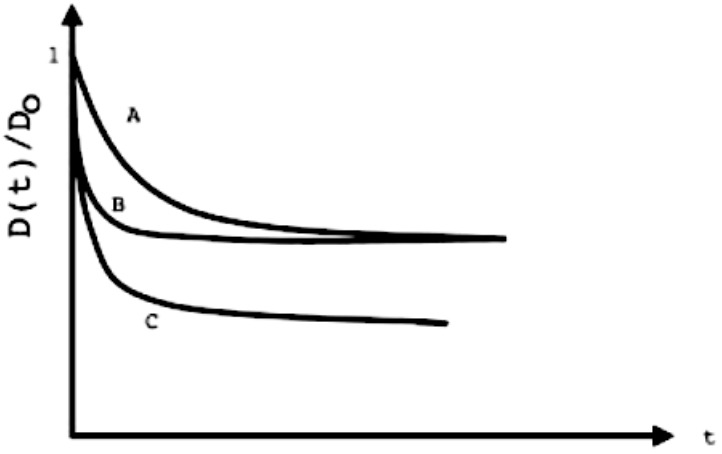

Figure 1.4: Three time-dependent diffusion coefficient related to three types of porous media. The initial slope corresponds to the short time limit and give us the surface-to-volume ratio; the long time plateau is determined by tortuosity [13].

For long times, 1.29 behaves as:

$$\lim_{t \longrightarrow \infty} \frac{D_{app}(t)}{D_0} = \frac{1}{\alpha} + \frac{\left(1 - \frac{1}{\alpha}\right)}{t} + O\left(\frac{1}{D_0 t}\right)^{3/2} = \frac{1}{\alpha} + \frac{L^2}{t} + O\left(\frac{1}{D_0 t}\right)^{3/2} \tag{1.31}$$

where $L^2 = Gl^2$ is an effective length squared and G is a geometric factor.
Instead, for short times, 1.29 behaves as:

$$\lim_{t \longrightarrow 0} \frac{D_{app}(t)}{D_0} = 1 - \frac{4}{9\sqrt{\pi}} \frac{S}{V} \sqrt{D_0 t} + O(D_0 t) \tag{1.32}$$

For example, Latour *et al.* [12] tested the equation on monosized sphere packs and on a biological sample (Fig 1.5), obtaining excellent agreement between surface-to-volume ratio established by NMR diffusion measurement and the values based on the known sphere diameters, and between the tortuosity and the values obtained by computer simulations.

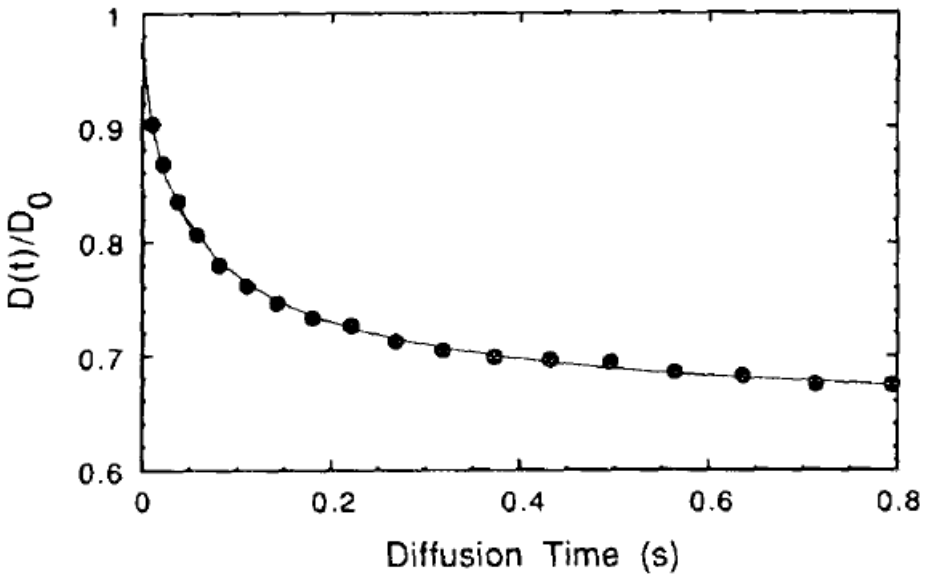

Figure 1.5: Diffusion coefficient as a function of diffusion time for distilled water in the pores of a monosized sphere pack: the filled dots are the experimental values and the line is the Padé approximant. For the long time limit, the diffusion ratio reaches the value of inverse tortuosity [12].

1.3 Diffusion and magnetic field gradient

NMR techniques, thanks to their noninvasive nature, represent an important device to study molecular dynamics in chemical and biological systems [3]. In this field, the spin echo attenuation forms the basis of translational diffusion studies. This phenomenon is caused by the dephasing of nuclear spins of nuclei set in a region of space wherein there is a magnetic field gradient. In order to understand the effects induced by a gradient in a magnetic field B_0, let us consider the Larmor equation

$$\omega_0 = \gamma B_0 \tag{1.33}$$

where ω_0 is the Larmor frequency (rad s^{-1}), γ is the gyromagnetic ratio (rad T^{-1} s^{-1}) and B_0 is the static magnetic field oriented in z direction.
B_0 is spatially homogeneous, thus ω has the same value in every part of the probe. Nevertheless that's not longer true in presence of a magnetic field gradient $\mathbf{g}$ (T m^{-1})

$$\omega_{eff} = \omega_0 + \gamma(\mathbf{g} \cdot \mathbf{r}) \tag{1.34}$$

where $\mathbf{g}$ is the gradient field component parallel to $\mathbf{B}_0$, i.e.,

$$\mathbf{g} = \nabla \mathbf{B}_0 = \frac{\partial \mathbf{B}_z}{\partial x}\mathbf{i} + \frac{\partial \mathbf{B}_z}{\partial y}\mathbf{j} + \frac{\partial \mathbf{B}_z}{\partial z}\mathbf{k} \tag{1.35}$$

where $\mathbf{i}$, $\mathbf{j}$, and $\mathbf{k}$ are unit vectors of the laboratory frame of reference.
Applying a gradient to the probe, the Larmor frequency becomes a spatial "label" with

respect to the direction of the gradient. Let us consider the case of a gradient oriented along z; **g** intensity is only a function of the time and is oriented along z-axis, $g_z = \mathbf{g} \cdot \mathbf{k}$, and we will call it simply g. From now, we describe the gradient effect on diffusion taking as an example the PFG (*Pulse Field Gradient*) sequence (Fig. 1.6).

From Eq. 1.34 the cumulative phase shift for a single spin is given by:

$$\phi(t) = \gamma B_0 t + \int_0^t g(t')z(t')dt' \tag{1.36}$$

where the first addend refers to the dephasing caused by static magnetic field B_0, while the second one corresponds to the contribution of the gradient. Then, we can see that the dephasing depends on the nature of the nucleus (i.e. γ), on the intensity of the gradient (i.e. g), on his duration (i.e. t) and on the nucleus displacement along the gradient direction.
In presence of a space and time constant gradient, we have:

$$\phi(\tau) = \gamma B_0 \tau + \gamma g \int_{t_1}^{t_1+\delta} z_i(t)dt \tag{1.37}$$

After a time τ (which is an half of the echo time t_E), the π rf pulse reverses the sign of the precession, thus, the second pulse applied at time $t_1 + \Delta$, with the same intensity g and the same duration δ, will cancel the effect of the first pulse, if the spins haven't diffuse during Δ. At the contrary, if the spins have diffused, the i-th spin cumulated phase, towards the one it should have if it hadn't moved from its position $z = 0$, at echo time will be:

$$\begin{aligned}\phi_i(2\tau) &= \left\{\gamma B_0 \tau + \gamma g \int_{t_1}^{t_1+\delta} z_i(t)dt\right\} \\ &- \left\{\gamma B_0 \tau + \gamma g \int_{t_1+\Delta}^{t_1+\Delta+\delta} z_i(t')dt'\right\} \\ &= \gamma g \left\{\int_{t_1}^{t_1+\delta} z_i(t)dt - \int_{t_1+\Delta}^{t_1+\Delta+\delta} z_i(t')dt'\right\}\end{aligned} \tag{1.38}$$

For a nucleus ensemble with different initial and final positions, the echo signal, towards the one should obtained in absence of a field gradient, is:

$$S(2\tau) = S(2\tau)_{g=0} \int_{-\infty}^{\infty} P(\phi, 2\tau)e^{i\phi}d\phi \tag{1.39}$$

Where $P(\phi, 2\tau)$ is the probability that the single spin has cumulated a ϕ phase, so, for definition:

$$\int_{-\infty}^{\infty} P(\phi, 2\tau)e^{i\phi}d\phi = 1 \tag{1.40}$$

Considering only the real component, reminding that:

$$e^{i\phi} = \cos\phi + i\sin\phi \tag{1.41}$$

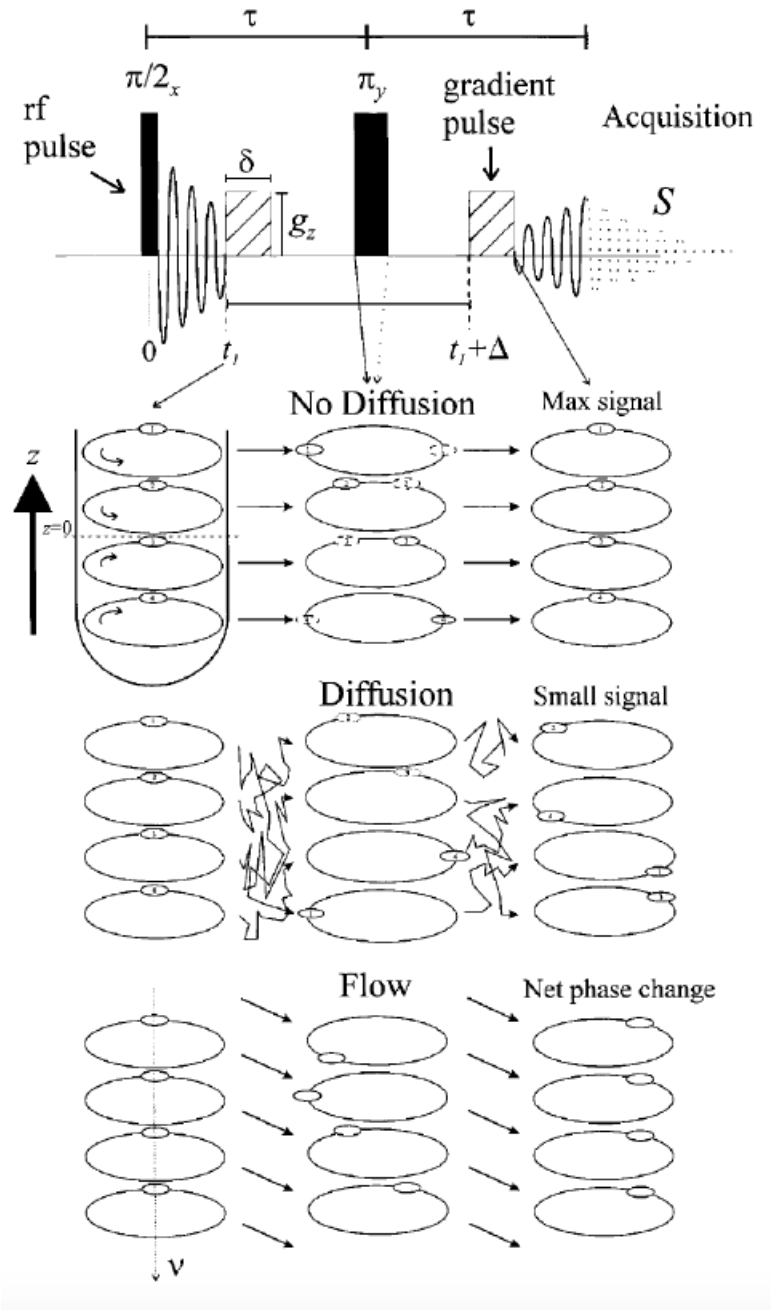

Figure 1.6: A schematic rappresentation of how a PFG sequence measures diffusion and flow. In the first line is presented a Hahn spin-echo pulse sequence with a rectangular gradient applied on z direction. In the second and in the third line the spin phase evolution respectively in absence and in presence of diffusion is shown. The last line illustrates the effect of flow along the direction of the gradient on the spins in absence of diffusion [3].

we have:

$$S(2\tau) = S(2\tau)_{g=0} \int_{-\infty}^{\infty} P(\phi, 2\tau) \cos\phi d\phi \tag{1.42}$$

Therefore, if there's not diffusion (or a field gradient), $\phi_i = 0$ for each i, so $\cos\phi_i = 1$, thus the maximum signal value will be acquired. If instead there is diffusion, $z_i(t)$ depends on time and the cumulated phase shift of a spin in the first period will not be canceled by the one of the second period. This means that the degree of miscancellation increases with the displacement for diffusion along the field gradient axis. These phase shifts are averaged on the nuclei ensemble and the observed NMR signal is not phase shifted but attenuated; the greater the diffusion, the larger the attenuation of the echo signal.
In absence of a field gradient we should have:

$$S(2\tau)_{g=0} = S(0)\exp\left(-\frac{2\tau}{T_2}\right) \tag{1.43}$$

where $S(0)$ is the signal at zero time, before any relaxation. Instead, in presence of a field gradient, due to the independence between the relaxation and the attenuation due to the field gradient we have:

$$S(2\tau) = S(0)\underbrace{\exp\left(-\frac{2\tau}{T_2}\right)}_{\substack{\text{attenuation due}\\ \text{to relaxation}}}\underbrace{f(\delta, g, \Delta, D)}_{\substack{\text{attenuation due}\\ \text{to diffusion}}} \tag{1.44}$$

Keeping τ fixed, it's possible to separate the field gradient contribution:

$$E = \frac{S(2\tau)}{S(2\tau)_{g=0}} = f(\delta, g, \Delta, D) \tag{1.45}$$

Therefore, we can obtain D through measures with different values of g, or of δ, or Δ
In a Spin Echo sequence, in the case of g constant, it can be demonstrated ([15]) that:

$$S(2\tau) = S(0)\underbrace{\exp\left(-\frac{2\tau}{T_2}\right)}_{\substack{\text{attenuation due}\\ \text{to relaxation}}}\underbrace{\exp\left(-\frac{2\gamma^2 D g^2 \tau^3}{3}\right)}_{\substack{\text{attenuation due}\\ \text{to diffusion}}} \tag{1.46}$$

This leads to the possibility of realizing a constant gradient experiment, however, in this case, only g could be varied independently of τ. Nonetheless the relaxation effect could be erased through a normalization. In this case, the experiment time scale is limited by T_2. By increasing the time scale, i.e. τ, would lead to a signal too small for being measured. In the case of PFG, Δ is set within range [1 ms, 1 s] and δ is set within a range [0 ms, 10 ms]. The g values usually employed are on the order of 20 T/m.

1.3.1 Gaussian Phase Distribution approximation

In order to illustrate the dependence of E on δ,g,Δ and D, we use a mathematical approach called *Gaussian Phase Distribution approximation* (GPD) [3].
Assuming that the gradient pulses have a rectangular shape, we consider the case of

one-dimensional diffusion along z direction, the gradient axis. Remembering Eq. 1.11, z is described by a gaussian distribution

$$P(0,z,t) = \frac{1}{\sqrt{4\pi Dt}} \exp\left(-\frac{z^2}{4Dt}\right) \tag{1.47}$$

Thus, also $P(\phi, 2\tau)$ is a gaussian distribution:

$$P(\phi,2\tau) = \frac{1}{\sqrt{2\pi \left\langle \phi^2 \right\rangle}} \exp\left(-\frac{\phi^2}{2\left\langle \phi^2 \right\rangle}\right) \tag{1.48}$$

where $\langle \phi^2 \rangle$ is the mean-squared phase change at $t = 2\tau$.
It's given by:

$$\begin{aligned}
\left\langle \phi^2 \right\rangle &= \gamma^2 g^2 \left\langle \left\{ \int_{t_1}^{t_1+\delta} z_i(t)dt + \int_{t_1+\Delta}^{t_1+\Delta+\delta} z_i(t)dt \right\}^2 \right\rangle_{av} \\
&= \gamma^2 g^2 \left\{ \int_{t_1}^{t_1+\delta} \left[\int_{t_1}^{t_a} 2Dt_b dt_b + \int_{t_a}^{t_1+\delta} 2Dt_a dt_b \right] dt_a \right. \\
&- 2\int_{t_1}^{t_1+\delta} \int_{t_1+\delta}^{t_1+\Delta+\delta} 2Dt_a dt_b dt_a \\
&\left. + \int_{t_1+\Delta}^{t_1+\Delta+\delta} \left[\int_{t_1+\Delta}^{t_a} 2Dt_b dt_b + \int_{t_a}^{t_1+\Delta+\delta} 2Dt_a dt_b \right] \right\} \\
&= \gamma^2 g^2 2D\delta^2 \left(\Delta - \frac{\delta}{3}\right)
\end{aligned} \tag{1.49}$$

Putting 1.48 in 1.42 we have:

$$\begin{aligned}
S(2\tau) &= S(2\tau)_{g=0} \int_{-\infty}^{\infty} \frac{1}{\sqrt{2\pi \left\langle \phi^2 \right\rangle}} \exp\left(-\frac{\phi^2}{2\left\langle \phi^2 \right\rangle}\right) \cos\phi d\phi \\
&= S(2\tau)_{g=0} \exp\left(-\frac{\left\langle \phi^2 \right\rangle}{2}\right)
\end{aligned} \tag{1.50}$$

Hence we obtain the diffusion contribution in the signal attenuation

$$E(2\tau) = \frac{S(2\tau)}{S(2\tau)_{g=0}} = \exp\left(-\frac{\left\langle \phi^2 \right\rangle}{2}\right) = \exp\left(-\gamma^2 g^2 D\delta^2 \left(\Delta - \frac{\delta}{3}\right)\right) \tag{1.51}$$

whose logarithm gives the Stejskal-Tanner equation:

$$\ln(E) = -\gamma^2 g^2 D\delta^2 \left(\Delta - \frac{\delta}{3}\right) = -bD \tag{1.52}$$

This means that the dependency on D could be linearized after had acquired measures for different values of one of the variables.
A plot of $\ln(E)$ as a function of $\gamma^2 g^2 \delta^2 \left(\Delta - \frac{\delta}{3}\right)$ (which represents the so-called *b-value*) will provide the D value by a linear fit (Fig 1.7).

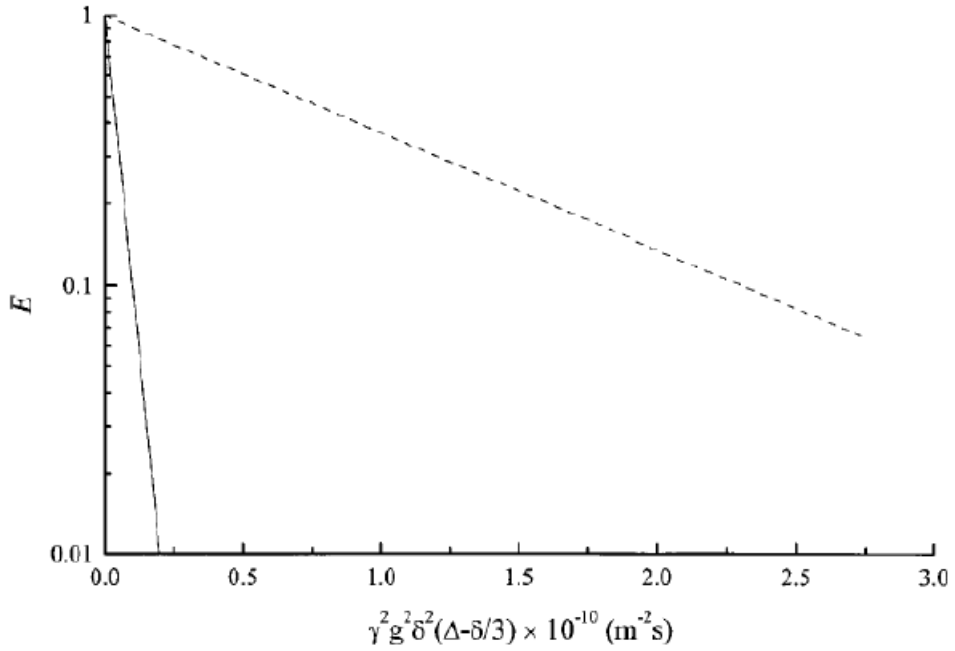

Figure 1.7: Signal attenuation due to diffusion as a function of b-value. Solid line stands for water, stippled line stands for protein [3].

Chapter 2

Profile NMR-MOUSE PM 10

In topics as diagnostic medical imaging or analytical chemical spetroscopy, NMR analysis consists in testing the sample with radio-waves inside stationary magnets. To ensure a good signal strenght and a good spetroscopic resolution, generally these magnets have high and homogeneous magnetic fields B_0. Their reduction were considered unacceptable, until in the oil industry was demonstrated that robust and mobile sensors can be built from permanent magnets that can be lowered into the bore hole of an oilwell for relaxation time analysis of the fluids in the surrounding porous rock formation.
This event has led to the principle of *inside-out NMR*, where the magnet is set inside the object (the earth), at the contrary of the ordinary NMR (or *outside-in NMR*) where the sample is set inside the magnet. Inside-out NMR is a form of single-sided or unilateral NMR, where an NMR sensor much smaller than the object is placed near the object to acquire signals from the object volume near the sensor. In 1995 the NMR-MOUSE (*MObile Universal Surface Explorer*) was built at RWTH-Aachen and now commercialized by Magritek: it consists in a small single-sided NMR sensor weighting of the order of 1 kg which generates a polarizing magnetic field up to 0.5 T with an adjustable gradient. It has been used and explored in such diverse fields as the non-destructive testing of rubber and polymer products, food and livestock analysis, as well as the state assessment of objects of cultural heritage. This in turn stimulates the development and understanding of NMR in highly inhomogeneous field [10].

2.1 Features

The NMR-MOUSE has a magnet in the shape of a horseshoe, obtained by opening up a conventional c-shaped magnet with a homogeneous field between its poles: it generates the polarizing magnetic field B_0 oriented parallel to the sensor surface. It has approximately quadratic profiles along x and z with a main gradient along the depth direction y; this feature can be applied to resolve depth profiles into the object simply varying the excitation frequency. In the gap between the two poles, a rf-coil is setted: it

produces the B_1 field perpendicular to B_0. In this arrangement, the sample is set above the gap in the stray fields of the magnet and the rf coil. Only a small portion of the sample can be reached in a single experiment, this is the so-called *sensitive volume*, a flat sensitive slice with a curvature of only a few μm over a region of about one cm^2 which depends on the magnet, rf-coil geometry and the pulse sequence applied (Fig 2.1 (a)). This flat region is obtained by minimizing the curvature with the arrangement of two simple horseshoe magnets in parallel leaving a small gap along the x-direction (Fig 2.1 (b)). This setup is known as the Profile NMR-MOUSE [16].

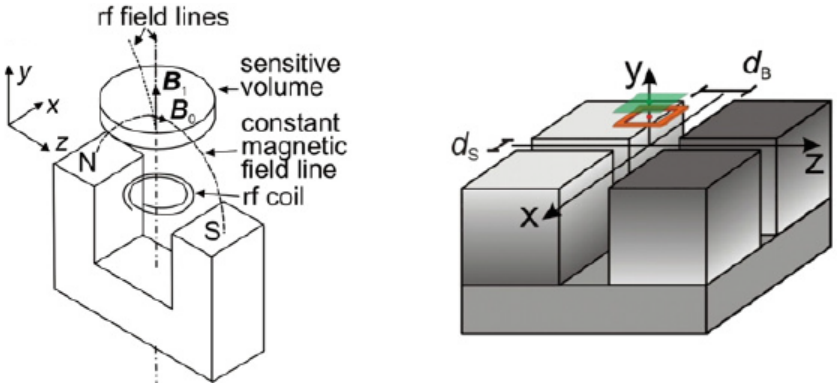

(a) (b)

Figure 2.1: (a) A scheme of a single sided sensor [10] (b) magnet arrangement for the Profile NMR-MOUSE which provides a constant B_0 in the xz-plane at one particular depth y [17].

The model we have used in our experiment is the Profile PM10 whose features are reported below:

- $B_0 = 0.327$ T
- $\nu = 13.9$ MHz for ^{1}H nuclei
- $\Delta\nu/\Delta y = 600$ kHz/mm
- Max Depth = 10 mm

Due to the dishomogeneity along y direction, B intensity varies on it:

$$g = \frac{\Delta B}{\Delta y} = \frac{2\pi}{\gamma}\frac{\Delta\nu}{\Delta y} \tag{2.1}$$

If we consider this equation for hydrogen molecules, $\frac{\gamma}{2\pi} = 42.58\ \frac{MHz}{T}$, we have $g = 14\ \frac{T}{m}$. The application of a rf pulse, causes the rotation of the net magnetization of an angle called *flip angle*:

$$\alpha = \gamma B_1(y)\Delta t(y) \tag{2.2}$$

where $\Delta t(y)$ is the Pulse Width (PW).

The distance of the sensitive volume from the magnet surface is fixed, but his distance from the rf-coil may be reduced by inserting spacers (each 2 mm thick) underneath it (Fig. 2.2 and Fig. 2.3). The more spacers you use, the better will be the sensitivity, hence the shorter will be the PW. The closer the rf-coil is to the sensitive volume the better will be the efficiency of the rf-pulses and the signal detection.

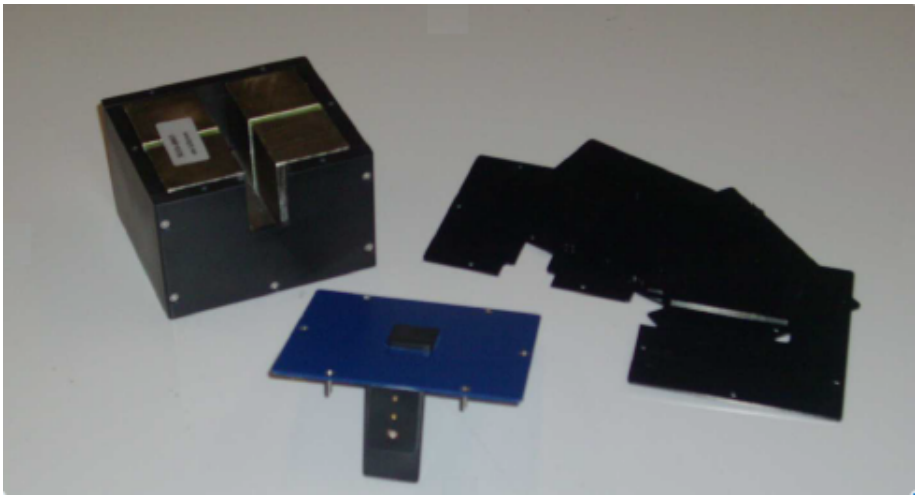

Figure 2.2: Profile NMR-MOUSE PM 10: the permanent magnet on the left, the rf-coil in the middle, and the spacers on the right.

Furthermore, it's possible to make a profile of the sample shifting the sensitive through it by displacing the sensor in depth direction; to realize it, the Profile MOUSE is mounted on a precision lift automatically controlled by a step motor. The maximum slice thickness Δy which can be excited by the sensor is defined by the excitation bandwidth and the gradient strength. Structures within Δy are resolved by Fourier transforming the echo. Larger depth ranges are scanned by moving the sensitive volume across the sample depth. This is achieved by changing the distance between the sensor and the sample surface in increments of Δy and combining the partial Δy profiles into one profile.

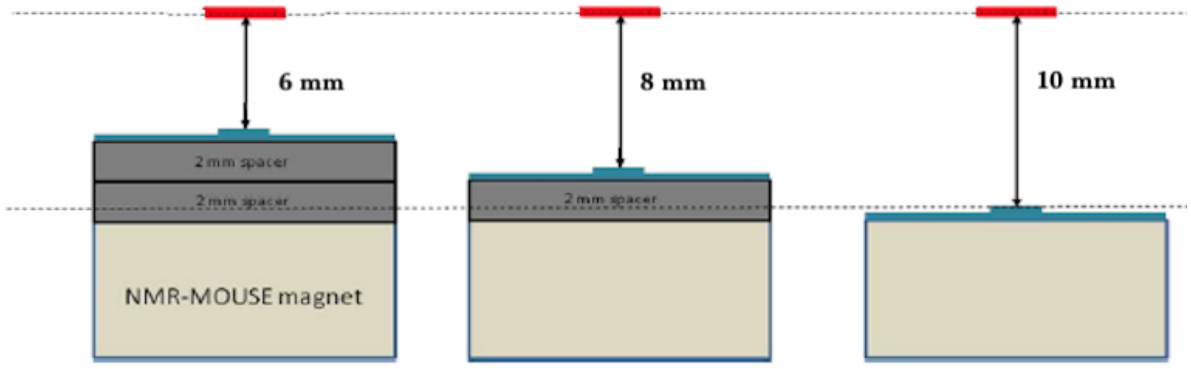

Figure 2.3: Profile NMR-MOUSE PM10 with different spacer configurations [16].

2.2 Kea-2 spectrometer

The Profile is connected to the Kea-2 NMR digital spectrometer from Magritek (Fig. 2.4). It consists of several modules (Fig. 2.5), all powered by a 24 V DC input. The range of pre-amplifier and duplexer module is between 12 MHz and 30 MHz. The Kea spectrometer connects to a PC via a USB interface through the software package Prospa, described in the following subsection.

Figure 2.4: Kea-2 spectrometer

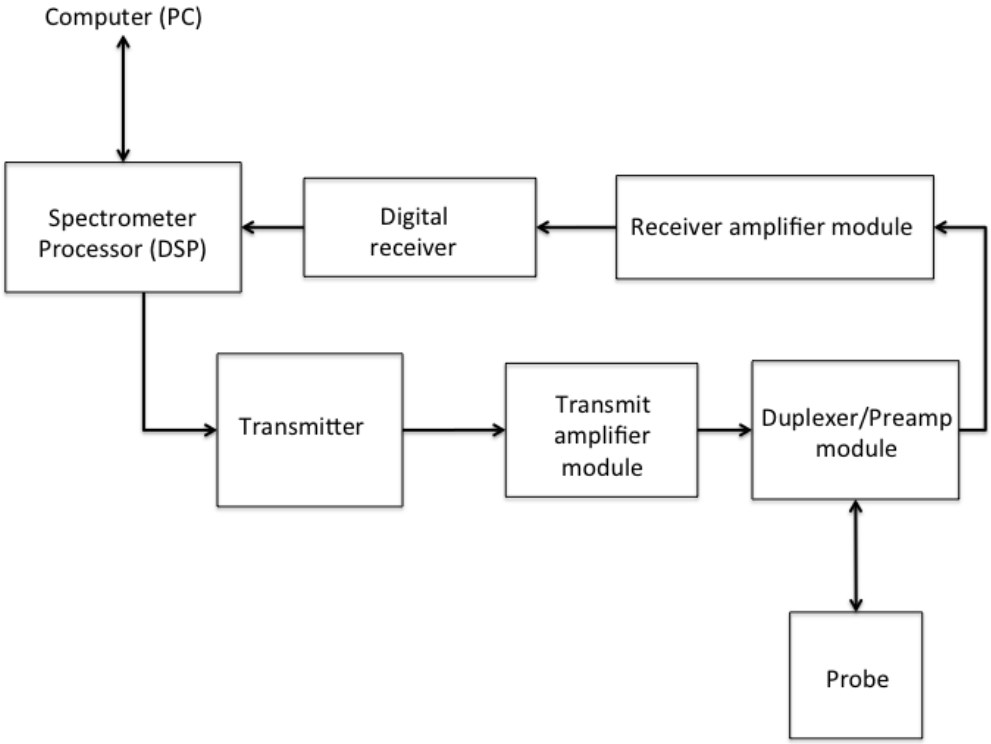

Figure 2.5: A block scheme of Kea-2 spectrometer

2.3 Prospa software

Prospa is a software package designed specifically for processing NMR experiments. With additional hardware (Kea 2 spectrometer in our experience) it can also be used to control an NMR experiment and collect the data. Prospa is based around a core of 400 or so commands which can be used to load, save, modify and view numerical data in matrix form. These commands can be combined together to form sophisticated script files called *macros* which can perform a wide variety of processing and interface functions.
The default Prospa configuration consists of 6 main windows. The main Prospa window acts as a container for the other 5 windows and provides a main menu. The main menu contains options for loading, saving, importing and exporting data files, and running macro files. The other 5 windows consist of:

- A command line interface (CLI), into which typed, single-line commands can be entered. This also provides an output interface for diagnostic message from other parts of the program.

- An editor into which macros can be entered, loaded, modified and saved. The editor provides syntax highlighting and command help to simplify the writing of macros.

- A 1D plot into which x-y type data can be displayed. It provides facilities to display real and complex data, error bars and multiple traces. Like the editor the 1D plot can be subdivided to display multiple data sets and additional plots may be opened.

- A 2D plot into which images can be displayed. They may be in the form of intensity or contour plots. Rows and columns from the current 2D data set can be easily displayed in the 1D plot.

- The 3D plot window can display a variety of plot types - for example a surface rendering of the data in the current 2D plot, an iso-surface rendering of a 3D data set and 3D lines and surfaces. Interactively selected planes from the 3D plot may also be viewed in the 2D plot.

All 5 subwindows provide their own menus and shortcuts. Although Prospa is supplied with the above interface as the default, all aspects of the Prospa interface are user definable.
An important feature of this software consists in the possibility for the user to see the real-time input signal, as shown in the following subsection.

2.4 NMR pulse sequences

The sequences used with the profile are a combination of an encoding period followed by a detection period, composed by an echo-train (Fig 2.6). This approach can lead to

an improving of the detection sensitivity by co-adding the echo composing the detection train (Fig. 2.7).

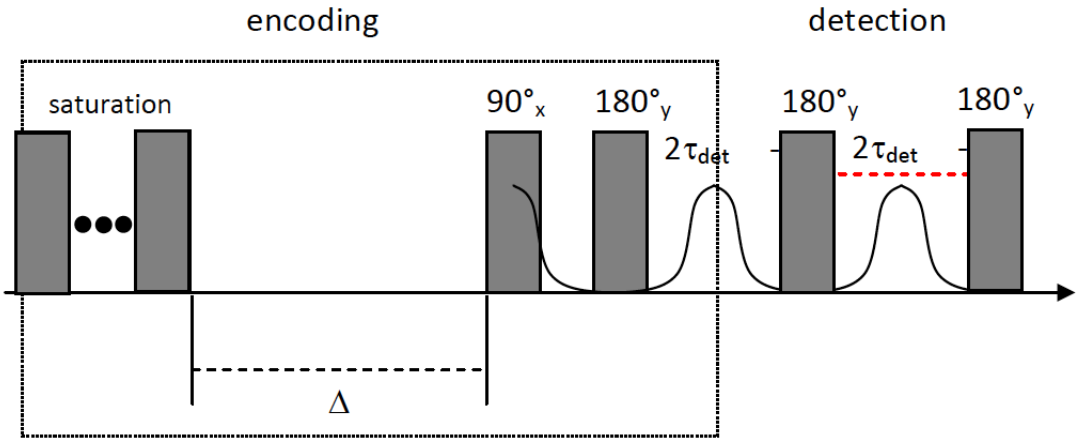

Figure 2.6: Saturation recovering + Hahn Echo sequence (encoding period) followed by CPMG detection train (detection period). By varying Δ the recovering of the M_z magnetization is sampled. The exploration to zero time of all echoes generated during the train is proportional to longitudinal magnetization [16].

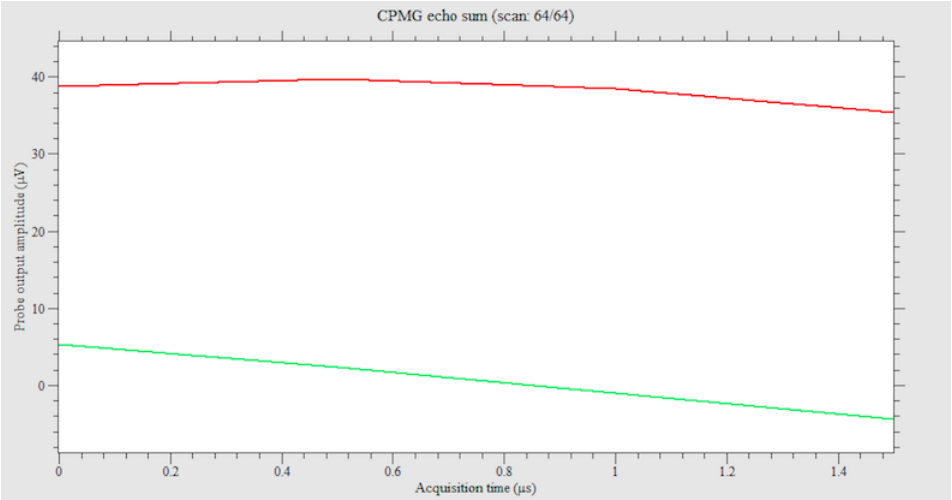

Figure 2.7: CPMG echo scan. The red line corresponds to the real component, the green line stands for the immaginary one: this has to be equal to zero, in order to consider only the real echo.

The main purpose of these sequences is to obtain the distribution of the following values:

- **Tranverse relaxation time T_2**: it states the decay constant for the component of the nuclear spin magnetization perpendicular to B_0. It corresponds to the process of decoherence of the tranverse nuclear spin magnetization.

- **Longitudinal relaxation time T_1**: it states the decay constant for the recovery of the component of the nuclear spin magnetization parallel to B_0 towards its thermal equilibrium value.

- **Apparent diffusion coefficient D**: it's largely described in chapter 1.

Before we describe the sequences used in this work, we illustrate the parameters for the detection period in the Pulse Sequence Tab of Prospa (Fig 2.8):

- **B_1 Frequency (MHz):** RF frequency.
- **Repetition time (ms):** Time between consecutive shots. For full recovery of magnetization the repetition time should be $5 * T_1$.
- **90 amplitude (dB):** RF output level for the 90°pulse. For 0 dB the full power is obtained (change of 6 dB means a change of 2 in the output).
- **180 amplitude (dB):** RF output level for the 180°pulse.
- **Pulse Length (μs):** Duration of all the RF pulses in the sequence.
- **Echo time (μs):** Time between consecutives echoes.
- **Number of echoes:** Number of 180°pulses/echoes in the detection sequence.
- **Echo shift (μs):** parameter to center the choes in the acquisition window

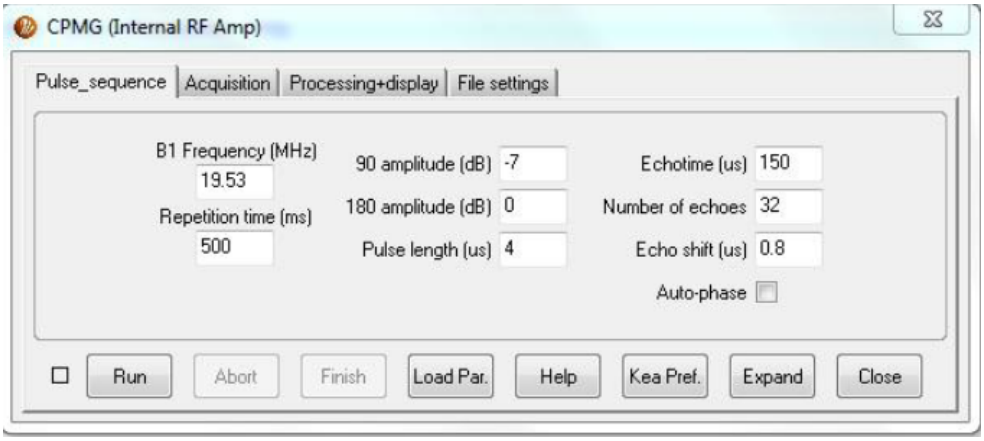

Figure 2.8: Pulse Sequence tab for CPMG [16].

In the Acquisition tab of Prospa (Fig. 2.9), the following parameters need to be adjusted:

- **Rx Gain (dB):** Receiver gain. It is recommended to keep it in 31 dB when working with NMR-MOUSE.
- **Rx phase (°):** Receiver phase. It must be set to put the signal in the real channel.
- **Number of complex points:** Number of points acquired per echo.
- **Dwell time (μs):** Delay between acquired points.

- **Number of scans:** Number of scans to be averaged in order to improve the SNR.

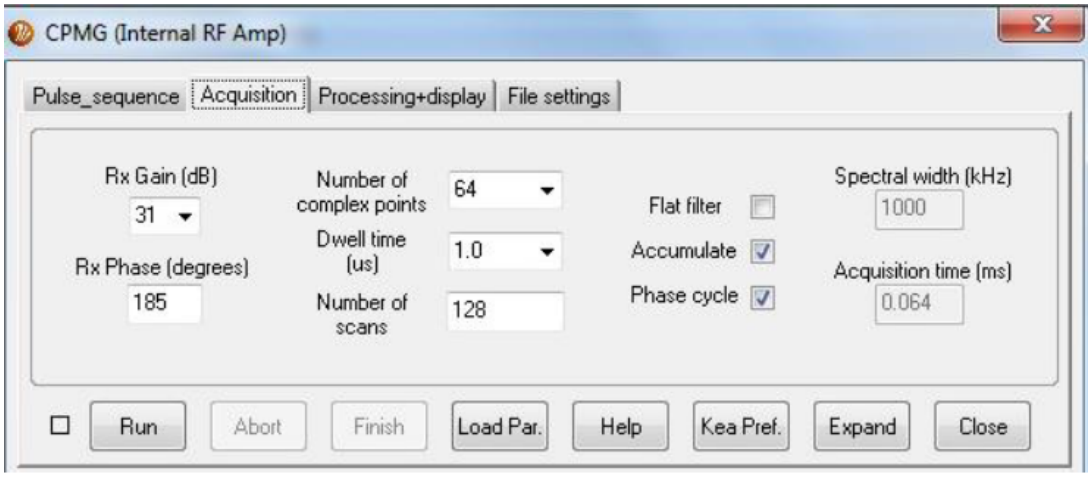

Figure 2.9: Acquisition tab for CPMG [16].

2.4.1 MonitorNoise

Before using the Profile, external noise level (induced by the coil, which is unshielded due to the characteristic of the NMR-Mouse) needs to be checked [16]. This task is performed by the sequence MonitorNoise: this application simply opens the receiver and acquires noise during a defined time. After each measurement, three windows are shown in Prospa: the values of the ratio between the RMS noise and the RMS of a 50Ω impedence (Fig. 2.10 left side), the corresponding frequency spectrum (Fig. 2.10 right side), and the acquired noise (Fig. 2.11).
During this experiment, we have worked with an average RMS noise ratio in the range 0.85-0.95.

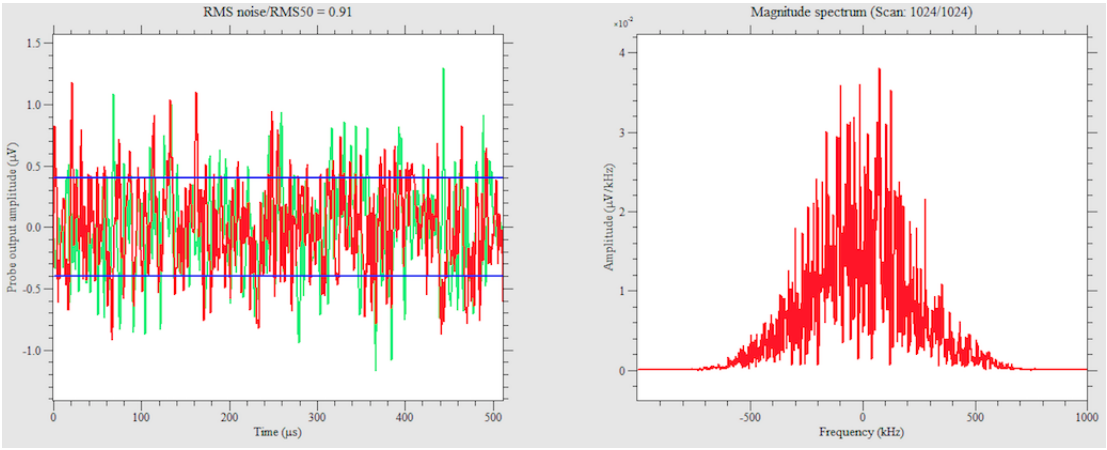

Figure 2.10: RMS noise - RMS 50Ω ratio (left), corresponding frequency spectrum (right).

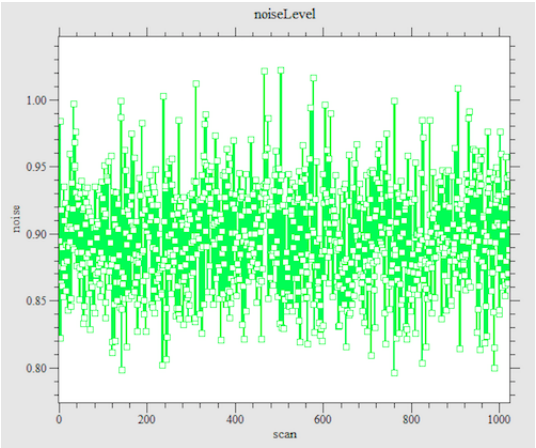

Figure 2.11: Acquired RMS noise.

2.4.2 CPMG

The CPMG sequence (Carr-Purcell-Meiboom-Gill) consists of a 90°pulse followed by a train of 180°, which generates a train of spin echoes, in order to refocus B_0 inhomogeneities [16] (Fig. 2.12).

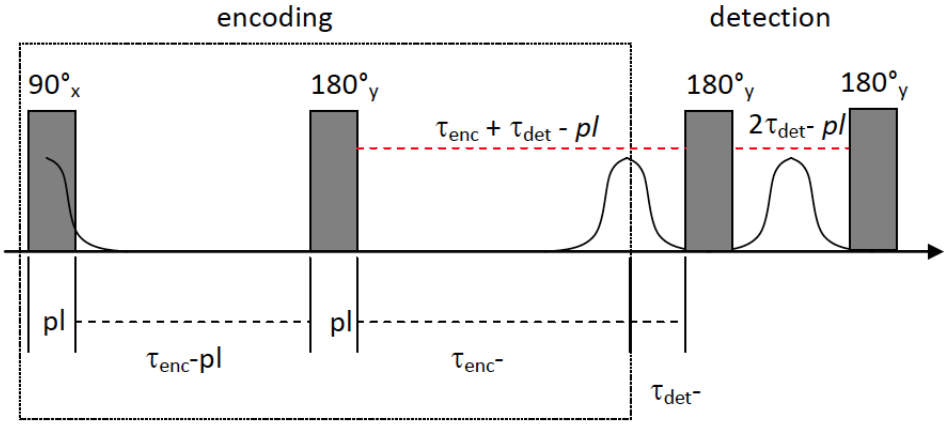

Figure 2.12: CPMG sequence [16].

In absence of the 180°pulses train, the T_2 extracted would be too low (T_2^*) as compared with the real one inherent of the system

$$\frac{1}{T_2^*} = \frac{1}{T_2} + \frac{1}{T_{inhom.}} = \frac{1}{T_2} + \gamma \Delta B_0 \tag{2.3}$$

The envelope of the decay can be used to obtain the spin density as well the T_2, the sensitivity increases with the echoes co-adding. While the spin density can simply be related to the initial amplitude of the decay, the effective transverse relaxation time T_{2eff} can be extracted from the signal decay (Fig. 2.13).

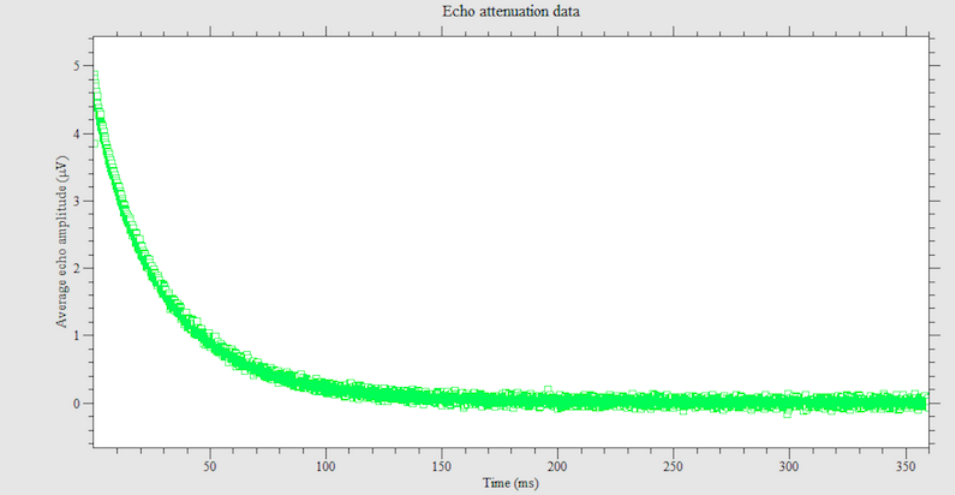

Figure 2.13: Signal attenuation during a CPMG sequence.

The total sampling time is given by the product of the echo time and the number of echoes. In principle, the best sensitivity is achieved when the minimum possible echo time is used and the number of echoes is adjusted to the length of the decay. When just the addition of the echoes is needed, as a measure for the spin density, the decays should be sampled until the signal amplitude decayed to one third of its initial value.

2.4.3 T_1 Saturation Recovery

The enconding part of this sequence (Fig. 2.14) is composed by a saturation period, in which a certain number of 90°pulses (more than one because of the B_1 inhomogeneity) are applied to cancel the longitudinal component of magnetization, followed by a recovery period, during which the magnetization is built up again with the characteristic time T_1 [16] (Fig. 2.15). Then, it follows the detection period, consisting in a CPMG train where the echoes are co-added to increase the sensitivity.

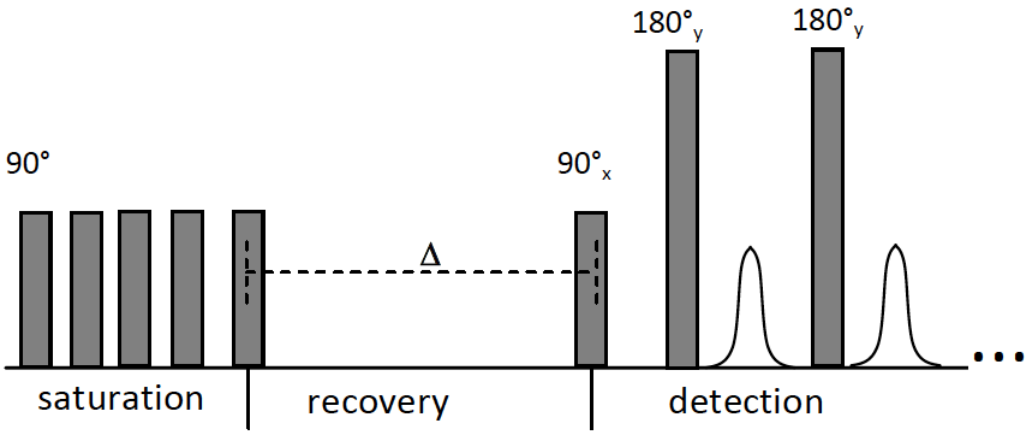

Figure 2.14: T_1 Saturation Recovery sequence [16].

A T_1-Sat experiment is composed by this sequence repeated for a certain number of increasing recovery times.

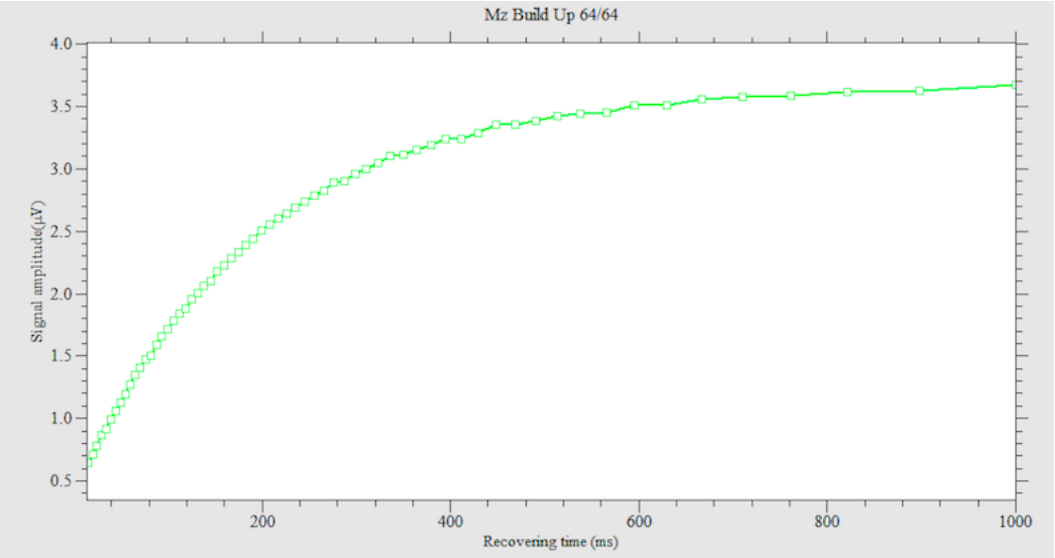

Figure 2.15: Longitudinal magnetization built up after a T_1 Saturation Recovery.

The following parameters, besides those already described, need to be adjusted (Fig. 2.16):

- **T_1 estimation (ms)**: in order to have a good fit, it's adviced to execute a first experiment with only a few point: the result would be put here.
- **Maximum recovery time**.
- **N°of T_1 points**: is the number of recovery times used in the experiment in order to build the T_1 curve.
- **Time increment**: it establishes the scale for the recovery time increment. It could be linear (*lin*) or exponential (*exp*).

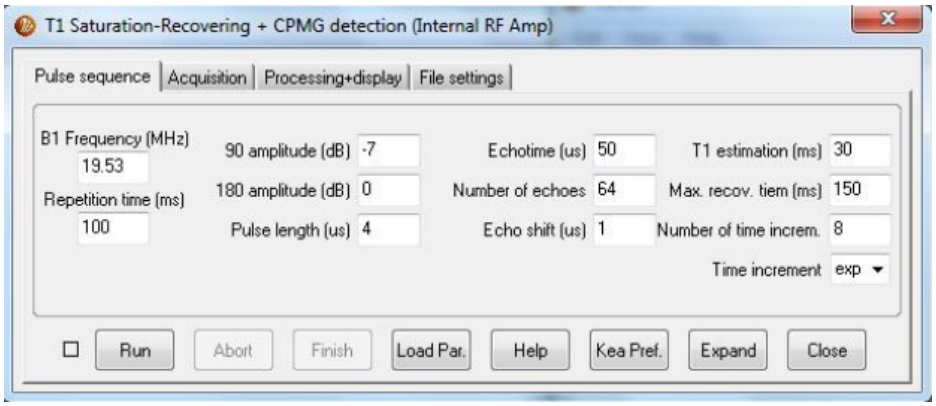

Figure 2.16: Pulse sequence tab for T_1 Saturation Recovery [16].

2.4.4 Saturation Recovery-CPMG

Respect to the T_1 Saturation Recovery sequence, here the data of CPMG decays are stored. At the final T_1 and T_2 data are available to calculate 2D relaxation spectra [16].

2.4.5 Stimulated Spin Echo

This sequence (called also SSE) is used to measure the self-diffusion coefficients of fluids [16]. After a first 90°pulse, the initial positions of the spins are enconded during the *encoding time* δ. It follows another one 90°pulse which brings the magnetization in y-direction for a time Δ; in this situations, the spin are free to diffuse, without any influence by the T_1. This is explained by the fact that $T_1 > T_2$, so we can use larger diffusion times if the magnetization is stored in z-direction, and the attenuation of the signal in this period is caused only by diffusion. After that, a third 90°pulse brings again the magnetization on the x,z plane and the final positions of the spins are encoded. Finally a train of 180°pulses occurs for the decoding (Fig. 2.17).

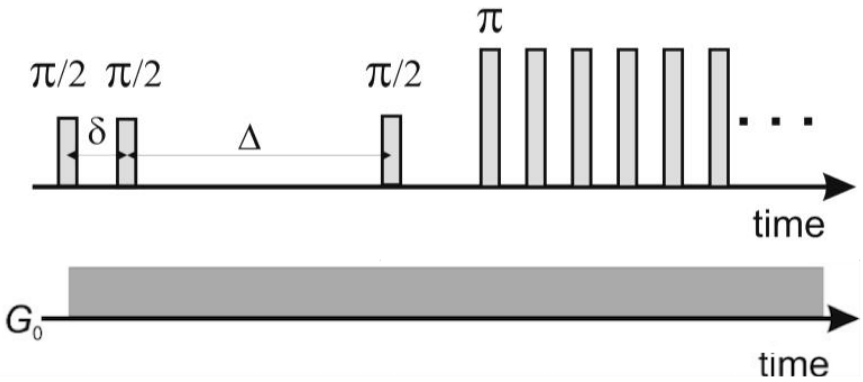

Figure 2.17: Stimulated Spin Echo sequence [16].

Varying δ for a fixed Δ, we can measure the apparent diffusion coefficient $D(\Delta)$, and the repetition of the experiment for different Δ values lets us to probe length scales of restrictions.
The signal attenuation due to diffusion is described by:

$$\ln\left(\frac{I(\delta)}{I_0}\right) = -\gamma^2 g^2 D\delta^2\left(\Delta + \frac{2\delta}{3}\right) \tag{2.4}$$

where I_0 is the initial signal intensity.
In addition to the standard parameters listed previously, in the Acquisition Tab (Fig. 2.18) there are the following ones:

- **Gradient (kHz/mm)**
- **D (μm^2/ms)**: Here the expected self-diffusion coefficient should be setted.

This parameter will be taken into account only if the Time increment parameter is setted as exponential.

- **tau min (ms):** is the minimum value given to δ.
- **tau max (ms):** is the maximum value given to δ. Best accuracy is obtained, when the achieved signal amplitude for *tau max* is about 1/3 of the initial signal amplitude.
- **Delta (ms):** is the value given to Δ.
- **Number of tau increments:** is the number of δ used in the experiment.
- **Time increment:** as for the T_1 Saturation Recovery, it establishes the scale for the recovery time increment. It could be linear (*lin*) or exponential (*exp*).

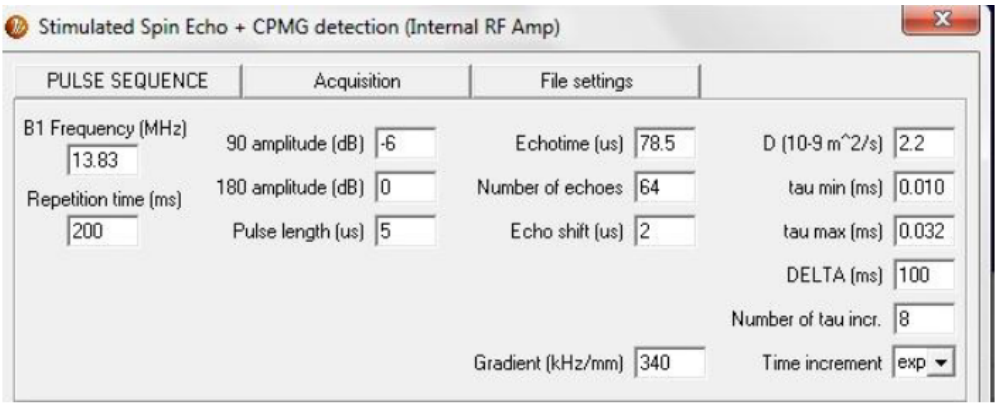

Figure 2.18: Pulse sequence tab for the Stimulated Spin Echo [16].

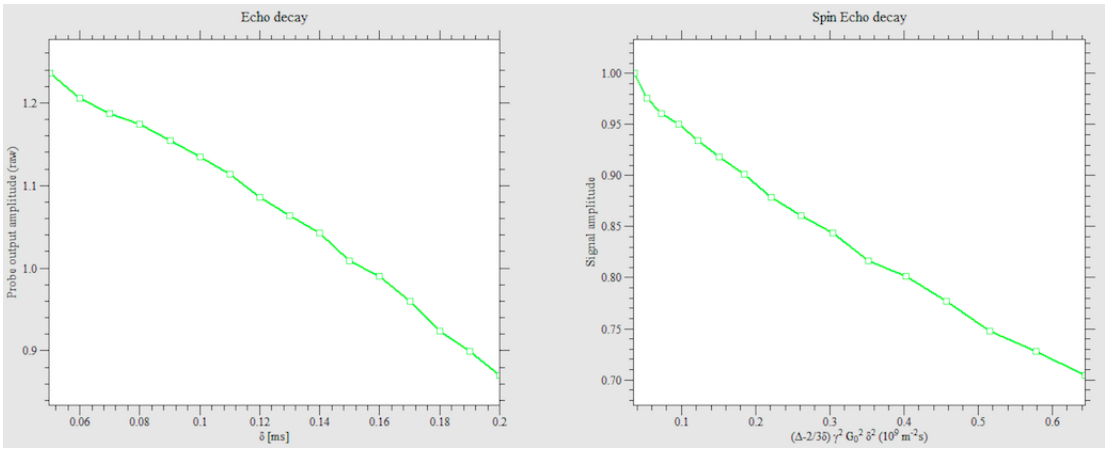

Figure 2.19: Acquired signal as a function of the encoding time δ (left), sicgnal attenuation as a function of the b value, where $b = \gamma^2 g^2 \delta^2 \left(\Delta + \frac{2\delta}{3}\right)$ (right).

2.4.6 SSEdec

Respect to the Stimulated Spin Echo sequence, here the data of CPMG decays are stored (Fig. 2.20). At the end, D and T_2 data are available to calculate 2D spectra [16].

File Edit Sheet Column Data Math Plot Window Help

Ready

	Column1	Column2	Column3	Column4	Column5	Column6	Column7	Column8
1	1.1298	1.6204	1.4840	1.5171	1.4366	1.3308	1.4090	1.3950
2	1.2179	1.6242	1.4649	1.4501	1.4609	1.4061	1.4810	1.4952
3	1.2156	1.4594	1.4425	1.3267	1.3704	1.4123	1.4933	1.3578
4	1.1445	1.3483	1.2353	1.4052	1.2493	1.4123	1.2432	1.3673
5	1.1249	1.3550	1.4200	1.4012	1.1819	1.2439	1.3422	1.3897
6	1.1094	1.3577	1.5523	1.2297	1.2401	1.2925	1.3313	1.2987
7	1.1398	1.3574	1.2449	1.2362	1.2355	1.2941	1.2816	1.2373
8	1.0059	1.3950	1.2468	1.2122	1.1757	1.2572	1.2783	1.2624
9	1.0097	1.2802	1.1817	1.1792	1.1786	1.1810	1.2351	1.1969
10	0.9366	1.2273	1.1421	1.1703	1.0436	1.2170	1.1530	1.2850
11	0.9518	1.2221	1.1392	1.1068	1.1040	1.1674	1.1353	1.1725
12	0.9248	1.1623	1.1457	1.2294	1.0896	1.1905	1.1680	1.1031
13	0.8629	1.2145	1.0180	1.0596	1.0531	1.0553	1.0953	1.1062
14	0.8880	1.0804	1.0372	1.0852	1.0565	1.1427	0.9379	0.9521
15	0.8943	1.1102	1.0682	1.0784	1.0488	0.9373	1.1418	0.9898
16	0.7722	0.9668	0.9792	0.9580	1.0332	0.9204	0.9803	0.9209
17	0.8531	0.9406	0.9627	0.9641	0.9469	0.8390	0.8917	0.8871
18	0.7596	1.0519	0.9139	0.8250	0.9238	0.9184	0.9621	1.0171
19	0.7362	0.9712	0.9163	0.8656	0.9227	0.9375	0.9086	0.8892
20	0.6008	0.8671	0.8581	0.8790	0.8217	0.8823	0.7673	0.8383
21	0.7058	0.8615	0.8836	0.8277	0.7955	0.8664	0.8437	0.7686
22	0.7215	0.8831	0.7765	0.9708	0.7615	0.8976	0.7749	0.8164
23	0.5084	0.8374	0.7588	0.8892	0.7964	0.8066	0.8148	0.7882
24	0.6472	0.8227	0.7649	0.7639	0.7762	0.7917	0.6482	0.7439
25	0.6252	0.8591	0.6840	0.7132	0.6677	0.7631	0.7696	0.6648
26	0.6250	0.7207	0.6607	0.6796	0.6635	0.6439	0.7492	0.7059
27	0.5038	0.6610	0.6700	0.6362	0.6232	0.6936	0.6164	0.6581
28	0.6096	0.6320	0.5473	0.6745	0.6376	0.5840	0.6657	0.7712
29	0.5024	0.5996	0.5839	0.7200	0.5478	0.6656	0.4966	0.6261
30	0.4875	0.6546	0.6448	0.5589	0.6163	0.5824	0.6958	0.7414
31	0.6429	0.6545	0.5815	0.6008	0.5908	0.5516	0.5166	0.5921
32	0.5037	0.5123	0.5518	0.6856	0.6721	0.5269	0.5757	0.5697
33	0.3868	0.5376	0.5647	0.5230	0.5137	0.5780	0.5273	0.5580

Figure 2.20: Part of data acquired by SSEdec sequence: each column corresponds to a SSE (thus each column corresponds to a δ); each row corresponds to the acquired CPMG data.

Chapter 3

Data analysis

The pulse sequences described in the section 2.4 allow one to acquire the signal decays; the following data analysis then often involves a Laplace inversion to obtain a distribution of relaxation times or diffusion constants. For samples as bulk water, the spins are exposed to the same environment, thus their relaxation is described by a monoexponential function. This is not longer true for more complex samples as tissues or biological systems, whose relaxation has a multiexponential trend.
It can be supposed that a discret number of components M exists, realizing a fit assuming a discrete number (k=M) of time constant T_k, each with an amplitude a_k. In this case, the signal measured for a sperimental time t_i will be:

$$S(t_i) = \sum_{k=1}^{M} a_k \exp\left(-\frac{t_i}{T_{(1,2)k}}\right) \tag{3.1}$$

The method of least squares seems to be good solution for the a_k and T_k extraction, but the more the parameters, the more the risk of a solution which doesn't represent correctly the real physical system. It's shown to be more realistic to assume a continous relaxation times distribution [1] characterised by a *signal density function* $f(T_{1,2})$, such that

$$S(t) = \int_0^\infty f(T_{1,2}) \exp\left(-\frac{t_i}{T_{(1,2)k}}\right) dT_{1,2} \tag{3.2}$$

The problem of the inversion from the measured times scale t to the relaxation times one $T_{1,2}$ is the fact that $S(t)$ isn't a theoretical function, but it's given by experimental values affected by noise, for each t we have:

$$S(t) = \int_0^\infty f(T_{1,2}) \exp\left(-\frac{t_i}{T_{(1,2)k}}\right) dT_{1,2} + \epsilon \tag{3.3}$$

It could be expressed as a discretized matrix form

$$S = KF + N \tag{3.4}$$

where S and N are the data and noise vectors, matrices K, and F are discretized version of the kernel, and $f(T_{1,2})$, respectively.
The noise brings **infinite solutions** to the problem, thus there are infinite $f(T_{1,2})$ distributions which could be obtained. Hence this inversion is ill-conditioned: a small noise in the data can cause significant changes in the resulting distribution. This problem has been solved using two different approaches for the 1D and the 2D Laplace inversion.

3.1 1D Laplace inversion

In order to solve the ill-condition of the inversion, a first approach is the introduction of some smoothing terms in the distribution. The risk of this method is represented by the fact that, given a distribution composed by a narrow peak and by a low intensity tale (i.e. fluid saturated porous media), a fixed smoothing coefficient could tend to enlarge the peak and to break the tail into peaks which are mathematical artefacts wrongly supposed as separated populations.
The UPEN algorithm (Uniform PENalty) [18] avoids the formation of these artefacts by imposing a *variable* smoothing coefficient which introduces the *same* penalty on the data along the distribution curve (Fig. 3.1).

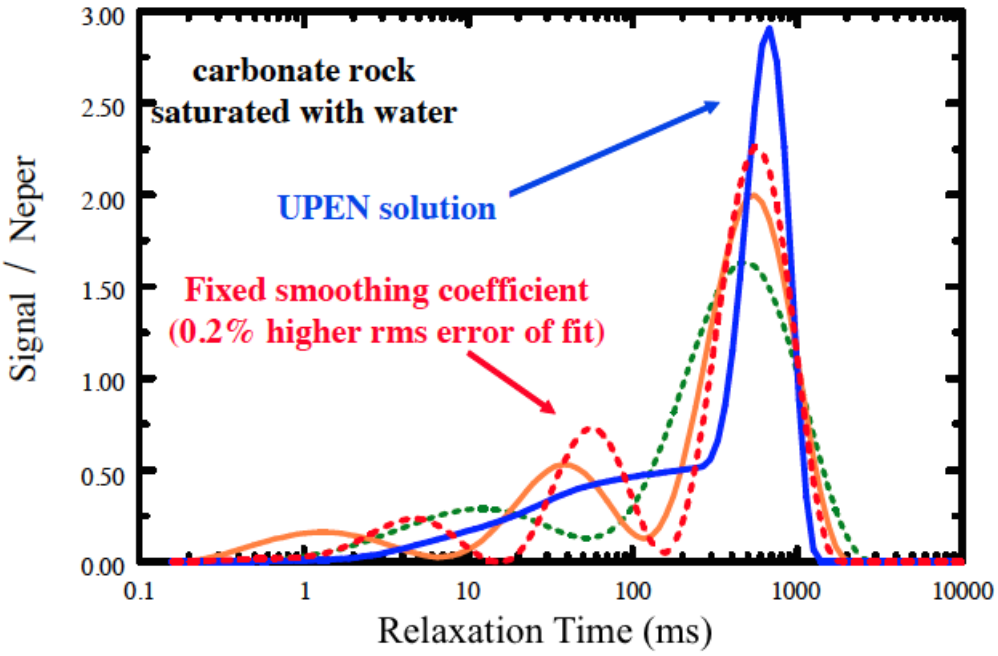

Figure 3.1: T_2 relaxation data of carbonate rock saturated with water. The dashed lines stand for an algorithm with different fixed smoothing coefficients; the solid one is obtained by UPEN [18].

This is possible by using a negative feedback algorithm which, through successive iterations, varies the smoothing coefficients, making them inversely proportional to the squared curvature of each point to whom they are associated. Comparing the UPEN approach

with the one which uses a constant smoothing coefficient, if the fit error is the same and the second method produces more details, it means that these details are artefacts without any relationship with the analyzed system.
The UPEN method is expressed by the following formula:

$$\underbrace{\sum_{i=1}^{N}\left(g_0+\sum_{k=1}^{M}g_k\exp\left(-\frac{t_1}{T_k}\right)-s_i\right)^2}_{\text{Sum of squared errors of fit}}+\underbrace{\sum_{k=2}^{M-1}C_k(g_{k-1}-2g_k+g_{k+1})^2}_{\text{Penalty term}} \tag{3.5}$$

where g_0 is the value of the signal at infinite time, and C_k is the coefficient for curvature smoothing, which varies for each distribution point g_k. In order to have a uniform penalty, a series of iterations, starting with a fixed C_k occurs and, for each iteration, it becomes inversely proportional to the square of the second difference from the previous equation. To avoid the risk of a distribution composed by straight-line segment, the uniform-penalty requirement is relaxed by using at each k the highest second-difference-squared values found at $k-1$, k, or $k+1$ from the previous iteration.

3.1.1 UPENWin

UpenWin is a 32 bit application developed in C++ and MFC (*Microsoft Foundation Class*) by means of Visual Studio 2005, that implements an interface to facilitate the use if UPEN and its related input files [19]. The user can pre-process the data file using the appropriate filter program, set the value for the parameters for UPEN and run a computation session.
The input data files for UPEN computaion are text files, formed by two columns of data acquired with NMR sequences corresponding, respectively, to the time and to the signal amplitude. These data are preprocessed by UPENWin functions T_2 *Filter* and T_1 *Filter* respectively used for CPMG data and Saturation Recovery data. For CPMG the filter averages the data points in windows of a width chosen according to the number of points (*windowing* operation) (Fig. 3.2). The output is a signal described by fewer points.
The output of filtering is then processed by the UPEN run, which computes the T_k distribution (contained in a .DAT file) and displays a .TST text file with some information on some parameters and computed values related to the data, including quantities that are hoped to have diagnostic value for identifying various data problems. The elaborated data are finally shown using the plotting software PSI-Plot developed by Poly Software International, Inc.

3.2 2D Laplace Inversion

At the present time, the UPEN algorithm is not yet available for the 2D case. Thus, for 2D inversion envolving data acquired by SR-CPMG and SSEdec sequences, we have

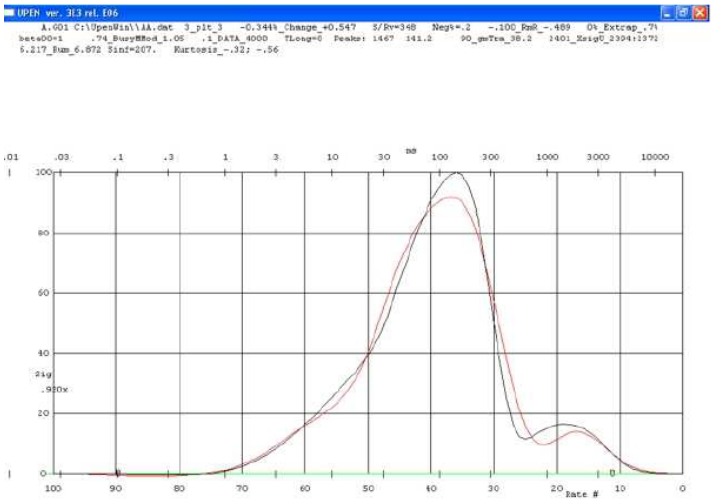

Figure 3.2: UPENWin on processing [19].

followed a different approach [1].
The regularization method (Tikhonov regularization [20]) obtains a fit to the data through minimization of the following expression:

$$\| S - KF \|^2 + \alpha \| F \|^2 \tag{3.6}$$

The first term measures the difference between the data and the fit, KF. The second term is a regularization whose amplitude is controlled by the parameter α. In order to accelerate the minimization, the filtering of the data and of the kernel is handled by applying a *singular value decomposition* (SVD) on K:

$$K = U\Sigma V^T \tag{3.7}$$

where Σ is a diagonal matrix with singular values in a descending order, U and V are unitary matrices.
The SVD on K, allow us to rewrite Eq. 3.6 in an equivalent form, but with compressed data ($\hat{S} = U^T SU$) and a smaller kernel. Hence the minimization has a greatly increased inversion speed.
In 2D case, this approach could be applied, but the kernel matrix will be huge, leading on very large computational times. We can solve this problem applying the Fast Laplace Inversion (FLI). It consists in rewriting the kernel as a product of two independent kernels. Taking as example the inversion of SR-CPMG data, we have:

$$k(t_1, t_2, T_1, T_2) = k_1(t_1, T_1)k_2(t_2, T_2) \tag{3.8}$$

In this case the kernels are:

- $k_1 = 1 - \exp\left(-\frac{t_1}{T_1}\right)$
- $k_2 = \exp\left(-\frac{t_2}{T_2}\right)$

Hence, Eq. 3.6 will be expressed as:

$$S = K_1 F K_2^T + N \tag{3.9}$$

where the kernel elements are expressed as $(K_k)_{ij} = k_k(t_{ki}, T_{kj})$. The SVD of K_1 and K_2 is followed by an approximated SVD of the product matrix. Because of the conversion of the problem from the 2D form to the 1D one, the computational times needed for the inversion will be greatly reduced.
Let us take the example of a 2D inversion of a SR-CPMG sequence performed on a water sample in bulk condition (Fig. 3.3): we can see that the signal is localised in a specific area of the map corresponding to the relaxation times of the sample. At the bottom of the plot, a small signal is shown: it's an artefact due to the data inversion, and it will be more evident in the inversion of restricted diffusion systems, especially at the proximity of inversion range limits (Cap. 5-6).

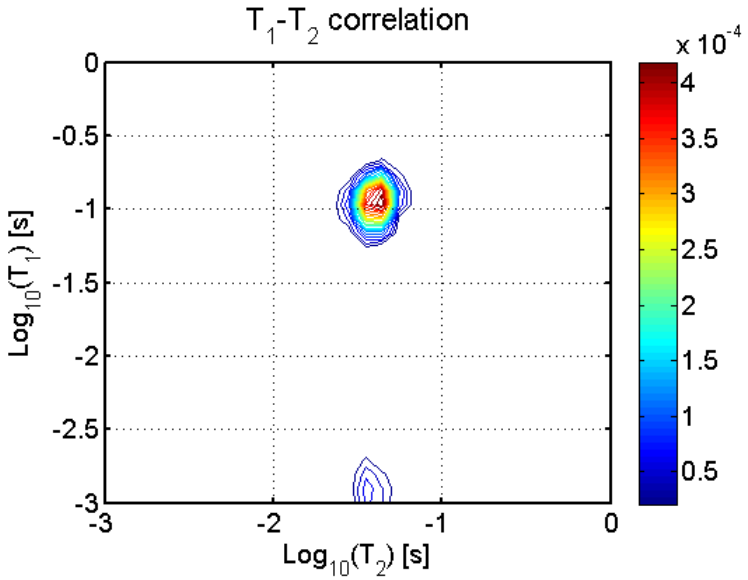

Figure 3.3: $T_1 - T_2$ map of a bulk water sample.

Chapter 4

Materials

In this chapter the materials and samples used in the measurements are described.

4.1 Soltrol

Soltrol 130 and soltrol 170 are paraffinic hydrocarbons commonly having a oily liquid colourless form [21]. Soltrol 170 is already known as dodecan, because it's a linear alcan composed by 12 carbon atoms ($CH_3(CH_2)_{10}CH_3$). They are used as solvents for organic synthesis and also as scintillator components. In our experiments, both samples were studied in bulk condition contained in a becker.

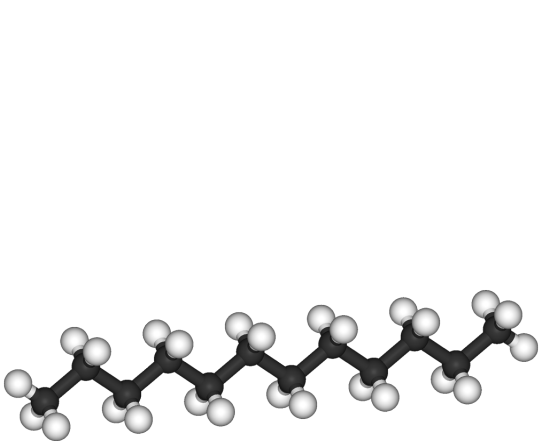

(a)

(b)

Figure 4.1: (a) Soltrol 170 atomic scheme [21]; (b) Becker containing Soltrol 170

4.2 CuEDTA

This sample is used in the measurements involving both bulk diffusion and both restricted diffusion conditions. EDTA (*EthyleneDiamineTetraacetic Acid*, $C_{10}H_{12}N_2O_8$) is a tetracarboxylic acid used as a chelating agent [22]. In fact, the presence of four carboxylic groups and of two nitrogen atoms allow the EDTA molecule to compose stable complexes with many cations: in our case it binds to the copper ion Cu^{++}.

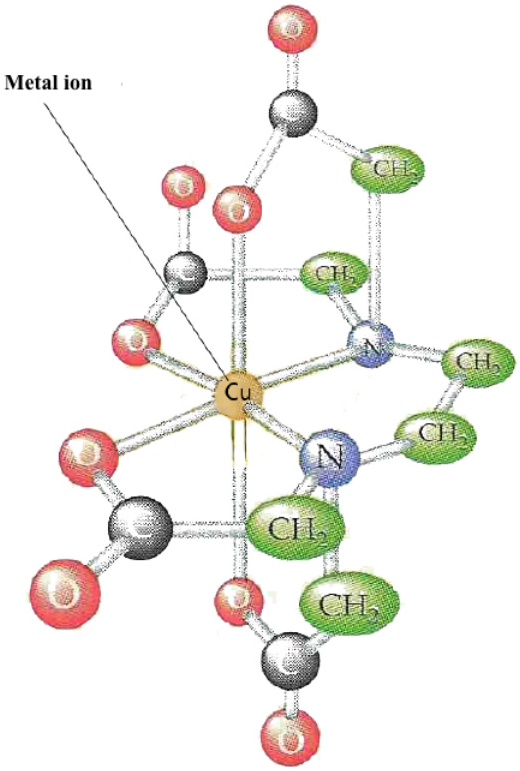

Figure 4.2: CuEDTA atomic scheme [23].

In NMR studies, this compound is used in order to strike down the samples relaxation times; this is due to the presence of Cu^{++}, which is paramagnetic.
In this work EDTA is present as small traces in a water sample used for bulk diffusion studies; but its paramegnetic behaviour is used in the restricted diffusion analysis, in order to greatly reduce the water signal component in diluted yeast samples.

4.3 Yeast

Yeasts are unicellular fungus, which mostly reproduce asexually by an asymmetric division process called budding [24]. They grow faster than filamentous mould, they differ from algae because they don't perform photosinthesis, and they aren't protozoa because of their rigid cell wall.
Yeast are important not only for bread fermentation, but also for fats, proteins and vitamins sinthesis from simple sugars; furthermore, they have contributed in the scintific progress as a cell model for studies on fundamental eukariota metabolic and biochemical process.

4.3.1 Yeast morphology

Yeast cells have a larger set of shapes: they are $1 \div 5$ μm large and $5 \div 30$ μm long, they could be ovoidal, stretched or spherical [24]. The most part of the information in our possession, was achieved by studying the *Saccharomyces cerevisiae*, which we have chosen as the main model in this experience.
The cell wall is thin in young yeast cells, it increases with increasing age. *S. cerevisiae* cell wall is mainly composed of two polysaccharides: glycan ($30 \div 34\%$) consisting of D-glucose unities, and mannan (30%). Furthermore proteins are $6 \div 8\%$ (w/w), and fats are $8{,}5 \div 13{,}5\%$ (w/w).

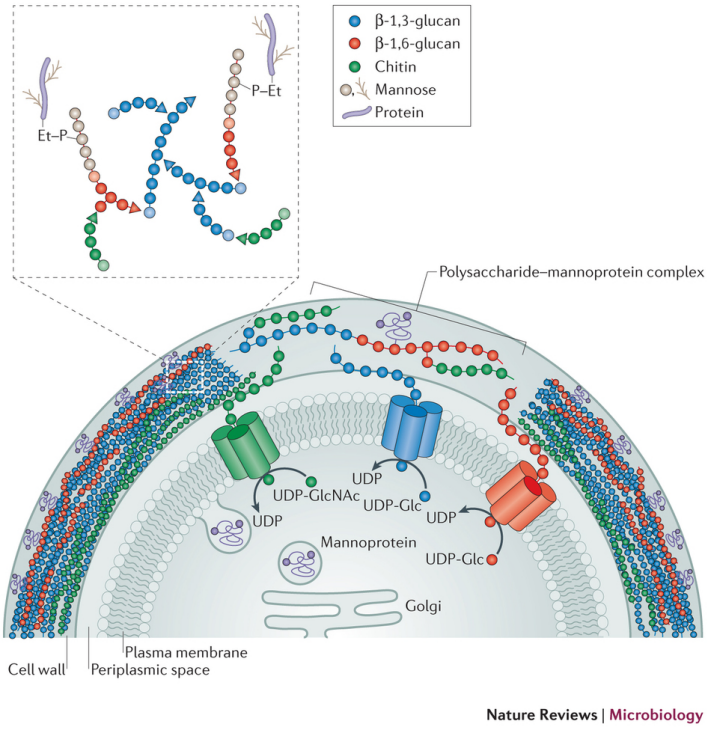

Figure 4.3: Schematic representation of cell wall assembly [25].

The cell membrane is composed of two layers. Isolated membrane fragments analysis has revealed the presence of lipids (among which phospholipids), proteins and polysaccharides. A typical yeast cell contains cytoplasm at semiliquid state, containing granular materials, ribosomes and organelles having own membranes.
The yeast nucleus is a well-defined organule confined by a selectively permeable membrane, which is functional for organism metabolism and reproduction.
The mithocondria have a 0,3÷1 μm diameter and they are confined by a double membrane. In the yeast cytosol is present a vacuole, an organule filled with water containing inorganic and organic molecules including hydrolytic enzymes (protease, ribonuclease) in solution.

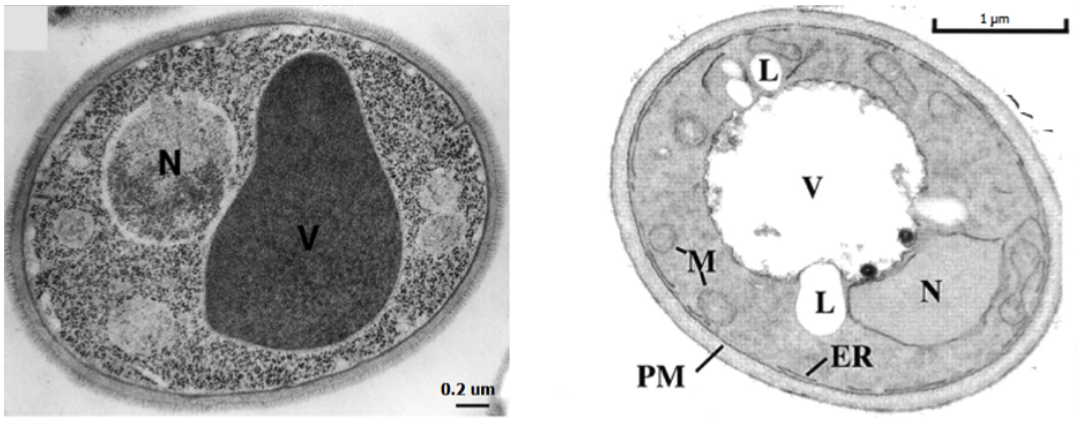

(a) (b)

Figure 4.4: (a) Electron microscopic observation of *S. Cerevisiae* (N=nucleus, V=vacuole) [26]; (b) Thin-section EM of *S. Cerevisiae* (L=lipid droplet, M=mitochondrium, N=nucleus, PM=plasma membrane, V=vacuole, ER=endoplasmic reticulum) [27].

Part II

Results

Chapter 5

Self-diffusion coefficient in bulk liquids

The first measurements performed involve three known samples in bulk condition:

- Soltrol 170;
- Soltrol 130;
- Water with small traces of CuEDTA.

The purpose of these experiments is to test the sequences described in the subsection 2.4 and to know how the change of some parameters could influence the results.
For every measure, the Profile was used with all the 4 spacers inserted underneath the rf-coil, ensuring the best possible rf-pulse efficiency. By the calibration sequence, the pulse duration has been set =4.5 μs

5.1 Soltrol 170

The CPMG parameters for the Soltrol 170 sample are listed below:

Number of echoes	8000
Repetition Time	25000 ms
Number of scans	64
Echo Time	50 μs

The *Number of echoes* parameter has a maximum limit of 8000, thus the T_2 relaxation acquired could be incomplete (Fig. 5.1). In order to expand the window, a longer echo time should be adjusted: the disvantage consists in a final T_2 value far from the effective value. This is caused by the fact that the spins have a larger time to diffuse, leading to a faster decay.

In the data inversion step, the entire signal evolution sampling is not needed, hence, the choice of a small echo time value is considered the priority in the parameters adjustment.

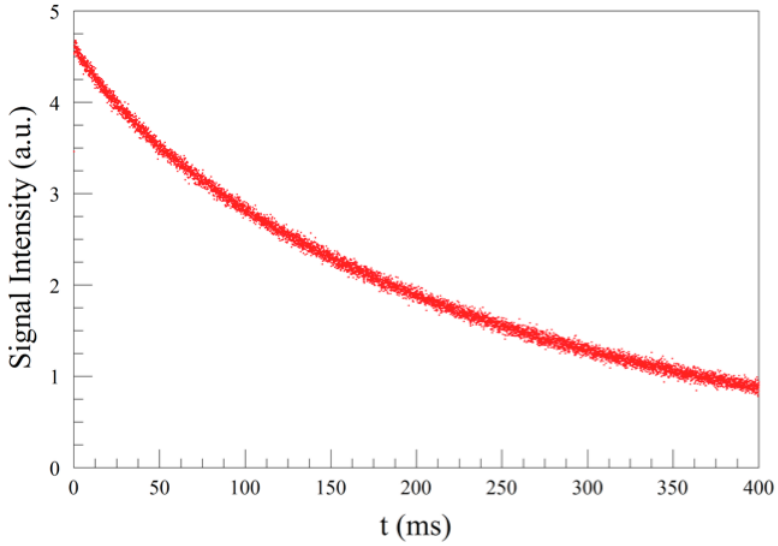

Figure 5.1: Soltrol 170 signal decay by a CPMG sequence.

From the data inversion analysis, we obtained a T_2 peak at about 300 ms (Fig. 5.2).

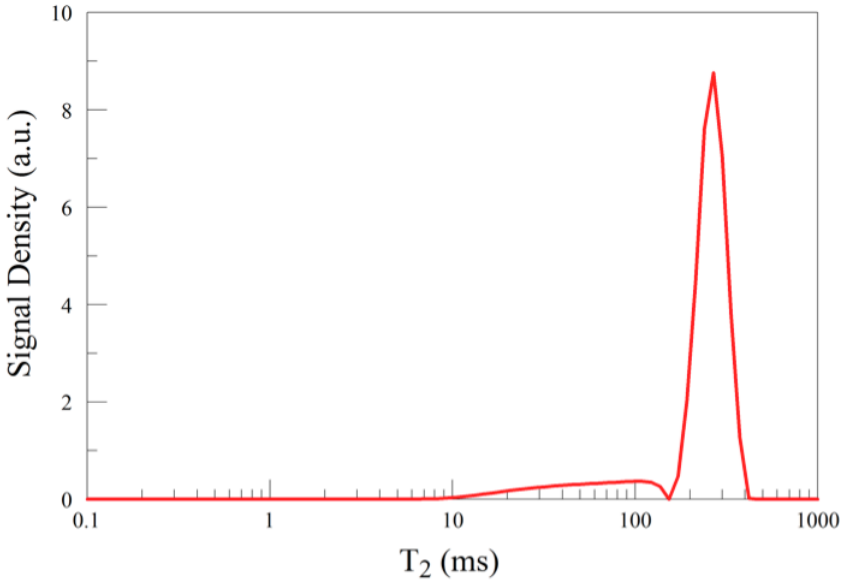

Figure 5.2: Soltrol 170 T_2 distribution.

The T_1 Saturation Recovery parameters are the following:

Number of echoes	128
Repetition Time	4000 ms
Number of scans	8
Number of points T_1	64
Echo Time	50 μs
Max Recovery Time	4000 ms
T_1 estimation	1000 ms

The corresponding distribution shows a peak of signal density at 600 ms in the range 300 ms÷ and 1 s (Fig. 5.3).

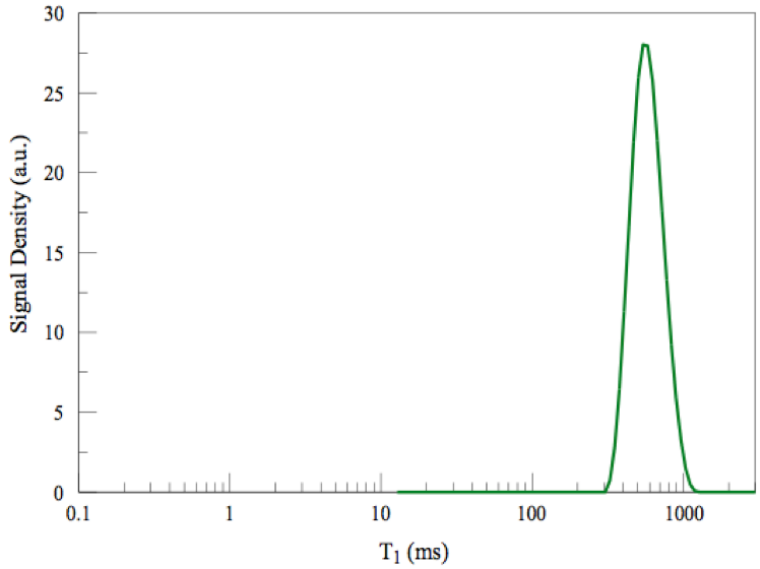

Figure 5.3: Soltrol 170 T_1 distribution by Saturation Recovery sequence.

The characterization of the Soltrol 170 sample ends with SSE sequences with different Δ values, to whom correspond squared averaged paths from 12 μm^2 up to 100 μm^2, according to Eq. 1.15.

Δ (ms)	**δ_{min} (ms)**	**δ_{max} (ms)**
1	0.02	0.4
5	0.02	0.2
10	0.02	0.14
40	0.02	0.07

Echo Time	50 μs
Number of echoes	128
Repetition Time	4000 ms
Number of scans	32
Number of points δ	32

The self-diffusion coefficients obtained by fitting the signal attenuations are very close to each other (Fig. 5.4). For equal δ, the Δ increase leads to a larger signal attenuation: the more is the diffusion time, the faster is the signal decay.

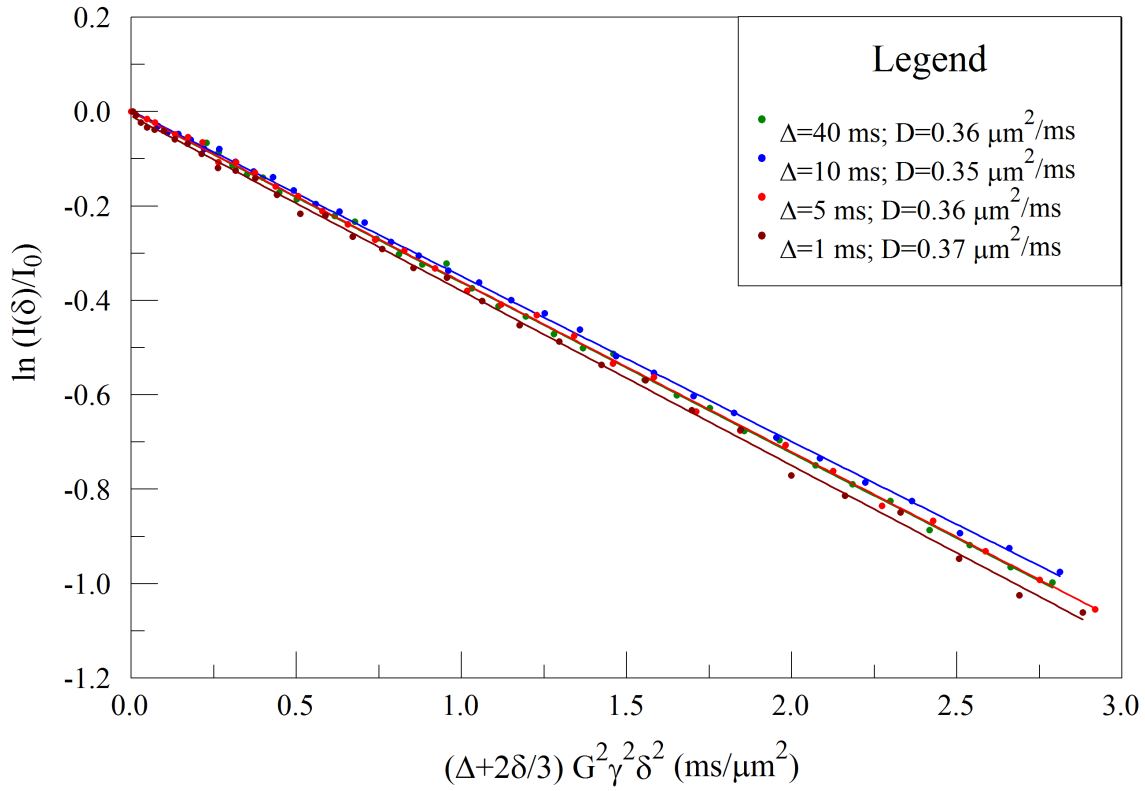

Figure 5.4: Soltrol 170 signal attenuation due to diffusion for different diffusion times.

5.2 Soltrol 130

The CPMG sequence with a Soltrol 130 sample has been executed with the following parameters:

Echo Time	50 μs
Number of echoes	8000
Repetition Time	25000 ms
Number of scans	64

The corresponding T_2 distribution has a signal density peak at about 160 ms (Fig. 5.5), and a tail between 5 ms and 60 ms.

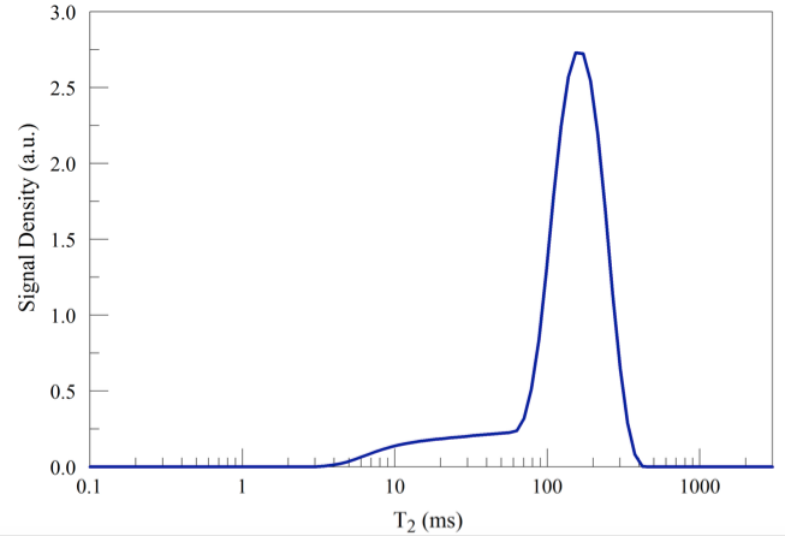

Figure 5.5: Soltrol 130 T_2 distribution by CPMG.

The SR sequence parameters are listed below:

Number of echoes	128
Repetition Time	5000 ms
Number of scans	8
Number of points T_1	64
Echo Time	50 μs
Max Recovery Time	5000 ms
T_1 estimation	1000 ms

The data inversion results in a T_1 density signal in the range 700 ms$\div$2 s with a density peak at 1 s (Fig. 5.6).

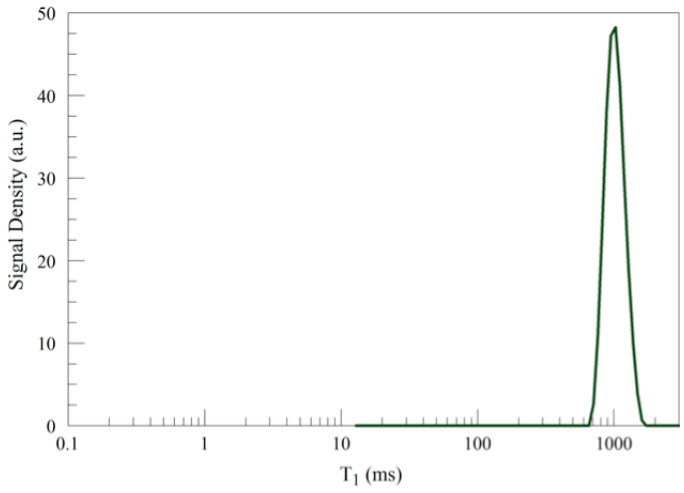

Figure 5.6: Soltrol 130 T_1 distribution by Saturation Recovery.

The SSE sequence was repeated several times: for each sequence, the data fit gave a selfdiffusion coefficient much higher than both the literature one (0.74 $\mu m^2/ms$) and the one measured in the same conditions previously (0.8 $\mu m^2/ms$). This is due to the fact that as temperature increases, the diffusion also grows. The sequences were performed using the following parameters:

Δ	20 ms
δ_{min}	0.02 ms
δ_{max}	0.07 ms
Echo Time	50 μs
Number of echoes	128
Repetition Time	4000 ms
Number of scans	32
Number of points δ	32

As shown in Fig. 5.7, a higher temperature leads to a higher diffusion coefficient, hence, on equal δ, the signal decay due to diffusion is faster.

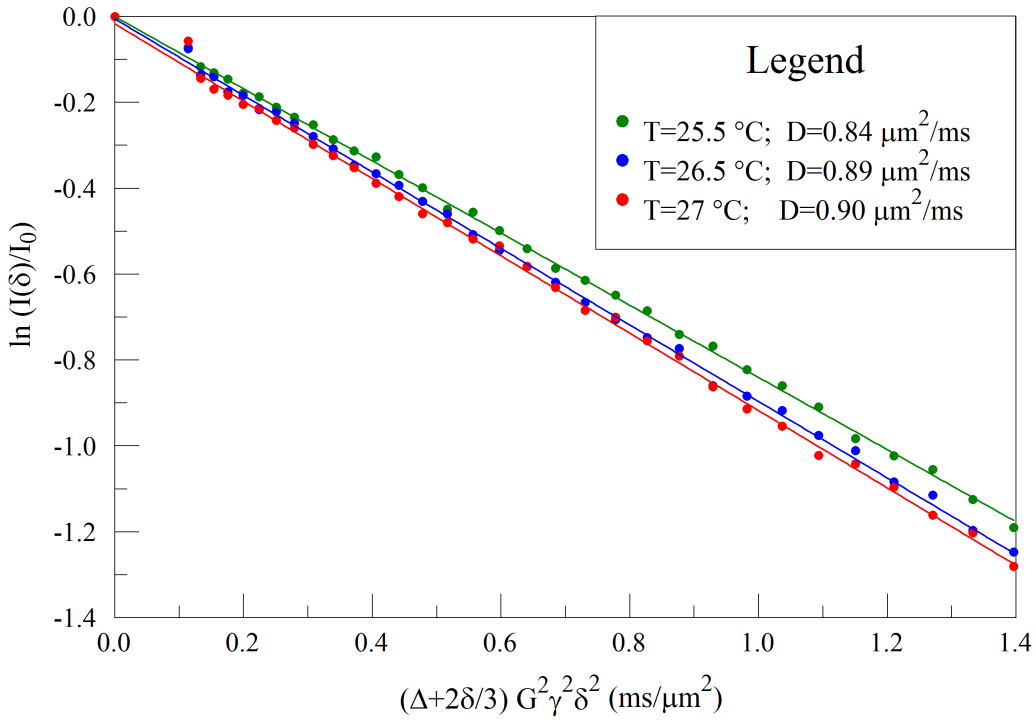

Figure 5.7: Soltrol 130 signal attenuation due to diffusion at different temperatures for fixed diffusion time Δ=20 ms.

5.3 Water with CuEDTA traces

For the water sample, the CPMG parameters are the following:

Echo Time	50 μs
Number of echoes	8000
Repetition Time	23000 ms
Number of scans	64

The corresponding analysis results in a main signal region, which represents the 92% of the entire signal, with a maximum density at 40 ms, and in a secundary one (the remaining 8%) corresponding to spins relaxing with shorter relaxation times (Fig. 5.8).

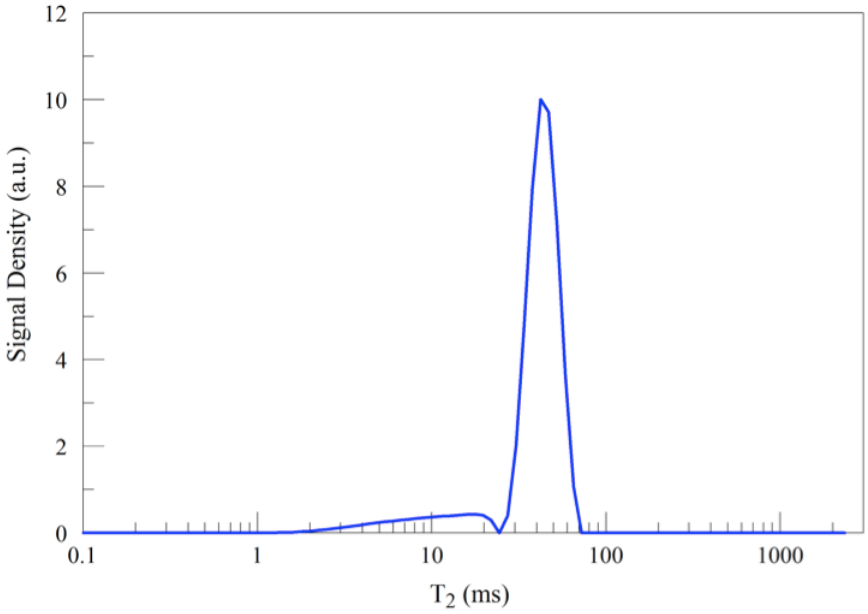

Figure 5.8: Water T_2 distribution by CPMG.

The SR sequence was setted as follows:

Number of echoes	128
Repetition Time	1000 ms
Number of scans	8
Number of points T_1	64
Echo Time	50 μs
Max Recovery Time	900 ms
T_1 estimation	100 ms

The data inversion leads to a distribution with a narrow density peak at 100 ms (Fig. 5.9).

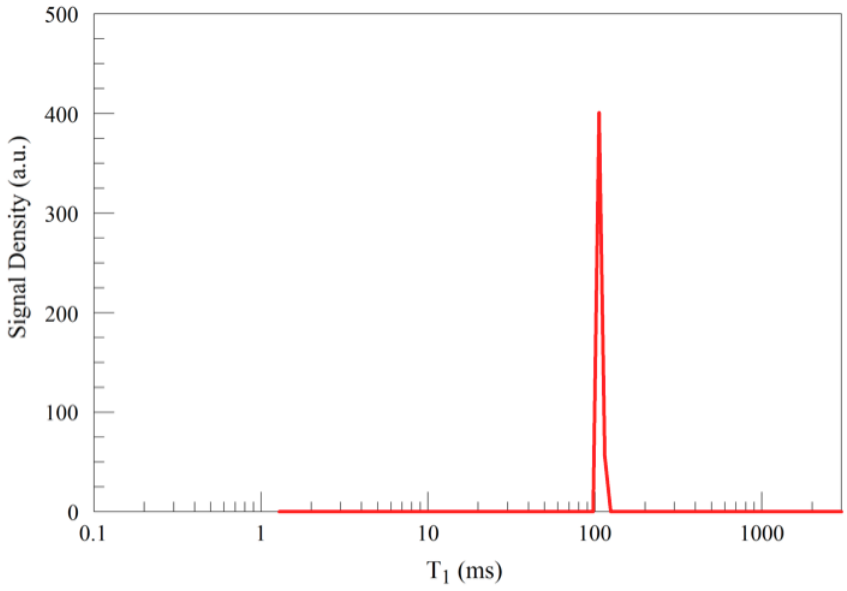

Figure 5.9: Water T_1 distribution by Saturation Recovery.

5.4 Comparisons

The last act of these introductory measurements is the comparison between the results of the SSE sequences on the three samples considered.

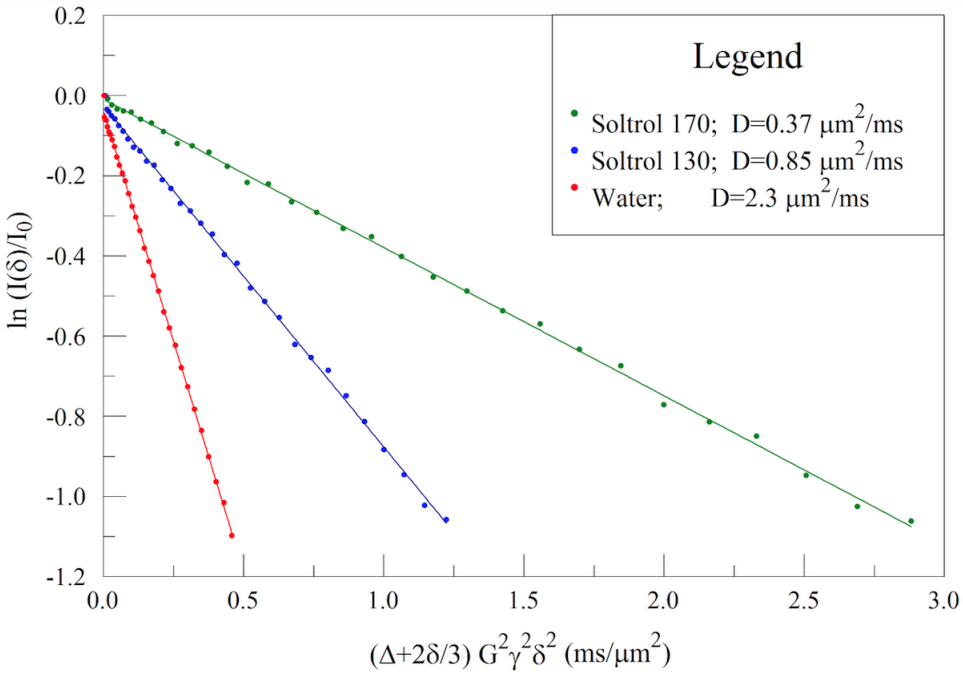

Figure 5.10: Signal attenuations comparisons for fixed diffusion time Δ =1 ms.

In the first comparison, the sequences were executed with Δ parameter fixed at 1 ms and different values for the δ_{max} parameter:

- 0.27 ms for Soltrol 170 and Soltrol 130 samples;
- 0.17 ms for water sample.

Fig. 5.10 shows that the water sample diffuses faster than the Soltrol 130 sample, which in turn diffuses faster than the Soltrol 170 sample.

A confirm of this behaviour is given by the second comparison (Fig. 5.11). In this one, we have fixed the averaged squared path (100 μm^2), hence we can compare the samples evolution on equal δ_{max} (fixed at 0.07 ms).

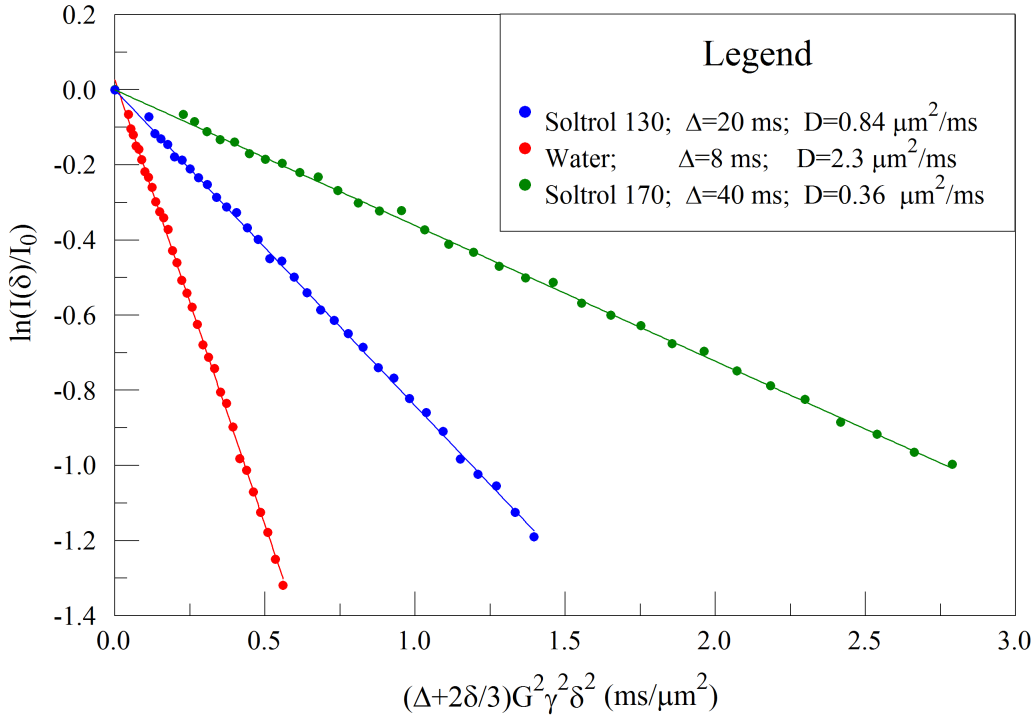

Figure 5.11: Signal attenuations comparisons for fixed averaged squared path ≈100 μm^2.

The differences between the samples selfdiffusion coefficients could be explained by their molecular composition: we can notice that the greater the number of atoms assembling a molecule, the lower the corresponding D.
In the following table, the selfdiffusion coefficients obtained are compared to the ones present in literature:

Sample	$D_{lit.}(\frac{\mu m^2}{ms})$	$D_{meas.}(\frac{\mu m^2}{ms})$
Soltrol 170	0.401 [28]	0.36±0.01
Soltrol 130	0.728 [28]	0.84±0.02
Water	2.3 [29]	2.3±0.1

where the errors are the standard deviations of the fits computed by PSI-Plot.
Nontheless the data fits very well, the error bands reffering to the soltrols $D_{meas.}$ don't include the corresponding D_{lit}; it is due to the fact that, as already stated in 5.2, these sequences were performed without a fixed external temperature because of technical issues.

Chapter 6

Measurements on solid yeast

Solid yeast (Fig. 6.1) has been chosen as sample for restricted diffusion studies because it's easly available and because it could be a good system (spherical shape) for testing the approach described in this work. Each sequence has been performed at constant temperature, 25°C, and with 4 spacers inserted underneath the rf-coil.

Figure 6.1: Block of solid yeast.

6.1 CPMG optimization

In order to obtain the nearest T_2 value to the real one, the attenuation effect due to molecular diffusion must be reduced: hence we have determined the lowest echo time available to have better results from CPMG sequences.
This task has been handled using again the water sample. Comparing the data inversions of CPMG with different echo times, we can observe that the geometrical mean T_2 value for $t_E = 50\mu s$ CPMG is the double (40 ms) than for $t_E = 35\mu s$. For lower echo times, it's impossible to achieve a good measure because of instrumental limits, thus the following sequences were acquired setting $t_E = 35\mu s$.

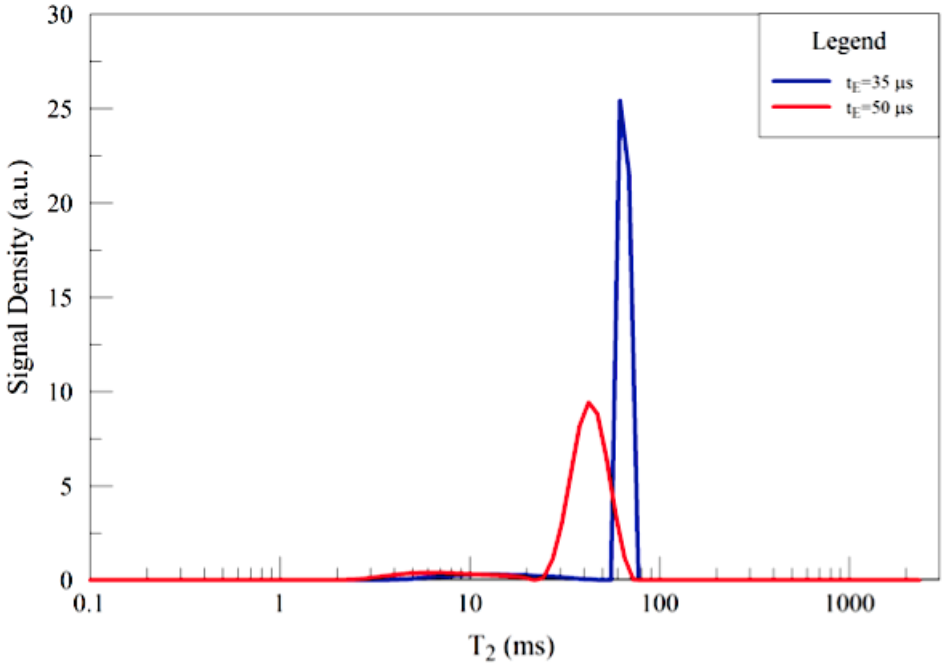

Figure 6.2: Water T_2 distributions comparison for different echo times by CPMG sequences.

6.2 Introductory measurements

Once the echo time had been chosen, SR and CPMG sequences have been performed on the solid yeast sample. The parameters setted are listed below:

CPMG Parameters

Echo Time	35 μs
Number of echoes	6000
Repetition Time	18000 ms
Number of scans	64

SR Parameters

Echo Time	35 μs
Number of echoes	128
Repetition Time	1000 ms
Number of scans	8
Number of points T_1	64
Max Recovery Time	1000 ms
T_1 Estimation	300 ms

The 1D data inversion gives as result that the geometrical mean values for T_1 and T_2 are respectively 200 ms and 40 ms: this information is important for the SSEdec acquisition and inversion. The Δ parameter should be short enough to avoid a T_1 relaxation; thus we have used as maximum diffusion time value $\Delta = 50$ ms, a quarter of the longitudinal relaxation time.
The T_2 range, instead, could help us to distinguish in the 2D maps the signal peaks due to the sample diffusion and relaxation from the artefacts.

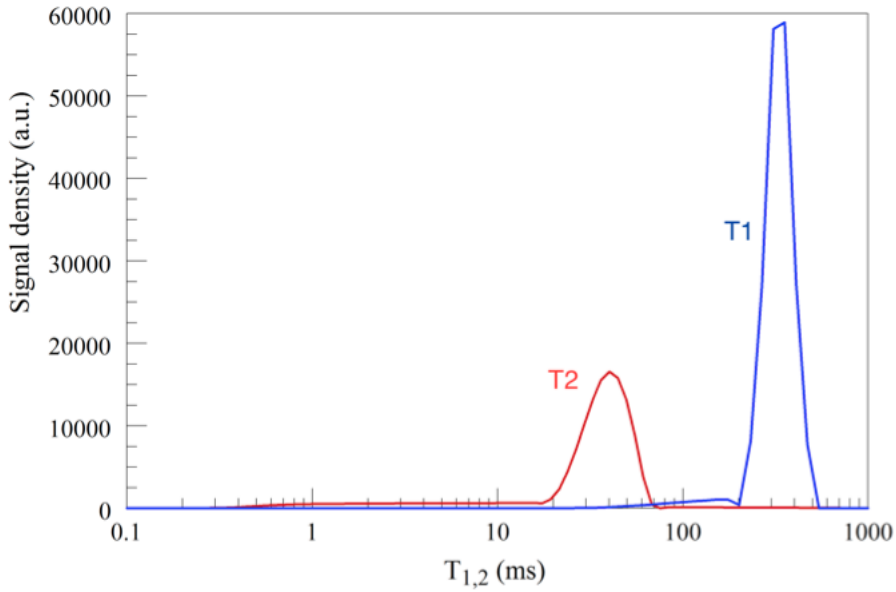

Figure 6.3: Solid yeast T_1 and T_2 distributions by SR and CPMG respectively.

First, SSE sequences were performed, repeating the approach used for the three bulk samples, for several diffusion times:

Echo Time	35 μs
Gradient	600 kHz/mm
Number of echoes	6000
Number of points δ	100
Number of scans	16
Repetition Time	18 s
$\boldsymbol{\delta_{min}}$	0.02 ms

The following plots show the signal intensity for increasing b-values (i.e. for increasing δs) for two different diffusion times.

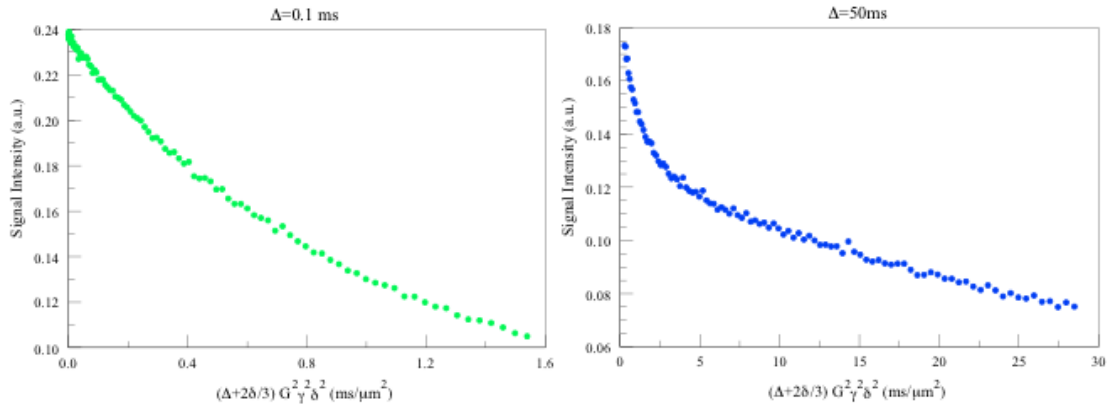

Figure 6.4: Signal attenuation due to diffusion with Δ=0.1 ms (left) and Δ=50 ms (right).

The plot on the left shows the acquired data with the shortest diffusion time ($\Delta = 0.1$ ms): the monoexponential trend suggests the presence of only one diffusing hydrogens family. For greater diffusion times the trend is no more single exponential. In fact, the greater diffusion time, the greater the fraction of hydrogens experiencing the walls: if the sample studied has diffusion spaces with different sizes, we obtain more D_{app} values corresponding to more diffusing hydrogens families.
The plot on the right shows acquired data for the largest diffusion time ($\Delta = 50$ ms): it suggests the presence of more compartments with different sizes in the studied system.

6.3 SSEdec sequences

In the view of the above section, in order to have a better understanding of the phenomenon, it's necessary to execute SSEdec sequences: for each of them, acquired data are then inverted into a 2D map having T_2 values on x-axis and D values on y-axis.
On the basis of previous comments, in the following we will use the symbol D for the diffusion coefficient, but it is clear that it is an apparent diffusion coefficient (D_{app}).
A MATLAB script has been developed to obtain the distribution of the two parameters along the two axis.
Here the SSEdec parameters initially setted are reported:

Echo Time	35 μs
Gradient	600 kHz/mm
Number of echoes	6000
Number of points δ	100
Number of scans	16
Repetition Time	21 s
$\boldsymbol{\delta_{min}}$	0.02 ms

The D-T_2 maps are realized with the following parameters:

- **Resolution:** 50×50
- **D range:** [10^{-2} $\frac{\mu m^2}{ms}$, 10 $\frac{\mu m^2}{ms}$]
- T_2 **range:** [10^{-3} ms, 0.3 ms]

The elaboration of each map takes about 5-10 minutes, with greater resolutions (i.e. 64×64) the computational time for the inversion is very long (30-40 minutes) and doesn't add significant details. The D and T_2 ranges chosen are the more restricted possible to avoid critical artefacts.
Each sequence takes around 9 hours, a very large time; hence we have optimised the parameters:

Echo Time	35 μs
Gradient	600 kHz/mm
Number of echoes	2000
Number of points δ	50
Number of scans	32
Repetition Time	7 s
$\boldsymbol{\delta_{min}}$	0.02 ms

The effects of these settings are the improvement of the Signal-to-Noise Ratio (SNR) of a $\sqrt{2}$ factor due to the doubling of the number of scans than the previous setted parameters; a 3 hours acquisition time due to the choice of the number of points δ and to the number of echoes, reduced from 6000 to 2000, enough to obtain a good sampling of the T_2 relaxation.
Repeating three times the new sequence on the same sample, the changes shown in Fig. 6.5 were observed, due to the exposition of the sample to the external environment.

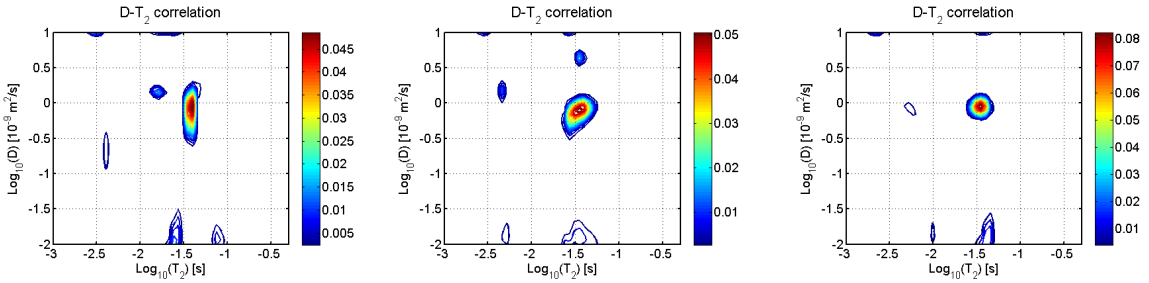

(a) (b) (c)

Figure 6.5: D-T_2 maps obtained for three consecutive SSEdec sequences on the same sample of solid yeast, Δ =0.1 ms.

Below the inversion map and their signal ditribution along D-axis for short, intermediate and long diffusion times are shown.

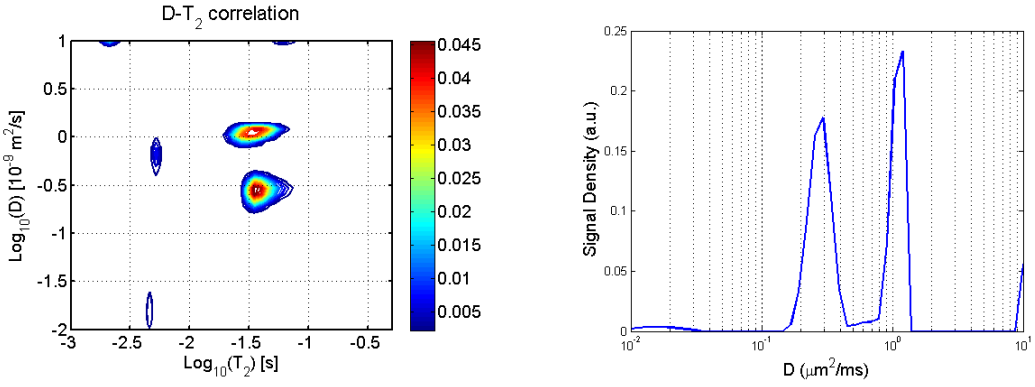

(a) (b)

Figure 6.6: (a) Solid yeast D-T_2 map for Δ=1 ms; (b) The corresponding signal distribution along D-axis.

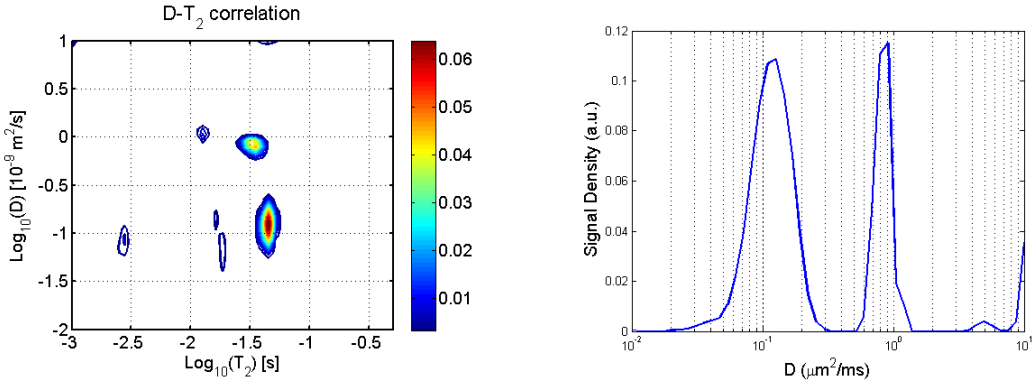

(a) (b)

Figure 6.7: (a) Solid yeast D-T_2 map for Δ=8 ms; (b) The corresponding signal distribution along D-axis.

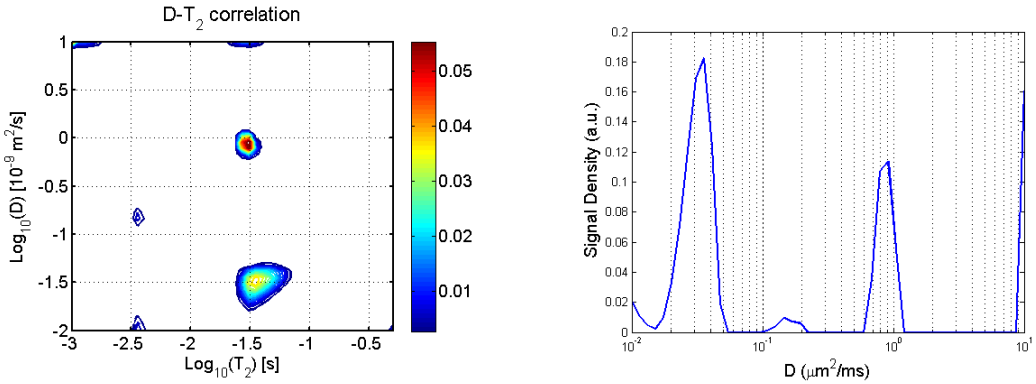

(a) (b)

Figure 6.8: (a) Solid yeast D-T_2 map for Δ=35 ms; (b) The corresponding signal distribution along D-axis.

We can observe the presence of two signal distributions for Δ=1 ms (Fig. 6.6): the longer is Δ, the more separated along D-axis are the distributions (Fig. 6.7-6.8).
In the plot in Fig. 6.9 we show the evolution of diffusion distributions for growing diffusion lengths $\sqrt{D_0\Delta}$ (from the top to the bottom).

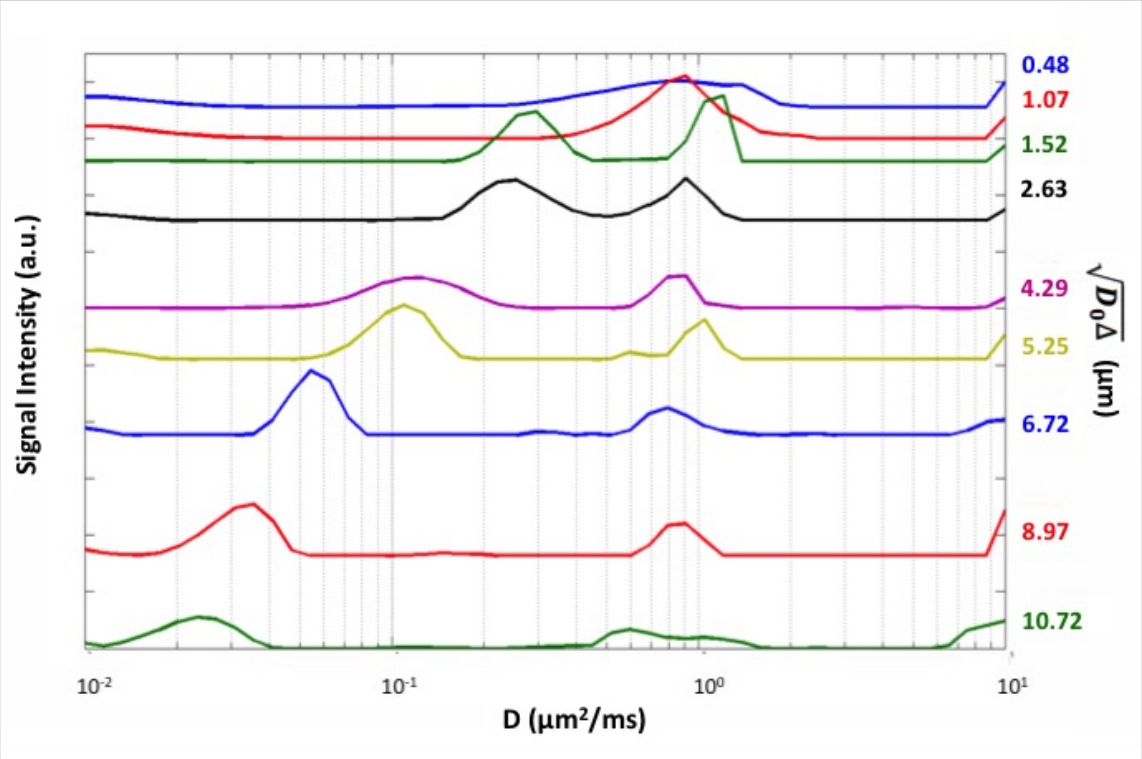

Figure 6.9: Signal distributions on D-axis for all the diffusion lengths considered. The third distribution from the top corresponds to Δ =1 ms diffusion time.

From the distributions along D-axis we can suppose that the two families stand for an *intracellular signal* (the lowest peak for each diffusion length) and for an *extracellular signal* (the highest one).
The separation in two hydrogen families is evident for $\Delta \geq$1 ms: for lower diffusion times we have a single family. We can suppose that the diffusing time is too low for molecules experiencing the cell walls, so we should obtain a bulk selfdiffusion coefficient ($\approx 2.3(\frac{\mu m^2}{ms})$). Despite this, these peaks are lower than the ones referring to extracellular water with greater Δ.
Hence, there could be a data inversion problem, maybe due to a too small percentage of extracellular water, which represents around the 30% of the two compartments signals sum (Fig. 6.10). The error bars have been computed the 3% of the percentages shown according to repeated measurements.

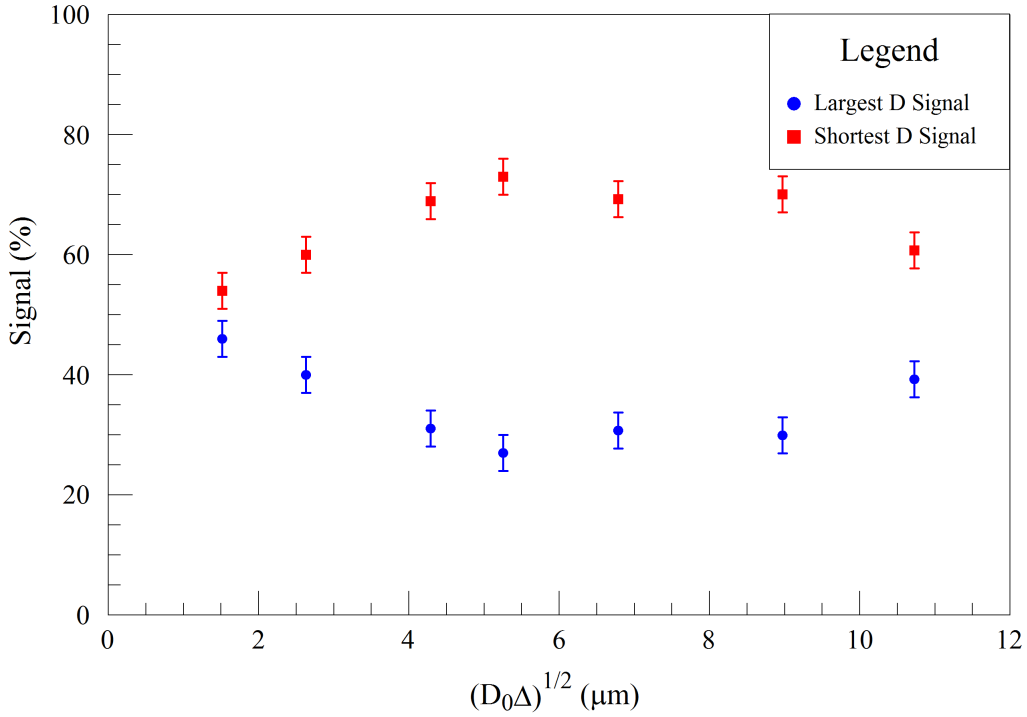

Figure 6.10: Percentage of the two compartments signals in solid yeast sample.

Chapter 7

Measurements on diluted yeast

Under the same conditions of the solid yeast measurements (25°C, 4 spacers inserted) we have performed CPMG for different dilutions of yeast in distilled water.
The data inversion shows a set of T_2 distributions having geometric peaks within a restricted range [50 ms; 70 ms]; their signal are shifted to the value of the solid yeast as a result of the presence of distilled water, which, in these experimental conditions, has longer T_2 ($\approx$ 200 ms).

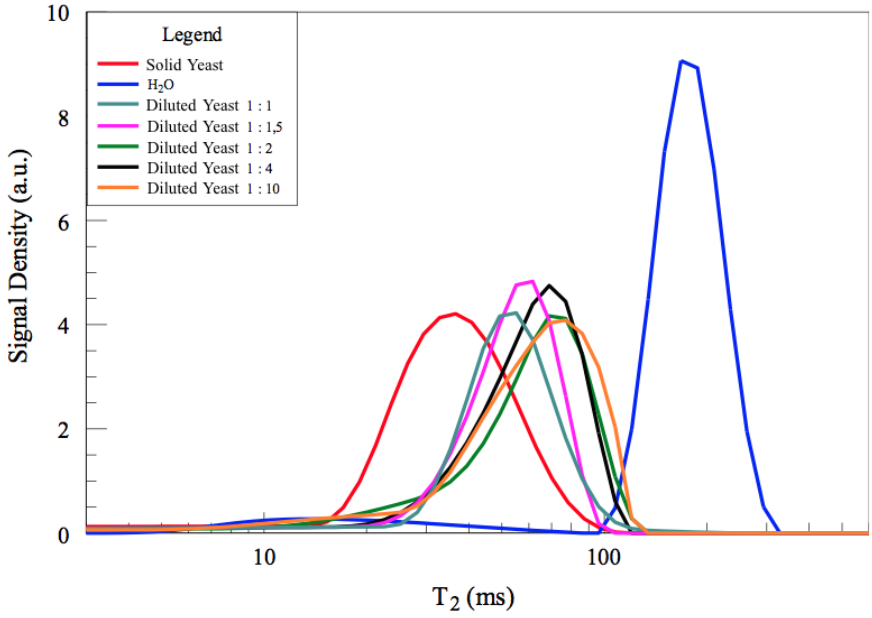

Figure 7.1: T_2 distributions comparison between solid yeast, bulk water and various yeast dilutions.

We have chosen the dilution 1 : 1.5 (w/w) for our measurements.
The 1:1 ratio has been rejected because the sample appears almost solid; the other samples, which have similar T_2 distributions, might have a too intense water signal, that could hide the cell one.

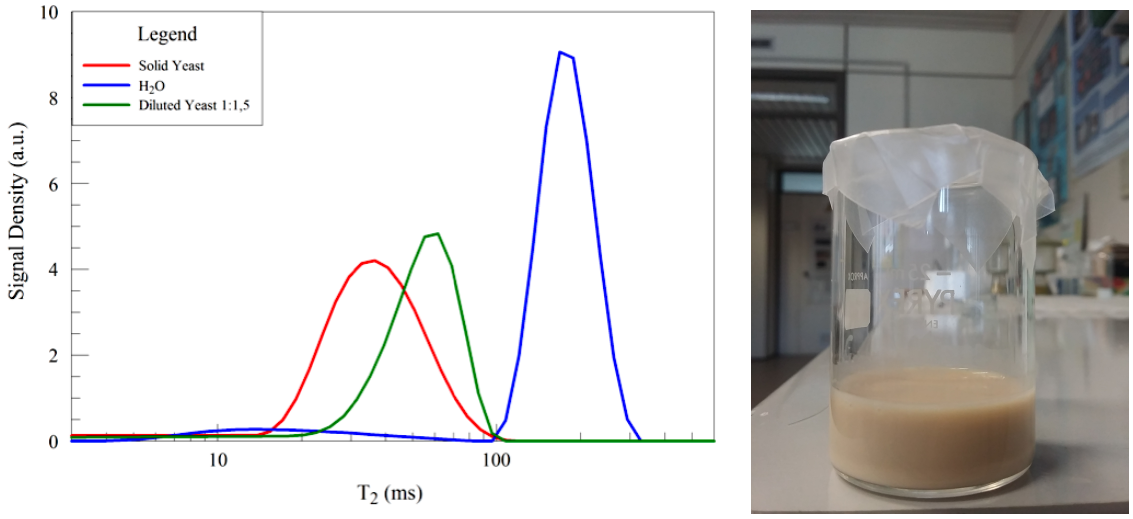

(a) (b)

Figure 7.2: (a) T_2 distributions of solid yeast, diluted yeast and free water; (b) Diluted yeast sample in a becker.

7.1 SSEdec sequences

The SSEdec sequences were used with the same parameters setted for the solid yeast sample. In Fig. 7.3, 7.4, 7.5 the inversion maps and the signal ditributions along D-axis for short, intermediate and long diffusion times are shown.

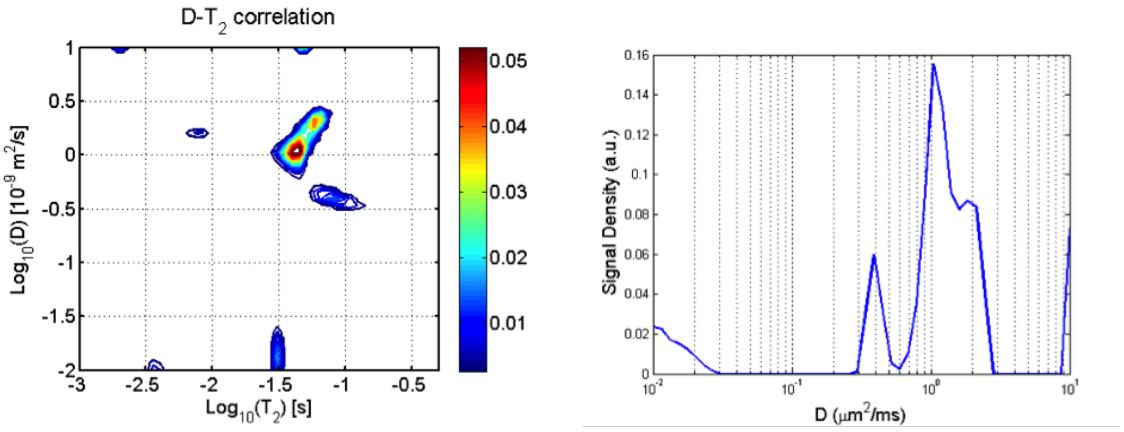

(a) (b)

Figure 7.3: (a) Diluted yeast D-T_2 map for Δ=0.1 ms; (b) The corresponding signal distribution along D-axis.

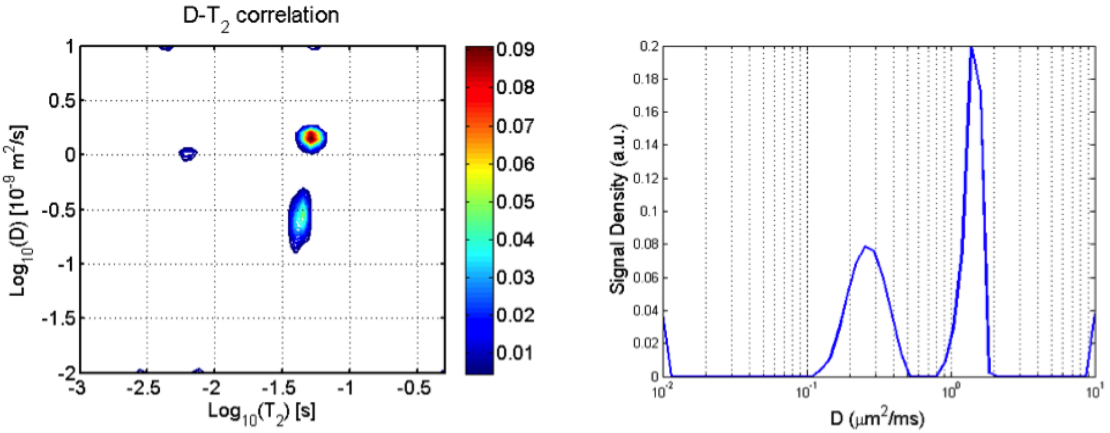

(a) (b)

Figure 7.4: (a) Diluted yeast D-T_2 map for Δ=3 ms; (b) The corresponding signal distribution along D-axis.

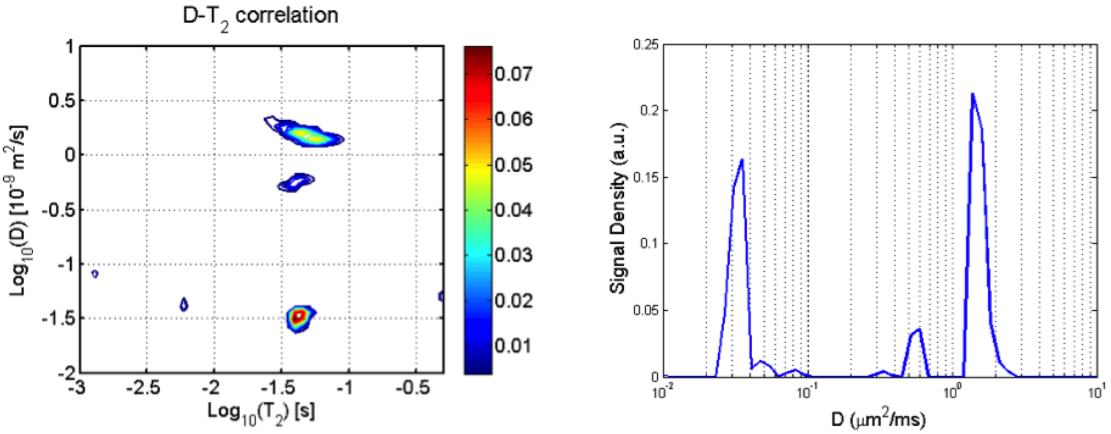

(a) (b)

Figure 7.5: (a) Diluted yeast D-T_2 map for Δ=35 ms; (b) The corresponding signal distribution along D-axis.

As for the solid yeast case, we have two families of diffusing molecules, which separation is more evident for longer diffusion times. In Fig 7.3 we can notice that the peaks distinction is already possible for Δ=0.1, and the longer D is very near to the bulk water selfdiffusion coefficient.
In Fig. 7.6 the two compartments signals are shown.
For shortest diffusion times ($\Delta \leq$1 ms), the longer D signal percentage is 2 times larger than the shorter D one, due to the short time given to the spins to experience the cell walls. In fact the diffusion length for Δ=1 ms is $L_D \simeq$1.5 μm, which is comparable to the cell size.
For $\Delta >$ 1 ms, the two signals are comparable, while for the solid yeast (Fig. 6.10) the

signal with larger D was smaller than the one with the shortest D.

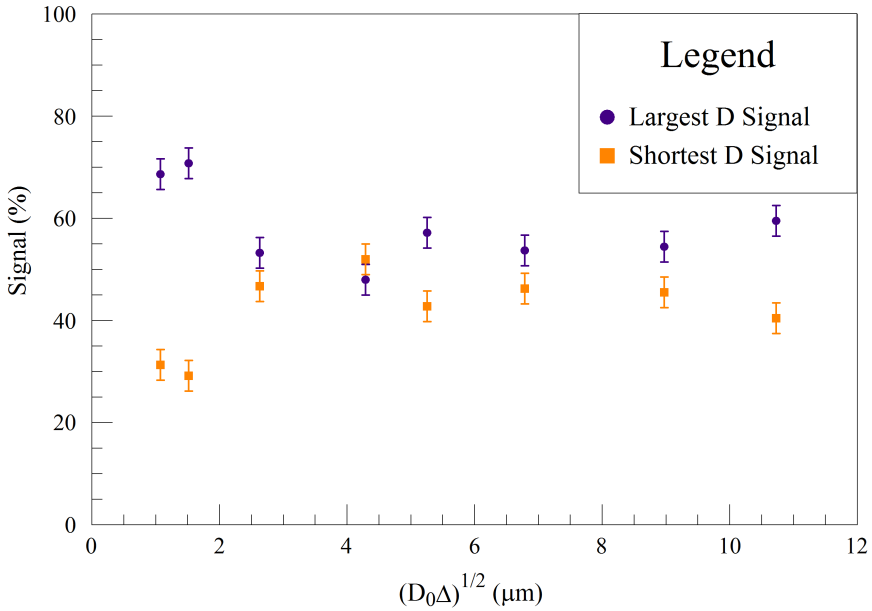

Figure 7.6: Percentage of the two compartments signals in diluted yeast sample, at increasing diffusion length $\sqrt{D_0\Delta}$.

The comparison of the percentages of sample signals over the total signal (Fig. 7.7) suggests that the diluted yeast measurements resulted in inversion maps with less artefacts than the ones elaborated from the solid yeast data.

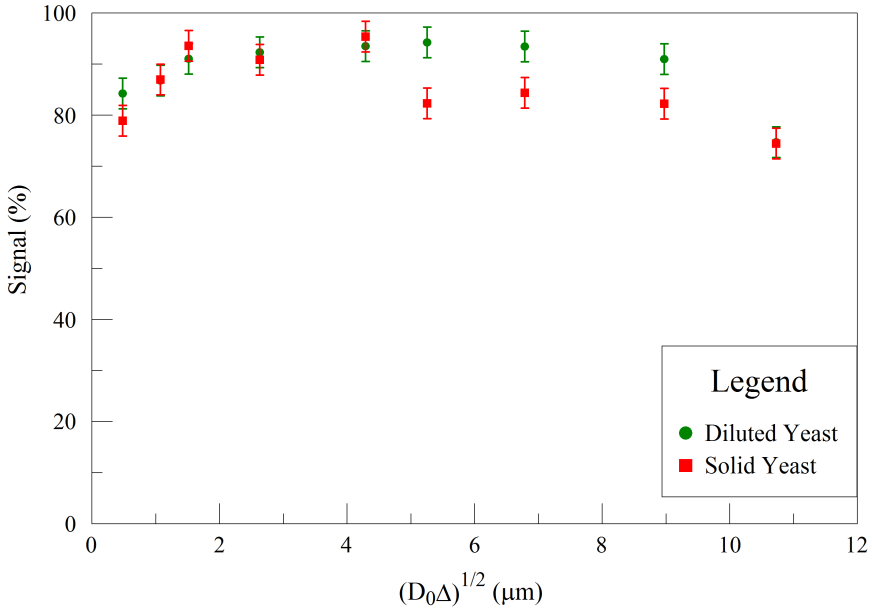

Figure 7.7: Percentage of the sum of the two compartments signals computed respect to the total signal of eache sample, at increasing diffusion length $\sqrt{D_0\Delta}$.

Comparing the signal distributions along D-axis (Fig. 7.8), we can see that the signal with greater D decreases as diffusion length increases; the one standing for the largest D remains almost constant for $\Delta \geq 1$ ms.

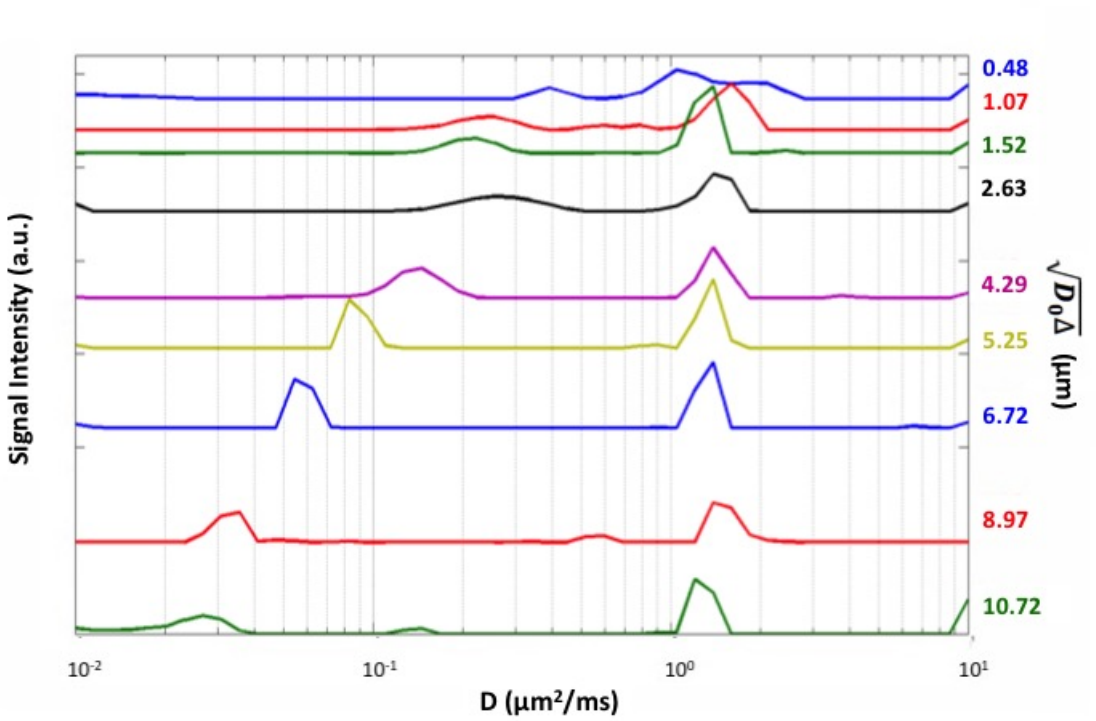

Figure 7.8: Signal distributions on D-axis for all the diffusion lengths considered for the diluted yeast sample.

7.2 SSEdec sequences on yeast diluted with doped water

We had supposed that the signal with the largest D corresponds to water external to the cell.
In order to validate this hypothesis, we have performed the SSEdec sequences on a yeast sample diluted (1 : 1.5 (w/w)) in CuEDTA-doped water. Because of its paramagnetic behaviour, CuEDTA will shorten the relaxation time of water.
Comparing (Fig. 7.9-7.10,7.11) D-T_2 maps of the doped sample (on the right) with the ones of the not-doped sample (on the left), we can notice that the T_2 of the two diffusing hydrogen families undergo a strong reduction. Especially, the family with the largest D has a T_2 which is one tenth of the one in absence of doping.

For $\Delta \geq 35$ms the largest D compartment of the doped sample is completely relaxed and the acquired signal belongs only to the shortest D compartment.

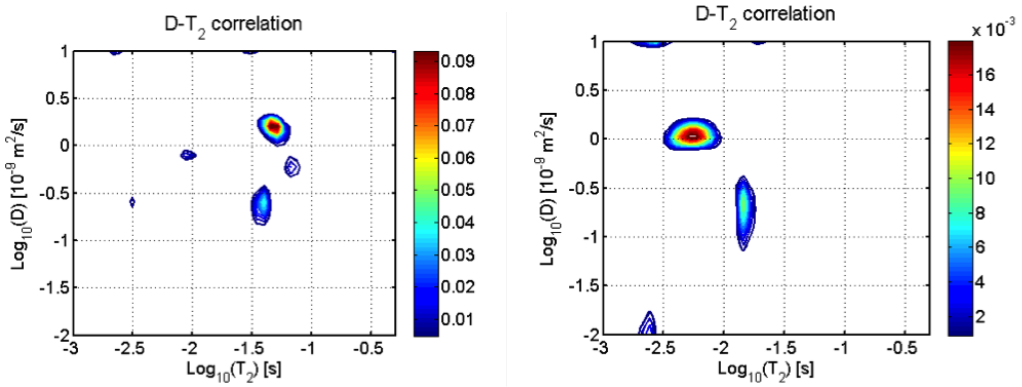

(a) (b)

Figure 7.9: (a) Yeast diluted in not-doped water D-T_2 map for Δ=0.5 ms; (b) Yeast diluted in doped water D-T_2 map for Δ=0.5 ms.

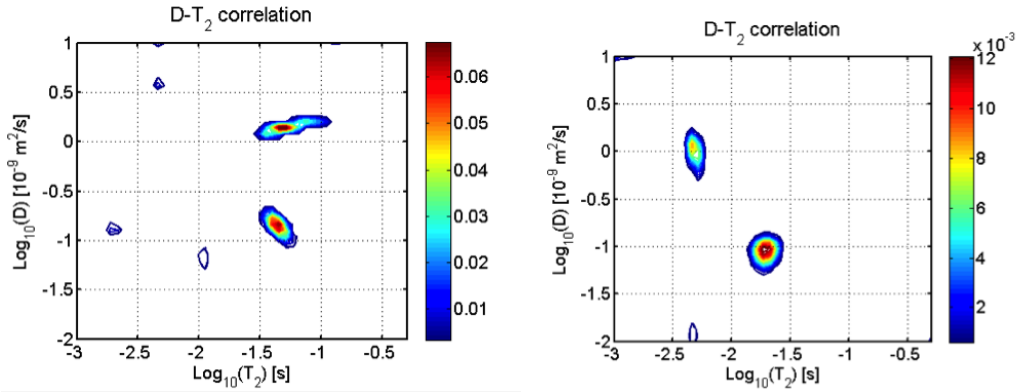

(a) (b)

Figure 7.10: (a) Yeast diluted in not-doped water D-T_2 map for Δ=8 ms; (b) Yeast diluted in doped water D-T_2 map for Δ=8 ms.

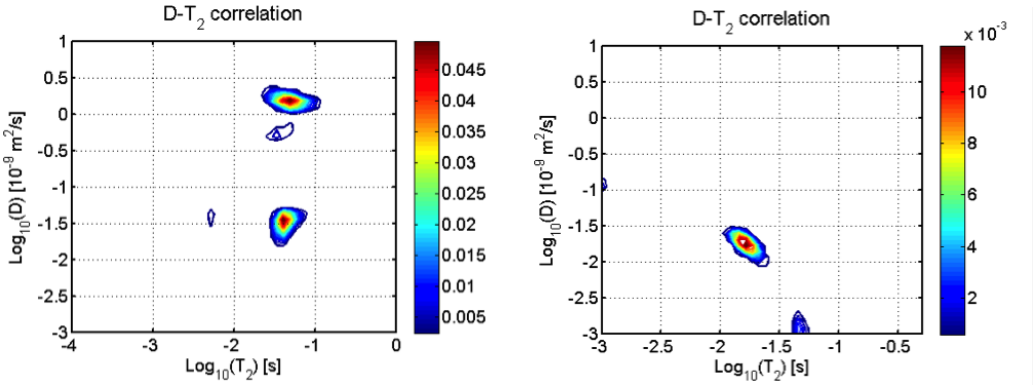

(a) (b)

Figure 7.11: (a) Yeast diluted in not-doped water D-T_2 map for Δ=35 ms; (b) Yeast diluted in doped water D-T_2 map for Δ=35 ms.

Comparing the largest D signal of the three samples considered (Fig. 7.12), we can notice that:

- The signal of the yeast diluted in doped water has values near to the ones belonging to the yeast diluted without doping.
- The two not-doped samples reach a plateu, the doped one decreases progressively until 0% for $\Delta \geq$35 ms.

Hence, in this cases we have only one signal compartment and we can adfirm that the one canceled by CuEDTA corresponds to water external to the cells.
The fact that also T_2 of the intracellular water in doped sample decreases in Fig. 7.9-7.11 as compared with not-doped sample is due to the effect of magnetic susceptibility difference between extra- and intra-cellular compartment in the doped sample.

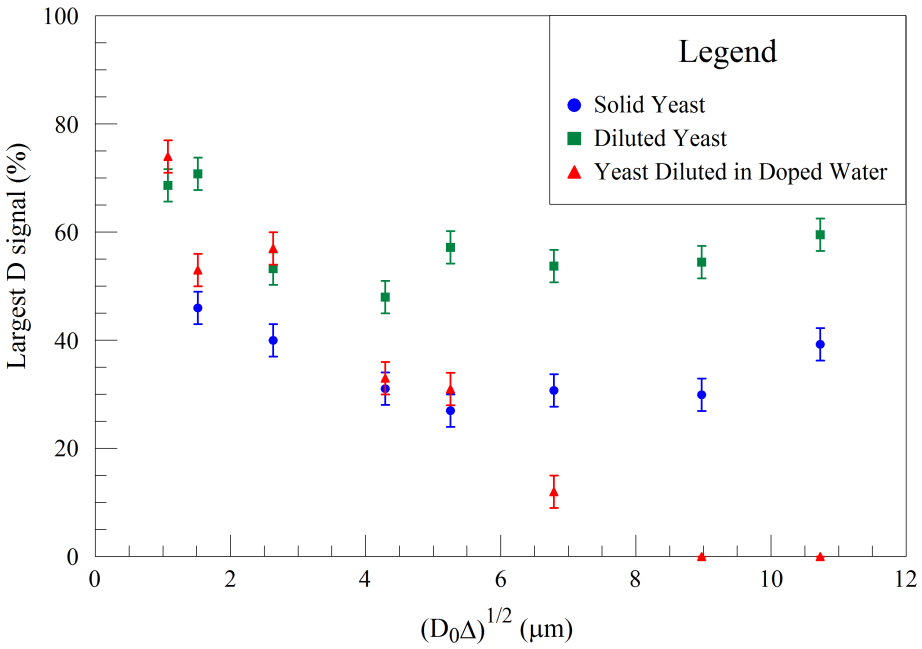

Figure 7.12: Percentage of the largest D compartment signal for the three samples: diluted, diluted doped, solid.

Chapter 8

Discussion

8.1 Apparent selfdiffusion coefficients

The signal peaks of the distributions on D-axis shown in chapters 6-7 exhibit a gaussian shape in a semilog axis, hence we have associate them to base-10 log-normal distributions. Considering the log-10 values

$$\log_{10} D = z \tag{8.1}$$

initially we have computed their mean and variance:

$$\mu = \frac{z_1 z_2 z_3 \dots z_N}{N} \tag{8.2}$$

$$\sigma^2 = \frac{\sum_{i=1}^{N} (z_i - \mu)^2}{N-1} \tag{8.3}$$

Then, we have defined the geometric mean and geometric variance of the base-10 log-normal distribution as:

$$GM[D] = 10^{\mu} \tag{8.4}$$

$$GVar[D] = 10^{\sigma^2} \tag{8.5}$$

Finally we obtain the arithmetic mean by:

$$E[D] = 10^{\mu + \frac{\sigma^2}{2}} = 10^{\mu} \cdot \sqrt{10^{\sigma^2}} = GM[D] \cdot \sqrt{GVar[D]} \tag{8.6}$$

In the following tables, we show the D_{app} values computed for the solid yeast and diluted yeast samples:

Solid Yeast

Δ(ms)	D_{app}^{intra} (μm^2/ms)	D_{app}^{extra} (μm^2/ms)
1	0.28± 0.08	1.06± 0.05
3	0.27± 0.08	0.86± 0.04
8	0.12± 0.04	0.80± 0.04
12	0.10± 0.03	0.98± 0.05
20	0.06± 0.02	0.81± 0.04
35	0.03± 0.01	0.86± 0.04
50	0.02± 0.01	0.65± 0.03

Diluted Yeast

Δ(ms)	D_{app}^{intra} (μm^2/ms)	D_{app}^{extra} (μm^2/ms)
0.1	1.13± 0.06	1.85± 0.09
0.5	0.22± 0.06	1.51± 0.08
1	0.22± 0.06	1.30± 0.07
3	0.27± 0.08	1.40± 0.07
8	0.15± 0.05	1.40± 0.07
12	0.09± 0.03	1.40± 0.07
20	0.06± 0.02	1.30± 0.07
35	0.04± 0.01	1.31± 0.07
50	0.06± 0.02	1.30± 0.07

The errors (1 SD) have been computed in according to the repeated measurements.

8.2 Data fit

In order to obtain information on the studied system, we have fitted the normalized data with the Padé approximant (Eq. 1.29) using PSI-Plot software, by assuming the following conditions:

- We have assumed the bulk water seldiffusion coefficient (=2.3 μm^2/ms) to normalize our data;
- In Eq. 1.29 the compartments are assumed to be spherical;
- The shortest diffusion time was assumed to be Δ =0.1 ms

- As reported in section 5.3, we haven't useful correct data for the short time limit in the case of solid yeast sample.

Because of the last consideration, we have firstly worked on diluted yeast data.
Rewrtiting the Padé approximant:

$$\frac{D_{app}(t)}{D_0} = 1 - \left(1 - \frac{1}{\alpha}\right) \frac{\left(\frac{4}{9\sqrt{\pi}}\right)\left(\frac{S}{V}\right)\sqrt{D_0 t} + \left(1 - \frac{1}{\alpha}\right)\left(\frac{D_0 t}{D_0 \theta}\right)}{\left(1 - \frac{1}{\alpha}\right)\left(\frac{4}{9\sqrt{\pi}}\right)\left(\frac{S}{V}\right)\sqrt{D_0 t} + \left(1 - \frac{1}{\alpha}\right)\left(\frac{D_0 t}{D_0 \theta}\right)}$$

we notice the presence of three free parameters: Surface-to-Volume ratio S/V, tortuosity α and the time fitting parameter θ.
The choice of letting them all free determined an overfitting of the data with non-physical results for the parameters (i.e. negative tortuosity). Hence, we have first extrapolated an estimation of S/V by fitting the short-time data using the short time limit (Eq. 1.32)

$$\lim_{t \longrightarrow 0} \frac{D_{app}(t)}{D_0} = 1 - \frac{4}{9\sqrt{\pi}} \frac{S}{V} \sqrt{D_0 t}$$

the value obtained for the parameter S/V was then inserted in the Padé approximant to estimate α and θ. The short-time limit fit on the intracellular signal gave us:

- $\frac{S}{V} = 3.5 \pm 0.2\ (\mu\text{m})^{-1}$

Taking it into the Padé approximant we obtained:

- $\frac{D_{eff}}{D_0} = \frac{1}{\alpha} = 0.03 \pm 0.02$
- $\theta = 0.11 \pm 0.03$ ms

Repeating the same process for the extracellular component we obtained:

- $\frac{S}{V} = 1.3 \pm 0.1\ (\mu\text{m})^{-1}$
- $\frac{1}{\alpha} = 0.58 \pm 0.02$
- $\theta = 0.15 \pm 0.05$ ms

In Fig. 8.1 the plots for the two compartments of the diluted yeast data with the corresponding fits are shown:

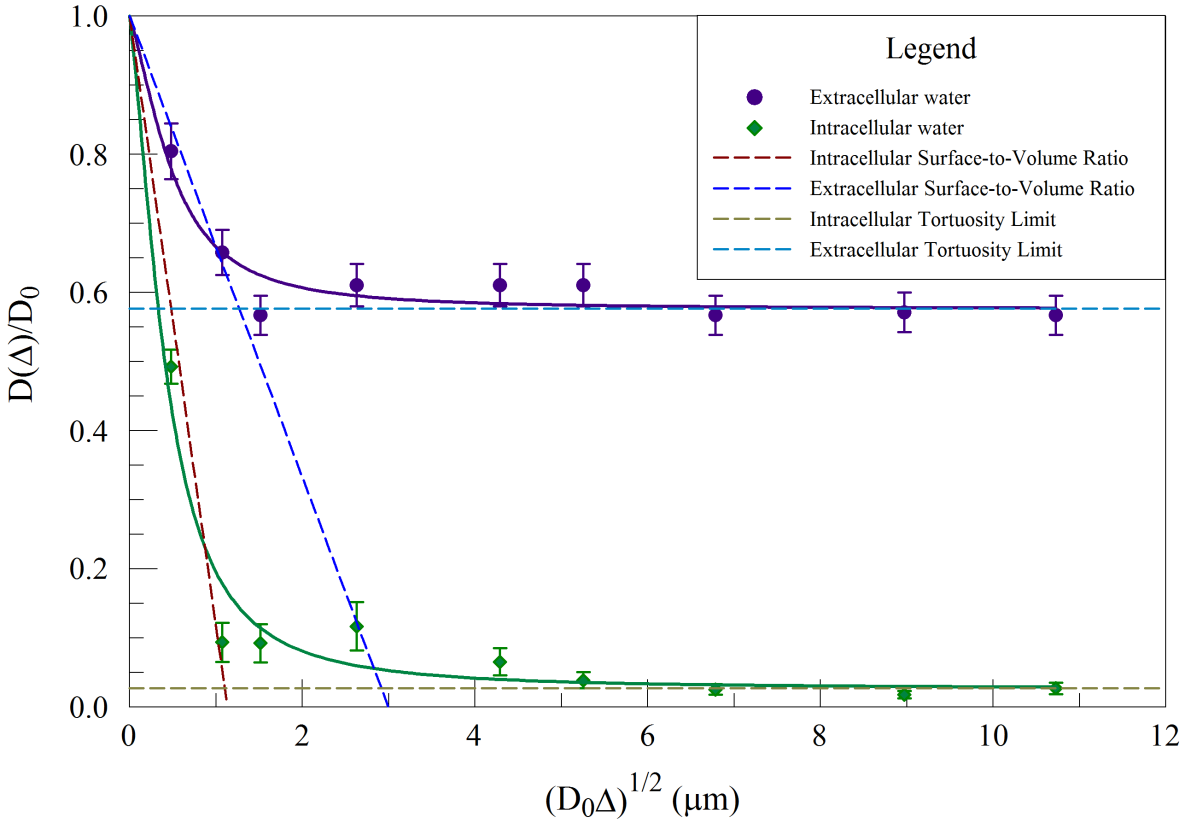

Figure 8.1: Diluted yeast sample data fitted with the Padé approximant.

By assuming a spherical shape for the compartments, an estimate of the radius can be obtained:

$$\frac{S}{V} = \frac{4\pi r^2}{\frac{4}{3}\pi r^3} = \frac{3}{r} \longrightarrow r = \frac{3}{S/V}$$

and

$$\Delta r = \frac{r^2}{3}\Delta(S/V)$$

Thus:

- $r = 0.9 \pm 0.1$ μm, intracellular compartment;
- $r = 2.3 \pm 0.2$ μm, extracellular compartment

According to this analysis, the cell membranes are on average about 2.3 μm separated; the intracellular compartment could be assume to be an about 1 μm radium sphere. Repeating this analysis to the yeast sample diluted with doped water, whose compartments are visibly separated already with Δ=0.5 ms (Fig. 7.9(b)), we obtain the values shown in the table below:

Yeast diluted in doped water

	Intracellular compartment	**Extracellular compartment**
$\frac{S}{V}$ $(\mu\text{m})^{-1}$	3.3± 0.2	1.9± 0.1
$\frac{1}{\alpha}$	0.028± 0.014	0.393± 0.012
θ (ms)	0.07± 0.03	0.10± 0.03
r (μm)	0.9± 0.1	1.6± 0.1

Comparing these results to the ones presented previously, we notice the intracellular compartment data are compatible.
This means we could fit the solid yeast data with Padé approximant using the $\frac{S}{V}$ computed on the other samples (Fig. 8.2).

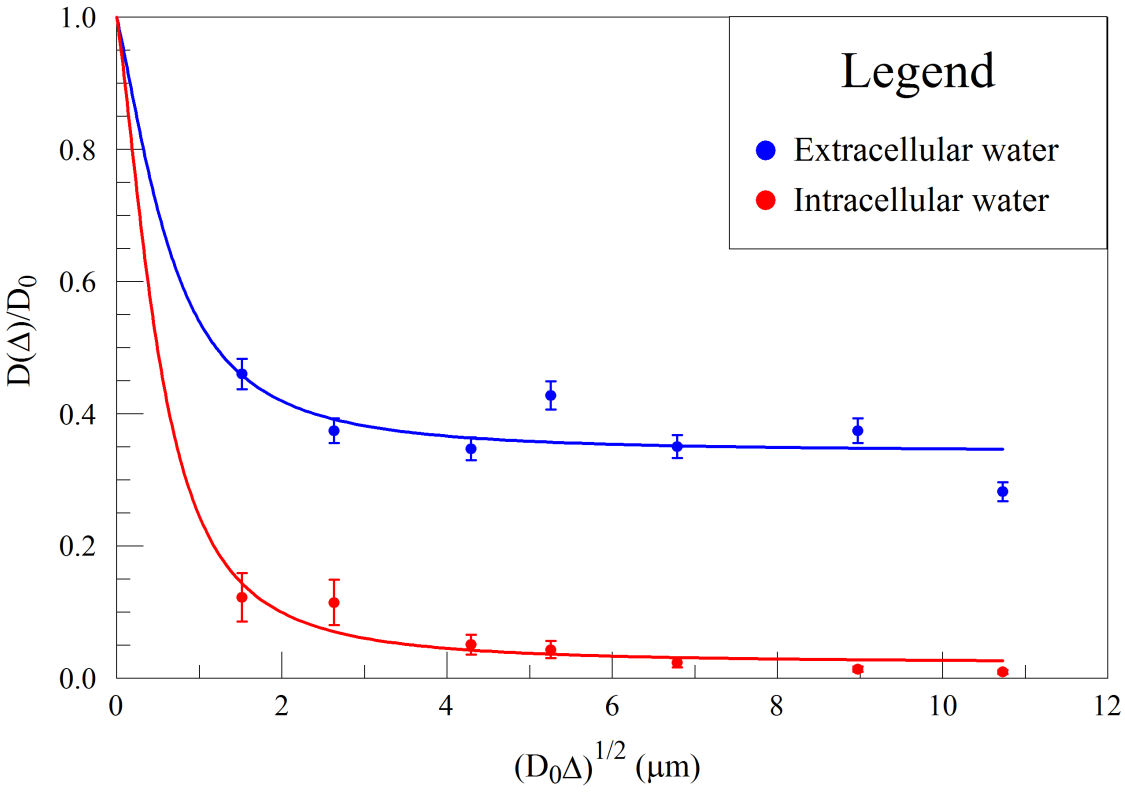

Figure 8.2: Solid yeast sample data fitted with the Padé approximant.

Hence we have obtained the following fitted parameters:

Solid Yeast

	Intracellular compartment	**Extracellular compartment**
$\frac{1}{\alpha}$	0.02± 0.02	0.34± 0.02
θ (ms)	0.17± 0.05	0.28± 0.17

In summary, two compartments are detectable. The largest D compartment is likely external water, and the one with the shortest D is due to signal of water inside the cells.

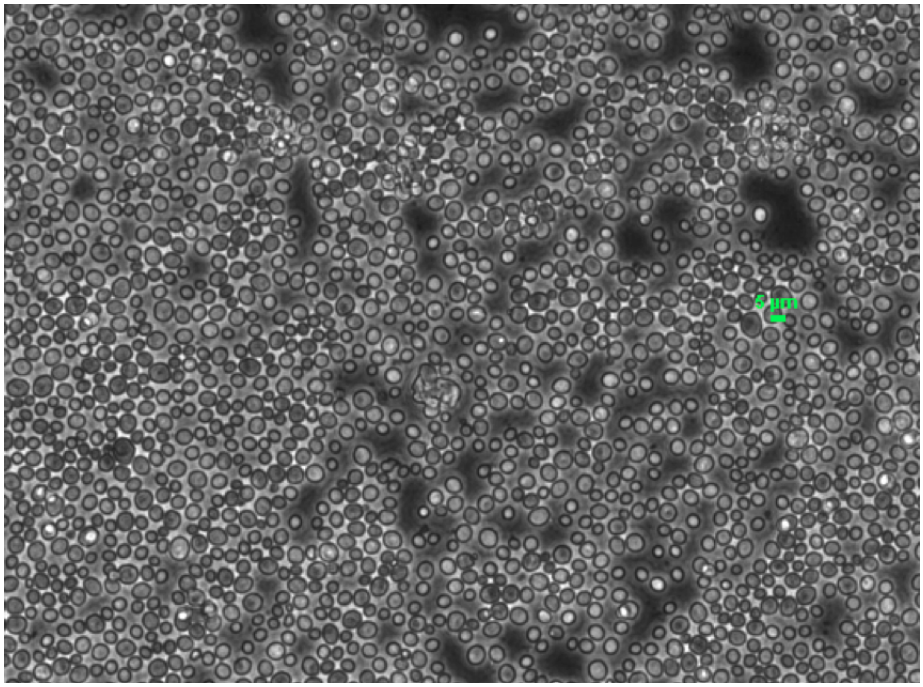

Figure 8.3: Yeast in 1:10 dilution 20X image by optic microscope (courtesy of Dr. Isabella Zironi).

In Fig. 8.3 an optic microscope 20X image of yeast on 1:10 (w/w) dilution is shown: the radius of the cells is distributed in the range 0.5-3 μm, consistent with the order of magnitude of the radius computed with the presented method.
The signal we have seen in our 2D elaborations is probably water exchanged between the organelles and the cytosol.

Conclusions

The object of this thesis is the feasibility study of the use of single-sided NMR devices to investigate the internal- external water compartmentalization in biological cells, through two-dimensional correlation maps, where the two variables are the molecular self-diffusion coefficient D of water and the transverse relaxation time T_2 of water ^{1}H nuclei.
Yeast cells in different diluition conditions have been chosen as model systems.

First of all, a set of preliminary tests were performed in order to test the procedures adopted to measure the molecular self-diffusion coefficients of bulk liquids by exploiting the intrinsic magnetic field gradient of the single-sided device of the NMR laboratory of the Department of Physics and Astronomy of the University of Bologna. The conditions for the localization of the NMR signal and the better use of the device were established. Then three different bulk liquids were analyzed and self-diffusion coefficients consistent with the literature values were obtained. At the tempearture of 25°C we obtained: $D = 2.3\pm0.1$ μm^2/s for water; $D = 0.84\pm0.01$ μm^2/s for soltrol 130; $D = 0.36\pm0.02$ μm^2/s for soltrol 170.

The second step was the optimization of the procedures for the study of compartmentalization by means of two-dimensional correlation maps in system characterized by restricted diffusion. These are systems in which the molecular self-diffusion is limited by walls, giving rise to measurements of appearent self-diffusion coefficients. For sake of semplicity, the symbol D will be used in the following, even if the symbol D_{app} would be physically more correct. Samples of solid yeast cells were used in these preliminary experiments. Sequences consisting in an encoding Stimulated Spin Echo followed by a decoding CPMG for different diffusion times have been used. By means of these preliminary experiments, the better choice for a correct timing of the events constituting the sequence (35 μs echo time, 2000 echoes, 50 increasing encoding times δ, 32 scans) and the experimental ranges of their possible temporal variations were established. By these sequences it is possible to distinguish in a sample families of ^1H nuclei characterized by different D and T_2 values. The families will appear as separated classes in a two-dimensional D, T_2 diagram. In solid yeast sample, the D-T_2 correlation maps have shown the presence of two ^{1}H families for diffusion times $\Delta \geq 1$ ms, which separation became larger for longer diffusion times Δ. The two families are characterized by two different self-diffusion coefficient. The separation became more and more evident with increasing Δ as a result of the restricted diffusion. In fact, as the diffusion time increases, more and more water molecules experience the restriction due to the cell walls. This determines a strong

reduction of the apparent diffusion coefficient of the family with the shortest D. For shorter Δs only one family is observed in the D-T_2maps: their peaks have lower D values than the ones belonging to the largest D signal for longer diffusion times, hence there have could be a data inversion problem. This was ascribed to the presence of a very low fraction of extracellular water.

The following step was the application of the procedures setted in the previous experiments to samples of yeast cells diluted by water. The CPMG sequences has shown the same T_2 range for different dilutions, in order to not have a too intense water signal, which have could hide the signal of water inside the cells, the dilution 1 : 1.5 (w/w) was chosen. These measurements have shown the presence of two ^{1}H families even setting short diffusion times ($\Delta \in$ [0.1-0.5 ms]). The D value of family with the shortest D decreased from D =1.13 μm^2/ms for Δ =0.1 ms to D =0.06 μm^2/ms for Δ =50 ms . The D value of family with the largest D decreased from D =1.85 μm^2/ms for Δ =0.1 ms to D =1.30 μm^2/ms for Δ =50 ms. For Δ =1 ms the D of the first famility is reduced respect to the bulk value of about 80%. The diffusion length for Δ=1 ms is L_D =1.5 μm, which is comparable to the cell size. All this suggested the the first family could correspond to intracellular water and the second family, with the largest D, to extracellular water.

In order to validate this hypothesis, we have repeated the measurements using as yeast cells sample diluted (1 : 1.5 (w/w)) in CuEDTA-doped water. This compound, that cannot cross the cell membrane, will shorten the T_2 of the external water because of its paramagnetic behaviour, and only sligthly reduce the T_2 of the internal water. If our hypothesis is true, we will observe a strong reduction of the signal intensity of the family with the largest D value. This is just the result observed. The comparison between the D-T_2 maps of the doped sample and the ones of the not-doped sample showed a strong reduction of the largest D compartment, until it completely disappeared for Δ >35 ms. This effect is almost neagligible for the shortest D family, which T_2 is reduced of a smallest amount, likely due to effects of the susceptibility difference between the doped compartment and the compartment without the paramagnetic compound.

This experiment has confirmed that the largest D compartment corresponds to extracellular water and the shortest one to the intercellular water.

Assuming the bulk water self-diffusion coefficient (2.3 μm^2/ms) for the data normalization, and the spherical shape for the compartments, we have fitted the data by two steps. The first step has allowed to compute an estimation of the Surface-to-Volume ratio of the two compartments using a short-time limit equation. The values obtained were then inserted in a Padé approximant in order to compute the estimation of the tortuosity values for the two compartments.

From the Surface-to-Volume ratio, by the assumption of spherical shape, the radius can be estimated. The fit of the data for the yeast diluted in not-doped water sample has resulted in r =2.3±0.2 μm for to the extracellular compartment and r =0.9±0.1 μm for the intracellular one; this last result has been confirmed by the same analysis on the yeast diluted in doped water. The errors associated to these estimates account only for

the best fit of the data to the short-time limit equation.
Of course they do not take into account other sources of errors, not easily quantifiable at the present time, as the assumption of spherical shape for the compartments. In particular, the presence of many organelles in the cytosol, which contribute to increase the Surface-to-Volume ratio, with water exchanging among these organelles and cytosol, could strongly influence the estimate of the size of the internal water compartment. Anyway if considered as estimates of the sizes, the values of r obtained for the two compartments are in good agreement (as order of magnitude) with the values observed by optical microscopy in the image obtained on a diluted sample of yeast cells.

In summary, the experiments performed for this thesis work have demonstrated not only the correctness of the procedures settled to measure bulk and restricted self-diffusion coefficients by a single-sided NMR device, but also the feasibility of studies of internal- external water compartmentalization in biological cells, through two-dimensional correlation maps.

Bibliography

[1] Song Y. Q., *Magnetic Resonance of Porous Media (MRPM): A perspective* Journal of Magnetic Resonance, 2013, 229, 12-24.

[2] Mitra P.P., Sen P.N., Schwartz L.M., Le Doussal P., *Diffusion propagator as a probe of the structure of porous media*, Physical review letters, 1992, 68(24):3555-3558.

[3] Price W.S., *Pulsed field gradient nuclear magnetic resonance as a tool for studying translational diffusion: Part 1. basic theory*, Concepts in Magnetic Resonance, 1997, 9(5):299-336.

[4] Latour L.L., Svoboda K., Mitra P.P., Sotak C.H., *Time-dependent diffusion of water in a biological model system.*, Proc. Natl. Acad. Sci. USA 91, 1994, 1229-1233.

[5] Mitra PP, Sen PN., *Effects of microgeometry and surface relaxation on NMR pulsed-field-gradient experiments: Simple pore geometries.*, Phys Rev B, 1992, 45(1):143.

[6] Mitra P.P., Sen P.N., Schwartz L.M., *Short-time behavior of the diffusion coefficient as a geometrical probe of porous media.* Phys Rev B, 1993, 47:8565.

[7] Sen, P.N., Schwartz, L. M., Mitra, P. P. and Halperin, B.I., *Surface relaxation and the long-time diffusion coefficient in porous media: periodic geometries*, Phys. Rev. B,1994, 49(1), 215-225.

[8] Latour L.L., Kleinberg R.L., Mitra P.P., Sotak C.H., *Pore-Size Distributions and Tortuosity in Heterogeneous Porous Media.*, J Magn Reson Series A, 1995, 112:83-91.

[9] Le Bihan D, *Diffusion and perfusion Magnetic Resonance Imaging: application to functional MRI.*, Raven, New York.

[10] Blumich B., Perlo J., Casanova F., *Mobile Single-Sided NMR, Progress in Nuclear Magnetic Resonance Spectroscopy*, 2008, 52,197-269.

[11] Gradshteyn I. S., Ryzhik I. M., *Table of Integrals, Series, and Products, Academic Press*, New York, 1994.

[12] Latour L.L., Mitra P.P., Kleinberg R.L., and Sotak C.H., *Time-Dependent Diffusion Coefficient of Fluids in Porous Media as a Probe of Surface-to-Volume Ratio*, J. Magn. Reson., 1993 A101, 342-346.

[13] Sen, P.N., *Time-dependent diffusion coefficient as a probe of geometry*. Concepts Magn. Reson., 2004, Part A 23 (1), 1-21.

[14] de Swiet T.M., Sen P.N.., *Time dependent diffusion coefficient* in a disordered medium. J Chem Phys 1996, 104-206.

[15] CarrH. Y., Purcell E. M., *Effects of Diffusion on Free Precession in Nuclear Magnetic Resonance Experiments*, Phys. Re.,1954, 94, 630-638.

[16] *profile NMR-MOUSE PM 10 user guide*, Magritek

[17] Perlo J., Casanova F., B. Blumich B., *Profiles with microscopic resolution by single-sided NMR*, J. Magn. Reson., 2005, 176, 64-70.

[18] Borgia G. C., Brown R. J. S., Fantazzini P.,*Uniform-Penalty Inversion of Multi-exponential Decay Data: II. Data Spacing, T_2 Data, Systematic Data Errors, and Diagnostics* Magn. Reson. 2000, 147, 273-285.

[19] *UPENWin Manual*

[20] Tikhonov A.N., Arsenin V.Y., *Solutions of Ill-Posed Problems*, John Wiley and Sons, New York, 1977.

[21] `https://en.wikipedia.org/wiki/Dodecane`

[22] `https://en.wikipedia.org/wiki/Ethylenediaminetetraacetic_acid`

[23] Brizi L.,*Studio NMR delll'autodiffusione molecolare: impiego di un gradiente di campo magnetico costante in condizioni di diffusione ristretta e non ristretta*, 2012.

[24] Krieg N.R., Pelczar M.J, Chan E.C.S., *Microbiology*, McGraw-Hill, New York, 1986.

[25] Cabib E, Arroyo J., *How carbohydrates sculpt cells: chemical control of morphogenesis in the yeast cell wall*, Nat. Rev. Microbiol., 2013 11:648-655.

[26] Misu K., Fujimura-Kamada K., Ueda T., Nakano A., Katoh H., Tanaka K, *Cdc50p, a conserved endosomal membrane protein, controls polarized growth in Saccharomyces cerevisiae.*, Mol. Biol. Cell, 2003, 14:730-747.

[27] Prinz W.A., Grzyba L., Veenhuisc M., Kahanab J.A., Silverb P.A., Rapoporta T.A., *Mutants Affecting the Structure of the Cortical Endoplasmic Reticulum in Saccharomyces cerevisiae*, J Cell Biol., 2000, 150:461-474.

[28] Borgia G.C., Brown R.J.S., Fantazzini P.,*Scaling of spin-echo amplitudes with frequency, diffusion coefficient, pore size, and susceptibility difference for the NMR of fluids in porous media and biological tissues*, Phys. Rev. E 51, 1995, 2104-2114.

[29] Mills R., *Self-diffusion in normal and heavy water in the range 1-45°*, Phys. Chem., 1973, 77 (5), 685-688.

Ringraziamenti

Volevo innanzitutto ringraziare la **Prof.ssa Paola Fantazzini** per la possibilitá che mi ha dato di approfondire un tema molto interessante e vasto come quello della Risonanza Magnetica applicata sui mezzi porosi, avvicinandomi all'approccio della ricerca scientifica e per avermi sempre dato i giusti consigli sia durante la mia esperienza in laboratorio che durante la stesura della tesi.
Volevo ringraziare il **Dott. Leonardo Brizi** per la costante disponibilitá che mi ha sempre fornito, anche in momenti impegnativi, per la grande pazienza dimostrata nei miei confronti, oltre che, ovviamente, per le tante indicazioni disposte durante il mio lavoro.
Ringrazio la mia famiglia, cui è dedicata questa tesi, mia madre **Franca**, mio padre **Giovanni** e mia sorella **Bianca** per il supporto che non hanno mai smesso di darmi.
Ringrazio **Alessandro**, **Andrea**, **Claudio**, **Davide** e **Lorenzo** con cui, tra molti alti e pochi bassi, condivido un rapporto d'amicizia sincero e ormai quasi storico.
Ringrazio **Andrea** e **Francesco**, per la grande intesa ("San Paolo" aggiungerebbe Francesco) che si è creata durante la mia esperienza universitaria.
Ringrazio **Marco** per il supporto morale (ricambiato, ovviamente) durante la stesura della tesi.
Ringrazio **Alessio**, **Alessandra**, **Carmine**, **Elisa**, **Fabio** e **Federico** per le serate e le chiacchere durante questi anni passati insieme in facoltá.
Ringrazio **Ivano**, col quale la scelta di un diverso curriculum non ha cancellato ciÃš che si é creato durante la laurea triennale.
Per lo stesso motivo ringrazio **Allegra**: "You don't ever need to worry about showing your true colours. You understand each other blindly, trust each other unconditionally and accept one another with all your special traits".
Infine volevo ringraziare **Roberta**, la mia ragazza, per esserci sempre stata prima, per esserci sempre adesso e, mi auguro, per esserci sempre in futuro.